AD-A149 237 MODELLING FOR FATIGUE CRACK GROWTH PREDICTION IN MIRAGE IIIO FRAME 26(U) AERONAUTICAL RESEARCH LABS MELBOURNE (AUSTRALIA) J M FINNEY ET AL. APR 84 ARL-STRUC-401 1/1

UNCLASSIFIED F/G 12/1 NL

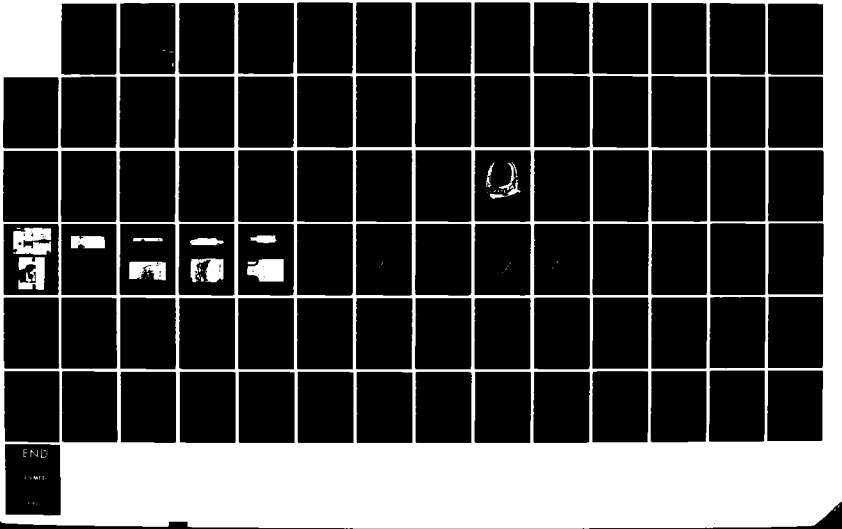

END

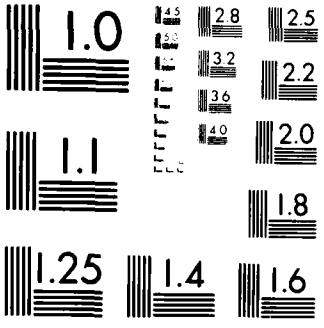

ARL-STRUC-REPORT-401

AR-003-015

DEPARTMENT OF DEFENCE

DEFENCE SCIENCE AND TECHNOLOGY ORGANISATION

AERONAUTICAL RESEARCH LABORATORIES

MELBOURNE, VICTORIA

STRUCTURES REPORT 401

MODELLING FOR FATIGUE CRACK GROWTH PREDICTION IN MIRAGE IIIO FRAME 26

by

J. M. FINNEY
F. G. HARRIS
R. A. PELL
C. S. DENTRY
C. T. STEFOULIS

APRIL 1984

COPY No

84 12 31 054

AR-003-015

DEPARTMENT OF DEFENCE
DEFENCE SCIENCE AND TECHNOLOGY ORGANISATION
AERONAUTICAL RESEARCH LABORATORIES

STRUCTURES REPORT 401

MODELLING FOR FATIGUE CRACK GROWTH PREDICTION IN MIRAGE IIIO FRAME 26

by

J. M. FINNEY
F. G. HARRIS
R. A. PELL
C. S. DENTRY
C. T. STEFOULIS

SUMMARY

Constant- and variable-amplitude fatigue crack growth data have been obtained for A7-U4SG-T651 (2214) ~~aluminium~~ alloy applicable to frame 26 of Mirage IIIO aircraft, enabling calibration of computer models of crack growth. Of the four crack growth retardation models examined—Wheeler, Willenborg, modified Willenborg and Crack Closure—the Wheeler and modified Willenborg models are the most satisfactory but both require calibration by test. Even so, crack growth is not accurately predicted when the specimen geometry and the test sequence are varied from those used in calibrating the models.

Apart from the crack growth models, the main sources of inaccuracy in predicting crack growth are the inadequacy of the growth rate basic data, incorrect assumptions of crack shape, and uncertainty in stress history. Thus, crack growth life may not be confidently predicted to better than a factor of two on actual life and, in some cases, the factor may be as high as ten.

POSTAL ADDRESS: Director, Aeronautical Research Laboratories,
Box 4331, P.O., Melbourne, Victoria, 3001, Australia

CONTENTS

A-1

1. INTRODUCTION

To determine inspection intervals for assuring integrity of an aircraft structure against fatigue the following aspects require consideration:

* a specification of flight loading:
* the stress distribution, to convert the loading history into a stress history and to establish potentially-critical areas:
* a crack growth prediction model:
* utilization of the model with materials crack growth data to predict growth rates in critical areas:
* a procedure for asserting safety using inspections for detecting cracks.

This report deals with one aspect of the structural integrity of the Mirage IIIO aircraft operated by the Royal Australian Air Force (RAAF), namely, crack growth prediction models. It is restricted also to one part of the structure—frame 26 of the fuselage. This frame, shown pictorially in Fig. 1, is a composite of two forged aluminium alloy frames and connecting plates, and contains the attachment points for the main spars of the wings.

Crack growth models have been formulated on a variety of bases, such as dislocation behaviour, work-hardening processes, and crack tip geometries, but those most commonly used are based upon a development of fracture mechanics by Paris.[1,2] Paris postulated that

$$da/dN = f(\Delta K) \tag{1}$$

and specifically that

$$da/dN = C(\Delta K)^n \tag{2}$$

The fracture mechanics models are popular because they are simple to use and because they have, in many cases, provided good agreement with experimental results, at least better than most other models.

The Paris model (equation (2)) is recognized to have a number of deficiencies. It does not account for the substantial effect of load ratio, R, on crack growth rates, or for the threshold ΔK phenomenon and the K_c limit of stress intensity, or for load sequence effects.

The present work utilizes the extensive fracture mechanics background in order to establish a suitable model for predicting crack growth in frame 26. Constant-load-amplitude tests on frame 26 material provide basic growth rate data, evaluate the effects of R, and determine limiting growth rate conditions. Variable-amplitude tests allow the 'calibration' of crack growth retardation models and provide crack growth data for comparison with predictions.

2. LOAD SEQUENCES

2.1 Load-Time Histories

The loading sequence used for the 'calibration' crack growth tests was derived from that used by the Swiss Federal Aircraft Factory (F + W) at Emmen, Switzerland for testing Mirage III aircraft. The sequence was thought to be sufficiently representative of RAAF Mirage flying for the computer model calibration.

The F + W sequence is a flight-by-flight type with 200 flights per program.[3] The 200 flights are not all unique; there are 24 unique or 'typical' ones repeated to give selected occurrence frequencies. One program contains approximately 39,000 turning points and the occurrence distribution is given in Table 1. The maximum load of 7·5 g occurs in only one of the typical flights (number 2), but this flight is used twice in the 200 flight program, once as flight 48 and once as flight 150. The 7·5 g load occurs within these flights at turning point number 116. The *g*-levels in Table 1 are only nominal designations. Stresses in the specimen tests were chosen arbitrarily and were directly proportional to the *g*-values listed. It is useful to retain the *g* nomenclature in discussing the fractographic and crack growth modelling aspects of this report.

A different Mirage load-time history was applied to two specimens as a check on the computer model calibrations. This sequence was derived from the 'all-time-average' of RAAF Mirage flying applicable up to late 1976. It was based on Fatigue Meter records which were used to derive a strain sequence at a particular control point on frame 26, namely, the area around the 6 mm fastener hole in the 8 mm thick outer flange at the bottom of the frame (Reference 4 gives the derivation). The sequence consists of 500 flights (all different) per program and one program encompasses approximately 108,000 turning points. The occurrence distribution is given in Table 2. The maximum load is equivalent to 7·8 g and occurs only once—in flight 65, turning point 43. The derived strain sequence is location dependent and the conversion from *g* to strain depends on whether the aircraft was fitted with centreline tanks. Only 6·64% of all flights utilized these tanks and for the present task it is satisfactory to describe the stress level in the specimens tested under this sequence as a certain gross area stress per *g*, obtained by dividing the stress under the maximum load by 7·8. (This gives scaled levels for ready comparison with the levels of the F + W sequence).

2.2 Constant-Load-Amplitude Tests—R Values

For the F + W sequence described above, Table 3 was compiled using range-mean-pair counting, to show the frequency of occurrence of *R*-values associated with a range of maximum *g*-levels. Three *R*-values were chosen for obtaining constant-amplitude data, namely +0·7, +0·2 and −0·7. They were chosen to cover most of the load excursions counted (to reduce the amount of extrapolation), but not to include the extremes which cover relatively very few excursions.

3. MATERIAL AND SPECIMENS

3.1 Regions Modelled

Two regions of the forged parts of the frame were chosen for the purpose of calibrating crack growth models and these are illustrated in Fig. 2. Figure 2(*a*) shows the flange area around hole 18 from which cracks have grown during full-scale testing. The metal is nominally 5 mm thick at this hole, although the thickness measured on some frames has been as low as about 3 mm. Figure 2(*b*) shows the bottom of the forged frame near the aircraft centreline where the bulk of the material is 20 mm thick and the outer flange is 8 mm thick. Various stress analyses[5] have indicated this region of the frame to be that most highly stressed.

The thickness and bolting arrangements in these two regions are considered to be sufficiently representative of most other regions in the forgings and for the purpose of calibrating crack growth models.

3.2 Material

The material specified for the frame 26 forgings is the French A-U4SG aluminium alloy (equivalent to the US 2014 and the British L104 specifications). A 55 mm thick rolled plate to the current specification of this alloy, A7-U4SG-T651, was available and used for the testing

program. It is equivalent to the US alloy 2214. The tensile and fracture properties of this plate are given in Table 4. Figure 3 shows the locations of fatigue specimens within the thickness of the plate.

3.3 Specimens

3.3.1 Standard Crack Growth Specimens

Because of the need to apply compressive forces in obtaining some of the crack growth data, a centre-cracked-tension (*CCT*) configuration was adopted, Fig. 4. This design conforms to the ASTM standard, E647-81 for obtaining constant-load-amplitude fatigue crack growth rates. Two thicknesses were used, 5 mm and 20 mm, appropriate to the generic regions of the frame noted above.

3.3.2 Simulation Specimens

The flange area around hole 18 is simulated by a 5 mm thick plate having a central hole with a 5 mm diameter interference-fit screw, as illustrated in Fig. 5 (denoted hole-18 simulation specimen). The plate thickness, hole finish, hole-to-edge distance, screw type and torque all conform to the practice for hole 18.

The bottom-of-the-frame area is simulated by the configuration shown in Fig. 6. The specimen (denoted frame-bottom simulation specimen) has retained the essential dimensions of the frame but the geometry has been modified to a symmetrical cross-section to avoid bending strains during test.

4. TEST TECHNIQUES

The constant-load-amplitude tests were made according to the definitions and requirements of ASTM E647-81. (The one exception to recommended practice was that testing was stopped overnight with the load sustained at the mean load of the cycle. No transient effects on subsequent growth rate were observed.) A single electrohydraulic fatigue machine of dynamic capacity 330 kN was used for all tests except those of the frame-bottom simulation specimens, for which a 600 kN machine was used. For most tests on 5 mm thick specimens the loading accuracy was increased by fitting a 44 kN load cell to the machine. Figure 7 illustrates the test arrangements.

To conserve testing time two values of cyclic load were used during the course of most constant-amplitude tests. After precracking, the loading was set to give growth rates in the region of 4×10^{-9} m/cycle. After sufficient readings were taken to locate the $da/dN - \Delta K$ curve around this growth rate the maximum and minimum loads were increased by 40–50% and kept constant until failure.

For *CCT* specimens the crack lengths were measured manually during the test. A grid with 1 mm spacings between lines was applied using photoresist and a contact printing technique. The grid lines were used as references and crack lengths between the lines were measured using X40 microscopes with scaled graticules. Measurements were recorded to the nearest 0·02 mm. Crack lengths were measured on both faces for the 20 mm thick *CCT* specimens, but only on one face for the 5 mm thick specimens.

The cyclic frequency for all constant-load-amplitude tests was 15 Hz and a sinusoidal wave form was used. Constant velocity and acceleration rates were used for the sequence tests and the values set to produce the same average cyclic frequency with a sinusoidal-like waveform.

A standard controller was used for load control in the constant-load-amplitude tests. A PDP 11/20 computer with magnetic tape storage was used in the sequence tests to control

both waveform and turning-point value. A chart recorder fed from a peak detector gave a continuous record of load and allowed checks on the sequence as desired.

5. CRACK GROWTH DATA

5.1 General

5.1.1 Crack Length Measurements

Mostly, one specimen per condition was tested. With *CCT* specimens the manually-measured crack growth data were supplemented, where necessary, with fractographically-derived data. The supplementary data were required in two cases.

(i) A computer malfunction part-way through the F+W sequence test of a 5 mm thick *CCT* specimen (GZ1AJ1) resulted in no crack length readings being made after $2a = 30{\cdot}90$ mm. Scanning electron and optical microscopies enabled the remainder of the fatigue crack growth to be tracked (Fig. 18 shows the results).

(ii) Corrections to measured crack lengths were required when excessive crack front curvature was observed. All specimens were examined for this curvature and when it was large enough in any part of the fracture to result in a greater than 5% difference in calculated stress intensity (the ASTM criterion for correction), corrections to average recorded crack lengths were made as follows. The differences between recorded crack lengths (surface measurements) and average through-thickness crack lengths (using a 5-point measurement method) were determined. These differences were plotted against the surface-measured crack lengths and a best-fit straight line was used to make corrections to all recorded crack lengths for that specimen. Figure 8 shows an example of curvature and a correction line adopted.

Crack lengths in component simulation specimens were obtained entirely from fractographic analysis. Macrophotographs of the fatigue fractures in these specimens are shown in Fig. 9. The hole-18 simulation specimen, Fig. 9(*a*), failed through the central screw hole with major fatigue cracking commencing at several points down the bore of the hole and at the plate surface (screw head face) on one side of the hole approximately 3 mm from the hole edge. The latter origin appeared associated with one of a number of longitudinal scratches made on the 5 mm thick plate to assist in crack growth measurement.

The frame-bottom simulation specimens failed through an end pair of Huck fasteners (see Fig. 7(*b*)) although fatigue cracking was mostly around one fastener of the pair. In the early stages of fracture the fatigue crack can be classed as embedded. In the frame-bottom specimen tested under the F+W sequence, Fig. 9(*b*), crack growth was measured from the bore of the hole to the outer edge of the specimen in the 8 mm thick section. Crack growth rates on the opposite side of the hole were roughly similar. Cracking in the frame-bottom specimen tested under the RAAF 'all-time-average' sequence, Fig. 9(*c*), occurred in three regions. The major region, and that used to determine growth rates, was from the bore of the hole in the 8 mm thick section to the 20 mm thick interior of the specimen. Fretting induced cracking due to side plate rubbing occurred near the outer corner of the 8 mm thick section in the mid-plane section of the hole, and in the opposite 8 mm thick section at a plane coinciding with the end of the side plate.

5.1.2 Analytical Techniques

5.1.2.1 Crack Growth Rate Data

Two methods of obtaining $da/dN - \Delta K$ data from the recorded constant-amplitude crack growth data (crack length *v.* number of cycles) were investigated. One was to use cubic splines

to curve-fit the raw data and then differentiate to obtain growth rates. It was necessary to experiment with the placing of knots in this method to achieve a best-fit curve: Fig. 10 shows one such data set and fitted curve. Although first and second derivatives at a simple knot are continuous, rapid curvature changes may occur from one side of the knot to the other and unacceptable $da/dN-\Delta K$ plots follow. The other method was to use the seven-point incremental polynomial technique as given in ASTM E647-81: this was found to be satisfactory and was adopted for all the analyses.

5.1.2.2 Load Ratio (R) Effects

Cycle-by-cycle computer models of crack growth require estimations of crack growth rates over a range of R-values. Two methods of coping with this variable were utilized. One method was to define an effective ΔK in such a way that it correlates all the experimental R information available. This was achieved by using an equation due to Schijve,[6] namely,

$$\Delta K_{\text{eff}} = \Delta K[0{\cdot}55+0{\cdot}35R+0{\cdot}1R^2] \tag{3}$$

This equation is based on the concept of crack closure, where the stress to open (and close) the crack is a function of the maximum stress and R-value. A comparison of Figs 12 and 13 shows that the equation above satisfactorily accounts for the R variable.

The other method (contained in the CRACKS IV[7] crack growth prediction program) makes simple interpolations and extrapolations using a linear ΔK scale and a logarithmic da/dN scale. The data are stored in arrays of crack growth rate and ΔK for the various R-values. Negative R-values are treated as zero (except for the crack closure retardation model—Section 6.3.4) and R-extrapolations are not made. Determination of growth rates outside the ΔK data limits, for particular R-values within the stored arrays, occurs by straight-line extrapolation (on log/linear scales) of the first or last two data points.

5.1.2.3 Threshold Stress Intensities

Threshold ΔK values, defined as those which give a growth rate of 10^{-11} m/cycle, were estimated for the constant-amplitude test results on 20 mm thick material by combining the location of the present $da/dN-\Delta K$ curves with the threshold ΔK data given in ESDU 81031.[8] The values arrived at were;

R	ΔK_{th} (MPa m$^{\frac{1}{2}}$)
+0·7	0·70
+0·2	1·63
−0·7	2·21

The threshold value of ΔK_{eff} was calculated to be 0·80 MPa m$^{\frac{1}{2}}$ by using the values above with the Schijve equation (Section 5.1.2.2) and taking an average.

5.2 Test Results

Table 5 lists the various specimen numbers and test conditions used in the present investigation. Figures 11 and 12 show the crack growth rate data* derived from test results for 5 mm and 20 mm thick *CCT* specimens respectively. Only one repeat of any test condition was made during the present test series—a 5 mm thick *CCT* specimen tested at $R = +0{\cdot}2$. The results

* Following standard practice, $\Delta K = K_{\max}$ for $R \leqslant 0$.

are given in Fig. 14 which shows that scatter in crack growth rates is less than a factor of two; a usual result. Figures 15–17 show that material thickness (5 mm–20 mm) has no substantial effect on crack growth rate, considering normal scatter.

The crack growth results using the F + W sequence are given in Figs 18 and 19 for the *CCT* specimens and in Fig. 20 for the simulation specimens.

6. CRACK GROWTH MODELLING

6.1 Crack Growth Model

The deficiencies of the Paris model of crack growth, as noted earlier, have been overcome to some extent by formulations which more closely resemble the shape of the crack growth rate curves and account for the mean stress effect (see, for example, References 9 and 10). Another possibility is to use experimental growth rate data instead of relying upon a particular-form equation. This approach was adopted for the present work and it was foreshadowed in Section 5.1.2.2 which described the analytical techniques used to cope with the load ratio effect on crack growth rate.

6.2 Crack Length Summations

The computing technique used calculates the crack growth increment arising from the current stress cycle and adds it to the length of the crack calculated up until that cycle, i.e.,

$$a_n = a_o + \sum_{i=1}^{n} f(\Delta K_i) \tag{4}$$

For any load history, such as the F + W sequence, the increments of crack growth are calculated for the stress cycles in the order in which they are applied to the specimens. The definition of a cycle in a variable-amplitude stress history and the use of discriminator levels on stress for efficient computer use may affect calculated crack lengths, but these aspects will be examined later when describing the results.

The following computer programs were utilized.

(i) An ARL program which incorporates the Wheeler model of retardation (described shortly) and which utilizes the Schijve definition of ΔK_{eff} (Section 5.1.2.2) and a cubic spline curve-fit to the crack growth rate data (see, for example, Fig. 13).

(ii) CRACKS IV[7] generated by Engle of the U.S. Air Force Flight Dynamics Laboratory. This program contains many options for the basic model, the retardation model, stress intensity factors and input formats.

6.3 Retardation

The sequence of load application is known to affect the rate of subsequent crack growth, the severest effect being a retardation after the application of one or a small number of high positive loads. Computations of crack growth ignoring retardation usually result in ultra-conservative predictions and this had led to models which modify the basic premise of equation (1).

Four retardation models have been examined, all options of CRACKS IV, and brief descriptions follow.

6.3.1 Wheeler Model

Wheeler[11] introduced a retardation parameter, C_p, bounded by zero and unity, which is calculated for each cycle and represents the state of strain at the crack tip during that cycle. It is used as a multiplying factor on the calculated increment of crack growth.

Specifically,

$$\Delta a = C_p f(\Delta K) \tag{5}$$

and

$$C_p = \left(\frac{R_y}{a_p - a}\right)^m ; \left(a + R_y < a_p\right) \tag{6}$$

where

R_y is the size of the current yield zone from the current crack length, a,

a_p is the distance, from zero, to the longest elastic/plastic interface caused by prior cycling,

m is a shaping exponent to be determined experimentally.

Descriptively, the amount of retardation is related to the extent to which the current-load yield zone penetrates the yield zone resulting from a prior high load. Wheeler found experimentally that the shaping exponent, m, was material dependent, having a value of 1·3 for a steel and a value of 3·4 for a titanium alloy.

6.3.2 Willenborg Model

Willenborg *et al.*[12] have operated directly on the crack growth driving function ΔK by computing an effective $\Delta K(\Delta K_{eff})$ from an assumed state of residual stress. Using the notation,

a_c = current crack length

a_p = maximum extent of plastic zone due to prior stressing,

the applied stress, σ_{ap}, necessary for the current yield zone to just reach the extent of the prior plastic zone is claculated by

$$\sigma_{ap} = \frac{\sigma_{yield}}{C\sqrt{\dfrac{2(a_p - a_c)}{a_c}}} \tag{7}$$

where C is a constant.

A stress reduction, σ_{red}, is then defined as

$$\sigma_{red} = \sigma_{ap} - \sigma_{max} \tag{8}$$

where σ_{max} is the maximum stress of the current cycle.

Note that for an overload $\sigma_{1(max)}$, followed by a cycle with a lower maximum stress $\sigma_{2(max)}$,

$$\sigma_{red} = \sigma_{1(max)} - \sigma_{2(max)} \tag{9}$$

However, for subsequent cycles of magnitude σ_2, σ_{red} will gradually decrease as the crack length increases.

The final step in this model is to reduce the maximum and minimum stresses of the current cycle by the amount σ_{red}, giving:

$$\sigma_{max(eff)} = \sigma_{max} - \sigma_{red} \tag{10}$$

$$\sigma_{min(eff)} = \sigma_{min} - \sigma_{red} \tag{11}$$

When an effective stress is less than zero it is set equal to zero. Crack growth is computed using these effective stresses with any desired crack growth model. Note that Willenborg *et al.* predict cessation of crack growth with an overload ratio ($\sigma_{1(\max)}/\sigma_{2(\max)}$) of two or more.

Retardation arises in two ways with this model.

(i) A reduction in R (when both effective stresses are positive).

(ii) A reduction in ΔK (and probably also in R) when one or both of the effective stresses is set equal to zero.

6.3.3 Modified Willenborg Model

Gallagher and Hughes[13] have noted that the overload ratio producing crack arrest (sometimes referred to as the shut-off ratio) is material dependent and is not the constant value of two as predicted by the Willenborg model. In addition, it is observed that there exists a threshold value of stress intensity for crack growth (K_{th}) which should be taken into account.

Their modification to the Willenborg model was simply to alter the σ_{red} calculated above by a proportionality factor ϕ, such that (using K rather than σ notation)

$$K_{red} = \phi K_{red} \text{ (due to Willenborg)} \tag{12}$$

where ϕ accounts for the shut-off ratio, S, and K_{th}. From Willenborg above,

$$K_{eff} = K_2 - K_{red} \tag{13}$$

and

$$K_{red} = K_1 - K_2 \tag{14}$$

before crack growth commences after the overload. Introducing the proportionality factor, ϕ, and noting that at crack arrest, i.e. when $K_1/K_2 = S$, $K_{eff} = K_{th}$ it follows that

$$\phi = \frac{(1 - K_{th}/K_2)}{S - 1} \tag{15}$$

It is claimed[13,14] that with a knowledge of S and K_{th} good predictions of crack growth in overload-affected zones are made.

6.3.4 Crack Closure Model

Eiber[17] has shown that in a cracked specimen subject to tension-tension loading the crack closed, upon unloading, at a positive value of load (due to plasticity effects behind the crack tip). Assuming that crack extension occurs only as the crack is opened, an effective stress for crack growth is defined.

$$\Delta\sigma_{eff} = \sigma_{max} - \sigma_c \tag{16}$$

where σ_c is the closure stress (requiring measurement).

Defining a closure factor, C_f, as

$$C_f = \frac{\sigma_c}{\sigma_{max}} \tag{17}$$

the equation above becomes

$$\Delta\sigma_{eff} = \sigma_{max}(1 - C_f) \tag{18}$$

Bell *et al.*[15,16] have formulated a crack growth model based on this concept of crack closure coupled with data from a variety of tests they conducted on 2219-T851 aluminium alloy and Ti-6Al-4V which investigated a number of important features such as multiple overloads and

growth rate transients. Unlike the previous models it allows both acceleration and retardation to be evaluated and it accepts negative stresses. Specifically they determined the influence on the closure stress, or the closure factor, of the stress ratio, the overload stress, and the number of overloads. The stress ratio effect is modelled by the equation

$$C_f = C_{f_{-1}} + (C_{f_0} - C_{f_{-1}})(1+R)^p \tag{19}$$

where

C_f is the closure factor at any R

$C_{f_{-1}}$ is the closure factor at $R = -1$

C_{f_0} is the closure factor at $R = 0$.

Note that from equations (18) and (19) the stress range at some R-value can be translated to a stress range at any other R-value on the basis that the effective stress is independent of R. Thus,

$$\Delta\sigma_{R2} = \Delta\sigma_{R1}\frac{(1-R2)(1-C_{f_{R1}})}{(1-R1)(1-C_{f_{R2}})} \tag{20}$$

(CRACKS IV requires that all stress ranges be translated to $R = 0$).

Bell *et al.* used crack growth data from overload tests to determine values of the closure factors and, because of the range of stress ratios covered by equation (19) negative stresses can be accounted for in crack growth prediction (unlike the Willenborg model which treats all negative stresses as zero).

Retardation due to an overload cycle is modelled by;

$$\sigma_c = \sigma_{c1} - \left(\sigma_{c1} - \sigma_{c2}\right)\left(\frac{\Delta_a}{R_y}\right)^b; \quad 0 \leqslant \Delta a \leqslant R_y \tag{21}$$

where

$\sigma_{c1,2}$ are the stabilized closure levels associated with the overstress σ_1 and the lower stress σ_2 respectively,

R_y is the overload plastic radius,

a is the crack growth increment subsequent to the overstress.

Equation (21) allows for the fact that the constant-amplitude closure stress is not established immediately after one or more cycles of overstress but takes until the crack reaches the limit of the overstress plastic zone.

Multiple overloads produce more retardation than a single overload, up to a limiting number, and this effect is modelled by assuming that the closure stress associated with the overload stress level is a function of the number of overload cycles. The equation used is;

$$\gamma = \gamma_1 + \left(1-\gamma_1\right)\left(\frac{N_{o1}-1}{N_{sat}-1}\right) \tag{22}$$

where

γ is the ratio of the closure stress after N_{o1} overloads to the stabilized closure stress (after N_{sat} overloads),

γ_1 is the value of γ for $N_{o1} = 1$.

The crack closure model thus requires as additional input the values of six parameters;

C_{f_0} closure factor at $R = 0$.

$C_{f_{-1}}$ closure factor at $R = -1$.

p exponent for determining the closure factor at any R.

b exponent for determining the decay in closure stress with cycles subsequent to an overload.

γ_1 the effectiveness of one overload in establishing the steady state closure stress of multiple overloads.

N_{sat} the number of overload cycles to achieve saturation in the closure stress.

7. CALIBRATION OF CRACK GROWTH MODELS USING RESULTS FROM CCT SPECIMENS TESTED UNDER THE F+W SEQUENCE

7.1 Wheeler Retardation Model

7.1.1 Calibration

Calibration of the Wheeler exponent, m, was achieved by comparing the experimental crack growth curve with the curves predicted using various m-values. In comparing these curves most emphasis was placed on the goodness of match over the whole of the data, and a minor emphasis was given to the prediction of the number of programs to failure. Little weight was attached to how well the final crack length was predicted since that can depend on the values chosen for K_c and initial crack length. The weighting was dictated by the subsequent use of the calibrated models—to determine inspection intervals and accurately predict small crack lengths.

Figure 21 gives the calibration results for the 5 mm thick specimen and an m-value of 1·1 is seen to be optimum. Figures 22 and 23 give the calibrations for the 20 mm thick specimens and indicate that optimum m-values are;

Stress (MPa)/g	m-value
17·98	1·50
13·33	0·75

It is evident that the m-value is not a material constant, as was initially envisaged by Wheeler,[11] and one solution to this problem is to cover a sufficiently wide range of stress/g values by test, so that a more-accurate m-value may be chosen for prediction. This approach has been used in the damage tolerance assessment of the F-4 aircraft[18] and Fig. 24 reproduces that data base. These data are for 7075-T651 aluminium alloy and are the most appropriate available for the present work. f_{max} is the maximum value of the gross-area stress in the sequence and Q is a crack shape factor (Q 1 for a through-thickness crack).

Two points are noted from Fig. 24. The calibration m-values given above lie within the scatter of the F-4 data, although towards the upper bound. Secondly, the scatter in m-values is quite large and indicates that the Wheeler model is unlikely to yield consistently accurate predictions. This is not to say that the model is useless, for there is a need to compare the scatter in predicted crack growth lives, using data such as those in Fig. 24, with uncertainties in other aspects of the prediction process. For example how well known is the time history of the stresses, and their magnitude, how accurate is the base growth rate data, and how good is the modelling of those data?

The Wheeler model calibrations above used CRACKS IV (Figs 21–23) and for the 20 mm thick specimens equivalent calibrations were made using the ARL program with the following results;

Stress (MPa)/g	*m*-value
17·98	1·1
13·33	0·5

The following sections now describe some of the decisions made in order to predict crack growth, and they also compare the ARL and CRACKS IV programs.

7.1.2 Stress State

Plastic zone sizes were calculated assuming a state of plane stress for the 5 mm thick *CCT* specimens and a state of plane strain for the 20 mm thick *CCT* specimens. From the fracture toughness and yield stress values in Table 4 a thickness greater than about 12 mm is calculated to be in plane strain and a thickness less than 1 mm is in plane stress. It is evident that the 5 mm thick specimens are in an intermediate stress state.

In section 8 where crack growths in simulation specimens are examined, a plane stress state is assumed, the critical-section thicknesses being 5 mm and 8 mm for the hole-18 and frame-bottom simulation specimens respectively.

7.1.3 Crack Shape

Crack growth predictions for all *CCT* specimens assumed a through crack. For simulation specimens (considered in Section 8) an embedded crack shape was assumed having a depth-to-length ratio of 0·33. Predictions assuming that the embedded crack grows into a through-thickness one were shown to be practically identical to those assuming an embedded configuration throughout the growth.

Predictions in this report have a clear advantage in that they are made only for specimens whose crack shapes are known by test (see Fig. 9). The effect of assuming other shapes is examined in Section 8.

7.1.4 K_c Value

The ARL crack growth program uses an equation for the basic growth rate data, $da/dN - \Delta K_{eff}$, based on cubic splines, and it is necessary to determine a K_c in order to cope with ΔK values above the limits of the data. It is also necessary to define a K_c fracture criterion for both computer programs. Rather than use K_{Ic} the approach taken was to determine a K_c value such that the final crack length was exactly predicted (using an optimum Wheeler *m*-value) for one specimen test result, and to then apply this value to all predictions. For the test results from the 20 mm thick *CCT* specimen GZ1AE1 a K_c value of 48·6 MPa m$^{\frac{1}{2}}$ (using an *m*-value of 1·1) gave the desired result. This value transforms to $\Delta K_{c(eff)}$ (Schijve) = 26·7 MPa m$^{\frac{1}{2}}$, based on the assumption that the load excursion producing fracture commences at zero load.

7.1.5 Load Sequence Truncations

To minimize computer time two truncations were investigated.

(i) For a sequence of turning points denoted 1, 2, 3, etc., assume that the turning point excursions 1–2, 3–4, etc. represent the full cycles 1–2–3, 3–4–5, etc. This practically halves computer time and was adopted for all predictions of crack growth. It was shown to give a nearly identical prediction to that using the complete set of half-cycle excursions 1–2, 2–3, 3–4, etc.

(ii) Editing of the load sequence to remove 'small' loads was investigated with two methods.

(a) Turning point pairs were deleted when their load range was below a specified value. 0·5 g was found to be the maximum truncation value which resulted in essentially the same prediction as the untruncated sequence, and this value was used with the ARL program.

(b) Turning point maxima were ignored when their magnitudes were below a specified value and, when such instances occurred, the turning point minima retained were the smallest ones occurring between the successive turning point maxima retained. Fig. 25 shows the effect of delimiter choice on crack growth prediction using the modified Willenborg retardation model (a similar result applies when using the Wheeler retardation model) and indicates that a value of 1·5 g is acceptable for reducing computer time without impairing the prediction. This value was used for all predictions made with CRACKS IV and its use reduced computer time by a factor of 2·5.

7.1.6 da/dN–ΔK Data Representations

Section 5.1.2.2 noted the use by CRACKS IV of experimental data tabulations, and by the ARL program of an effective ΔK (by Schijve) for the growth rate data. Also noted was the CRACKS IV extrapolation technique of fitting a straight line through the last two data points (log linear scales). Extrapolation with the Schijve ΔK_{eff} approach was made by fitting a curve with an arbitrary upper limit at $K_{c(eff)}$ and 1 metre/cycle.

These data representations were compared by making a specific crack growth prediction using CRACKS IV. For this purpose the Schijve ΔK_{eff} curve was inverted to a family of $da/dN - \Delta K$ curves, as shown in Fig. 26, which were then digitized. Fig. 27 shows that there is a sizeable difference (about 20% in life) between the crack growth predictions based upon these two schemes of representing the same data.

This difference could result from either the extrapolation technique, or the representation of the experimental data region, or both. Output from CRACKS IV had been arranged to show the percentage numbers of the cycles and the crack increments which use ΔK values outside the limits of the data. The percentages below are applicable to the prediction shown in Fig. 27 using experimentally-obtained $da/dN - \Delta K$ data. Type 1 extrapolation is from the lower growth rate end of the data to the threshold level: type 2 extrapolation is at the upper end and limited by K_c.

Stress g (MPa g)	Wheeler exponent (m)	Percent of crack length and cycles derived from extrapolation of growth rate data			
		Type 1		Type 2	
		crack length	cycles	crack length	cycles
13·33	0·5	0·2	16	54	2
17·98	1·1	zero	3·3	82	12

When the percentage crack length is very small, the percentage cycles, although sizeable—e.g. 16%, will be of little consequence because the number of flights, as distinct from cycles, predicted for a given crack length will be practically unaffected by the extrapolation. The results above allow the following inferences.

(i) The combination of data extrapolation and method of representation gives a 20% variation in predicted crack life as shown in Fig. 27, and extrapolation alone effects no more than 12% of the cycles. Thus, at least about half, and probably most, of the difference between the crack growth predictions shown in Fig. 27 arises from the different representations of the data over the range of ΔK values used in the experiments. (Simply because the percentage crack length or cycles predicted from extrapolated data points is sizeable for any one crack growth curve it does not follow that differences between two predicted curves result from the extrapolation technique).

(ii) The extrapolation technique used for the lower growth rate region of the $da/dN-\Delta K$ curve is immaterial, in fact practically the same growth curve would have been predicted if no extrapolation at all had been used. A corollary to this is that the experimental crack growth data could have been obtained commencing with a somewhat higher growth rate.

(iii) The method of extrapolating $da/dN-\Delta K$ experimental data in the high growth rate region has a greater potential for affecting growth predictions than extrapolations in the low growth rate region. Any extrapolation effect will become larger as the predicted crack length increases and, for this reason, predictions must be regarded as becoming less certain as fracture becomes more likely. If the aim of the predictions is to establish inspection intervals the foregoing should not present a great problem.

7.1.7 Comparison of ARL and CRACKS IV Programs

It was shown above (Section 7.1.1) that the ARL and CRACKS IV programs gave somewhat different m-calibrations for the same experimental crack growth data. The different $da/dN-\Delta K$ representations required for the two programs certainly contribute to this difference (see previous section) and it is possible, though thought not to be so, that other features of the programs contribute. The matter was resolved by using the inverted Schijve ΔK_{eff} constant-amplitude crack growth data (Fig. 26) with CRACKS IV and comparing the crack growth predicted with that obtained using the ARL program (requiring the Schijve ΔK_{eff} data curve as mentioned earlier).

Two cases were examined, using the F+W sequence and Wheeler retardation: $m = 1{\cdot}1$, stress = 17·98 MPa/g; and $m = 0{\cdot}5$, stress 13·33 MPa/g (the CRACKS IV prediction for the former case is shown in Fig. 27). As anticipated, in both cases the predictions were practically identical.

7.2 Modified Willenborg Model

The modified Willenborg model of retardation, like the Wheeler model, has one parameter available for calibration. In this case it is the shut-off ratio, S, originally envisaged[13,14] as being a material constant. Figures 28 and 29 compare predicted crack growth curves with those obtained experimentally for the two 20 mm thick *CCT* specimens tested under different stress/g conditions.

It is clear that the main problem encountered in calibrating the Wheeler model also exists with the modified Willenborg model, namely that the appropriate value of the disposable parameter is dependent on stress level. At a stress/g value of 17·98 MPa, a shut-off ratio of about 2·2 seems appropriate, whereas at a stress of 13·33 MPa a ratio of approximately 3·0 is appropriate. This problem could be treated similarly to that with the Wheeler model calibration

but this would require a considerable amount of test information (typified by that in Fig. 24) which is currently unavailable. It is therefore concluded that there is no advantage of the modified Willenborg model of retardation over the Wheeler model.

7.3 Crack Closure Model

The crack closure model of retardation requires six parameters to be specified (Section 6.3.4) and few data exist to guide in the selection of values. Three of the parameters model the stress ratio effect on crack growth rate (equation (19)), and used in conjunction with equation (18) they allow the determination of an effective stress range. (Thus far the model is similar in approach to the Schijve effective stress—section 5.1.2.2).

Eidinoff and Bell[19] have tabulated values of the parameters for some aluminium and titanium alloys: the alloys most relevant to the present investigation are 2219-T851, 2024-T851 and 2024-T3. Values for these materials are;

	C_{f_0}	$C_{f_{-1}}$	p	b	γ_1	N_{sat}
2219-T851	0·400	0·347	3·93	1·0	0·667	13·0
2024-T851	0·400	0·347	3·93	1·0	0·667	200·0
2024-T3	0·500	0·450	3·42	1·0	0·667	13·0

The first three columns permit translation of all ΔK values to those at $R = 0$ (equation (20)). Using the values for the T851 temper, the experimental constant-amplitude crack growth data for the 20 mm thick *CCT* specimens (Fig. 12) were replotted and are shown in Fig. 30. It is apparent that the parameter values chosen did not adequately correlate the *R*-effect. However, the values for 2024-T3 were then used and they provided a much better correlation—Fig. 31. (Because the data points in Fig. 31 overlap, and CRACKS IV requires a monotonic tabulation of constant-amplitude data, it was necessary to resort to fitting a curve from which monotonic values could be determined. The curve-fitting technique used was that described earlier (Section 6.2) when presenting the Schijve ΔK_{eff} data, and the result is given in Fig. 32).

The values of the parameters for 2024-T3 listed above were used to predict crack growth in the 20 mm thick *CCT* specimens tested under the F+W sequence and the results are shown in Fig. 33. Prediction of the 13·33 MPa/g crack growth is excellent (perhaps fortuitously so, considering likely scatter) and is within a factor of about two for the growth under the 17·98 MPa/g stress. Given that another set of parameter values make a better prediction of the higher-stress crack growth it is most unlikely that they will be as good as the 2024-T3 set in predicting the lower-stress crack growth. For this reason, and because the optimising of parameter values requires extensive testing outside the scope of the present work, calibration of the crack closure model was not attempted.

8. CRACK GROWTH PREDICTIONS

It is of interest to examine how satisfactory are the calibrations of the previous section for predicting crack growth in situations a little different from those used for calibration. Two main variations were examined, a change in geometry using simulation specimens, and a change in sequence using the RAAF 'all-time-average'.

The crack growth predictions described in this section were made with CRACKS IV and used the experimental $da/dN-\Delta K$ data in tabulated form. The stress states and crack shapes used in the predictions were noted in sections 7.1.2 and 7.1.3.

8.1 F-W Sequence, Simulation Specimens, Wheeler Retardation

Crack growth in the frame-bottom simulation specimen was predicted using a Wheeler exponent of 2·7 taken from the F-4 curve shown in Fig. 24. The prediction is compared with the experimental result in Fig. 34 and seen to be rather conservative. An m-value of 4·2, obtained by linear extrapolation from the two calibration values obtained with the 20 mm thick *CCT* specimens, was selected, as also was a value of 4·5, and the results are also displayed in Fig. 34. The m-value of 4·2 gives about the best overall prediction of the experimental result, but it is clear that no m-value will give an excellent prediction over the whole range of the experimental data.

The influence of the choice of crack shape on predicted crack growth was examined for this specimen. The results, shown in Fig. 35, illustrate a dramatic influence. (References 20 to 22 give the respective K-calibrations).

No prediction was made specifically for the hole-18 simulation specimen. It is evident from Fig. 20, which compares the experimentally-obtained crack growth in the frame-bottom and hole-18 simulation specimens tested under practically the same stresses, that most crack growth models would have difficulty in predicting both results. The predictions shown in Fig. 34 for the frame-bottom simulation specimen will apply without much change to the hole-18 specimen. The smaller bolt in the hole-18 specimen (5 mm dia. compared with 6 mm dia. in the frame-bottom specimen) means a slightly lower stress intensity and therefore slightly longer predicted life. But this cannot explain the eight-times longer life of the hole-18 specimen.

Crack growth in the hole-18 specimen is even more difficult to reconcile with that in the frame-bottom specimen when the crack that initiated at the plate surface is considered (Fig. 9(*a*)). It might be anticipated that this crack, by decreasing the net-section area, would, if anything, increase the growth rate of the cracks emanating from the bore of the hole.

8.2 RAAF 'All-Time-Average' Sequence

Crack growth in the 20 mm thick *CCT* specimen tested at a stress of 14·12 MPa/g was predicted by considering firstly, no retardation, and then some retardation using the four models described in section 6.3. Figure 36 compares experimental and predicted crack growths.

The Wheeler exponent (m = 0·97) was a linear interpolation of the calibration m-values determined in Section 7 (see Fig. 24), also based on *CCT* specimens. The m-value based on the F-4 curve, Fig. 24, is zero and hence gives the 'no-retardation' prediction. The modified Willenborg shut-off ratio S = 2·75 is also a linear interpolation of the Section 7 calibrations, and the crack closure retardation used the six parameter values for 2024-T3 given in Section 7.3.

The Willenborg and crack closure retardation models are highly non-conservative and obviously unsatisfactory. Quite reasonable predictions are made with the Wheeler and modified Willenborg models when a linear dependence of the retardation parameter on stress is assumed. The no-retardation assumption gives a prediction of crack growth that is not less than 0·63 of the experimental result.

Experimentally-obtained crack growth in the frame-bottom simulation specimen (from the area shown in Fig. 9(*c*)(ii) and described in Section 5.1.1) is shown in Fig. 37. Commencing at program number 112 (with corresponding crack length of 0·837 mm) there is a sudden increase in growth rate which coincides with the complete fracture of the outboard 8 mm thick section—see Fig. 9(*c*)(i). Though the shape of the crack growth curve is unusual an attempt was made to predict its behaviour using the two retardation models which seemed most promising from the *CCT* results above—the Wheeler and modified Willenborg models. The values of the Wheeler exponent (m = 2·4) and the modified Willenborg shut-off ratio (S = 1·24) were determined by linear extrapolation of the calibration values determined in Section 7.

The experimental crack growth data covered crack lengths ranging from 0·230 mm to 18·630 mm at which stage fracture occurred. At crack lengths of 0·230 mm and 0·837 mm the crack was embedded: at some larger dimension it became a through-crack and remained so until fracture. These features can be seen in Fig. 9(*c*)(ii).

Crack growth prediction using modified Willenborg, an asymmetric embedded crack, and an initial crack length of 0·230 mm is shown in Fig. 37. It is clearly non-conservative, even over the crack length range of 0·230 mm to 0·837 mm: in fact very little crack growth at all was predicted.

Similar conditions were used with Wheeler retardation in the hope of more-adequately predicting growth behaviour over the crack distance 0·230 mm to 0·837 mm. The prediction was conservative but still rather poor as shown in Fig. 37. An attempt was made to predict the higher growth rate portion of the data, also with the Wheeler model, by using the facts that at a crack length of 0·837 mm (from the bore of the hole) the 8 mm thick ligament fractured and the growth rate suddenly increased by a factor of 14. The inset in Fig. 37 illustrates the crack geometry at a crack length greater than 0·837 mm. Stress intensity for this configuration was modelled using the form;

$$K = C\sigma(L+a)^{\frac{1}{2}} \tag{23}$$

That is, for $a > 0{\cdot}837$ mm the length L is added to the expression. The value of the constant, C, is determined from the fact that there is a sudden 14-times increase in growth rate at $a = 0{\cdot}837$ mm; thus, assuming a fourth power Paris law of crack growth,

$$C_2 = 14^{\frac{1}{4}}\, C_1 \left(\frac{a}{L+a}\right)^{\frac{1}{2}} \tag{24}$$

where C_1, C_2 are the constants for growth at crack lengths less than (where $L = 0$) and greater than 0·837 mm respectively.

It was also assumed that from an a/t ratio of 0·5 (a = crack length, t = thickness) the value of C_2 changed linearly with crack length until a through-crack ($a/t = 1{\cdot}0$) configuration was reached. The value of C_2 from above was 1·33 and was applied up until $a/t = 0{\cdot}5$, and the final through-crack value was $\sqrt{\pi}$. As it eventuated this refinement had little effect on the prediction of crack growth.

Crack growth predicted on the bases above it shown in Fig. 37 commencing at program 112 and crack length 0·837 mm. Its gross inadequacy arises partly from an inappropriate determination of the Wheeler exponent and partly from the simplified characterization of stress intensity.

9. DISCUSSION

9.1 General

To summarize briefly, the Wheeler and modified Willenborg models of retardation, when calibrated, enable satisfactory predictions of crack growth in specimens having the same geometry (*CCT*) as those used for calibration (Fig. 36). The Willenborg and crack closure retardation models, and crack growth prediction without retardation, are unsatisfactory. Admittedly, a reasonable prediction may have followed if the crack closure model was properly calibrated, but there is a question of value-for-effort.

The success of the retardation models for crack growth prediction in more complex geometries is mixed. None of the models were satisfactory when the sequence was different from that of the calibration (Fig. 37), whereas the Wheeler model was satisfactory for the frame-bottom simulation specimen tested under the F + W sequence used for calibration (Fig. 34). Two other experimental facts of significance are that in complex specimens crack locations and geometries

are not predictable with certainty, and that hole-18 and frame-bottom specimens tested under the same stress and sequence gave markedly different (a factor of 8) crack growth lives (Fig. 20).

The words satisfactory, poor, reasonable, non-conservative, have been used above or in previous sections to describe how well crack growth predictions have matched experimental results. Expectations of prediction accuracy seem often to depend on the use to which the predictions are put. For aircraft structures operated by damage tolerance principles quite accurate predictions of crack growth are necessary. The number of flights predicted and the number utilized in service to produce a given length of crack should, ideally, differ by not more than about 10%. Progressively larger differences will result in increasingly poorer utilization of the structure if a given safety level is to be maintained. There are several factors, now discussed, which affect the accuracy, and hence our expectation, of crack growth prediction.

9.2 Accuracy of Stress History

The stress magnitudes in the test load histories used in the present work are known precisely, at least well within the $\pm 2\%$ allowed in ASTM E647-81. In complex structures, however, local stresses may be known only to within ± 10 to 50%—the accuracy depends upon the precision of load measurement, the complexity of the geometry and the loading, the stress analysis technique, and the effort expended. Using a fourth power Paris law for crack growth the foregoing stress accuracies transpose to a range of crack length prediction of approximately ± 50 to 500%: although this is taking the extreme case of the magnitudes of all stress cycles being biased in one direction.

Likewise, in the laboratory tests on the specimens, the number of cycles at any given stress and the order in which they are applied are known precisely. This is not usually so with aircraft structures in service, the result of which is to further degrade the accuracy of prediction.

9.3 Accuracy of da/dN–ΔK Data

There are several considerations which affect the accuracy of the crack growth rate data. The first point considered is how much scatter in growth rate may be expected—which leads to a determination of the number of replications required for a given confidence in the mean. The 'variability factor' on growth rate at any ΔK is likely to be of the order of two.[23] (The variability factor is defined as the ratio of maximum to minimum growth rates assuming a log normal distribution of growth rates and a spread of ± 2 standard deviations (thus capturing about 95% of all the growth rate data)).

Only one constant-load-amplitude test was repeated in the present investigation (Section 5.2) and from Fig. 14 it can be determined that the maximum variability in growth rate is a factor of approximately $1{\cdot}5$. Additional information on variability can be obtained by considering the trends of growth rates with R-value, Figs 11 and 12. It can be seen that;

(i) the general trend of increasing growth rate with R-value is similar in both 5 mm and 20 mm thick specimens, and accords in magnitude and direction with other published data,

(ii) variations in growth rate with R-value are of the order of potential scatter—e.g. in the mid-ranges of ΔK the growth rates at $R = 0{\cdot}2$ and $0{\cdot}7$ vary from one another by a factor of $3{\cdot}3$,

(iii) the excellent correlation of the various R information with Schijve's equation, Fig. 13, implies little scatter in the originals.

It follows that the present data sets are close to population means and that the average variability factor is likely to be less than $1{\cdot}5$.

A second consideration is the effect of the data reduction process on prediction: this was addressed in Section 7.1.6 and illustrated in Fig. 27. It was concluded that different representations of the experimental data can result in sizeable differences in prediction of the number of programs to achieve a given crack length. One of these representations was the ΔK_{eff} format by Schijve, and although his representation gave predicted lives at any crack length which differed

by about 20% from those using experimental data tabulations, it is not necessarily inferior. The Schijve treatment has one major advantage, namely that experimental data at one R-value only are required. (As an aside, the crack closure model of retardation also has the potential for correlating growth rates at various R-values (see Fig. 31) but in this case at least two sets of experimental data are required).

A similar influence of the $da/dN - \Delta K$ representation on crack life prediction has been noted by Hewitt.[24] Using five different representations he back-calculated constant-amplitude crack growth for three specimens of 2219-T951 aluminium alloy from growth rate data and using CRACKS IV. The variations in predicted crack growth life were 1 : 1·15, 1 : 1·15, 1 : 1·78 for the three specimens. Hewitt also compared the predictions of crack growth life with the original test data from the three specimens. Using growth rate data which contained data from the three specimens the predictions varied by as much as 25% from the actual test life (though in one case the variation was much greater).

A third consideration is the choice of data limits and extrapolation techniques. The lower limit of experimental growth rate obtained in the constant-load-amplitude tests was approximately 10^{-9} m cycle; threshold values (at 10^{-11} m/cycle) were determined as in Section 5.1.2.3. Section 7.1.6 showed that even if no extrapolation had been used at low growth rates the predictions would have been practically the same. Obviously, as stresses decrease and predicted numbers of flights increase, lower-growth-rate extrapolations will assume some significance. It was also shown in Section 7.1.6 that extrapolations at the upper-growth-rate end of the data have the potential for affecting the prediction.

The crack growth models investigated in this report (as do all others to the authors' knowledge) require a single value of K_c as the upper limit of growth rate. It is known[25,26] however, that stress history as well as geometry affect the value and it would seem that fatigue crack growth models should include K_c as a history-dependent variable. (An alternative view could be taken that the improvements in the accuracy of prediction would be small when compared with those possible by reducing variability from other sources).

A fourth consideration is the applicability of available constant-amplitude crack growth rate data. The data shown in previous sections are entirely applicable to the variable-amplitude crack growth predictions as they were derived using specimens taken from the same plate of material. Figure 38 compares the present growth rate results on 20 mm thick specimens with three other sets of data considered to be the most relevant of those located in the literature.[27,28] Two conclusions from this comparison are:

(i) forged and plate material give about the same growth rate—a conclusion of some significance to crack growth predictions for frame 26,

(ii) the present results are similar to, though not exactly identical with, those in the literature.

Some indication of the magnitude of batch effects on crack growth is available from the work of Schijve and de Rijk.[29] They measured crack growth in 2024-T3 alclad aluminium alloy obtained from seven manufacturers, the tests being made under both constant-amplitude and program load conditions. The ratio of highest to lowest crack propagation life was about 2 : 1 for the constant-amplitude tests and 1·5 : 1 for the program load tests. A more extreme result was found by Hewitt,[24] however, in his work noted above. Calculations of crack growth life, using various $da/dN - \Delta K$ representations were compared with experimental results from three specimens. When the growth rate data were taken from sources other than that with the experimental results, the predictions of crack growth life varied from the experimental lives by as much as a factor of six.

9.4 Assumption of Crack Shape

The necessary prior choice of crack shape can markedly influence the crack growth prediction as illustrated in Fig. 35. From the initial condition adopted, a 0·356 mm, there is a 7 : 1 difference in the predictions assuming embedded and through-crack shapes.

The U.S. Military Specification on damage tolerance[30] requires a corner flaw of quarter-circular shape at a hole. Pike and Kirkby[31] have shown, however, that even if such a crack

occurs initially, subsequent growth, until it becomes a through-crack, is more likely to be quarter-elliptical. That is, cracks tend to propagate faster down the bore of a hole than along the plate surface. Pike and Kirkby made crack growth predictions with both growth shapes under a variety of conditions including no retardation, two initial crack radii, three types of structural element, two materials, two stress spectra, and various stress per g values. The ratios of the quarter-circle to quarter-ellipse predicted crack growth lives varied between about 1 and 10, with values between 2 and 3 being most common.

A substantial bias can, therefore, be introduced into crack growth predictions by assuming a crack shape which does not eventuate in practice. Although the U.S. Military Specification appears to have taken a reasonable and conservative shape the study of Pike and Kirkby shows that there is a danger of cracks actually growing much faster than predicted or of the predictions being ultra-conservative.

9.5 Correctness of Crack Growth Models

Very little can be said about the absolute correctness of the various crack growth and retardation models. Scientifically they all have some plausibility and some deficiencies. To judge them on performance is, mostly, a test of their robustness since they are used in conjunction with the many factors noted above which can influence the prediction.

The present study supports the view that a model of retardation should be used in estimating crack growth to avoid ultra-conservative predictions. Of the four retardation models considered, that by Wheeler proved the most robust. Although simple in concept its 'shaping exponent' m varies with stress per g and with crack shape, and requires calibration by test. The linear calibration line from the present tests, Fig. 24, is a little different from that obtained on F-4 and associated tests. One reason for this could be that only single component simulation tests were made under any condition; no attempt was made to establish mean growth behaviour. Another reason comes from Section 7.1.1 where it was shown that the Wheeler m-values depend on the method of treating the basic crack growth data. Using the Schijve ΔK_{eff} approach the calibration m-values from the present tests are much closer to the F-4 curve. Consistency in usage is believed to be more important in retardation modelling than attempts to establish whether absolute calibrations are possible.

The development of retardation models has required the specification of an increasing number of parameters to cope with further insights into the complicated process of crack propagation under variable-amplitude loading. The crack closure model is a good example of this. The values of such parameters are obtainable only by test, and it remains to be seen how close the generation of this information comes to replacing prediction by test.

9.6 Total Variability

The discussion has covered most factors which, individually, contribute to inaccurate crack growth prediction. The crack growth model used and the crack shape assumed both give a bias to the growth prediction, the amount of which cannot be determined without test, although data such as are in this Report can provide guidance.

The accuracy of the $da\,dN$ - ΔK data and of the stress history can be transposed into a variability in prediction which may be statistically described. The combined effect of these two sources of variability may be described, approximately, by a summation of variances. Thus, assuming that variations in growth rate ($da\,dN$) and stress are distributed log normally, the variance in programs to failure is given as:

$$\sigma^2_{(\text{programs})} = \sigma^2_{(\text{growth rate})} + m\sigma^2_{(\text{stress})} \qquad (25)$$

where m is the Paris exponent, and σ^2 (in this case) is the variance (in logarithms). Taking the

variance ratio of the growth rate data as 2 (a minimum value), and the Paris exponent as 4, the following values of combined variance were obtained for different variance ratios of stress.

Variance ratio of stress	Variance ratio of number of programs
1·1	2·05
1·2	2·19
1·5	2·91

The variability in growth rate thus dominates and only very large uncertainties in stress magnitude contribute substantially to the variability in predicted life.

10. CONCLUSIONS

1. Ultra-conservative predictions of fatigue crack growth can occur when no retardation is incorporated in a crack growth model.

2. Of the four retardation models considered—Wheeler, Willenborg, modified Willenborg and Crack Closure—the Wheeler and modified Willenborg models are the most satisfactory, with the Wheeler model possibly being the better of the two.

3. Both the Wheeler and modified Willenborg models contain one disposable parameter which is not a material constant and requires calibration by test. A deficiency of the crack closure retardation model is that it requires a number of tests to determine the values of six parameters.

4. The Wheeler model of retardation enables satisfactory predictions of crack growth in specimens having the same geometry as that used in tests for calibrating the model. When the loading sequence and the specimen geometry are different from those used in calibrating the retardation models, none of the retardation models yield accurate predictions.

5. Of the various factors which may influence the accuracy of crack growth prediction, the adequacy of the $da/dN - \Delta K$ data and how they are treated, the assumption of crack shape, and the accuracy of the stress history appear to be the most important. Using the various crack growth and retardation models considered in this Report, and treating the case of an aircraft structure, an expectation of predicting crack growth life to better than a factor of two is unwarranted. It should be anticipated that some predictions will only be within a factor of ten of actual crack growth life.

REFERENCES

1. Paris, P. C. — 'The growth of cracks due to variations in load'. Ph.D. Dissertation, Lehigh University, 1962.

2. Paris, P. C. — 'The fracture mechanics approach to fatigue'. Fatigue—An Interdisciplinary Approach (eds J. J. Burke, N. L. Reed and V. Weiss), pp. 107–132, Syracuse University Press, Syracuse, 1964.

3. Anderson, B. E. — 'Preliminary Assessment to September 1977—of the panel failure in the F+W Mirage Fatigue test'. (Restricted). ARL-STRUC-TECH-MEMO-288, January 1979.

4. Sparrow, J. G. — 'Interim report on Task AIR 82 125 "Mirage Structural Integrity Investigation Part A" '. (Restricted). ARL STRUC-TECH-MEMO-350, October 1982.

5. Hoskin, B. C., Callinan, R. J. and Jones, R. — 'Interim damage tolerance analysis of Mirage frame 26; stress distribution, critical areas and critical crack sizes'. ARL-STRUC-TECH-MEMO-356, January 1983.

6. Schijve, J. — 'The stress ratio effect on fatigue crack growth in 2024-T3 alclad and the relation to crack closure'. Technische Hogeschool Delft, *Memorandum* M-336, August 1979.

7. Engle, R. M. — 'CRACKS—a Fortran IV digital computer program for crack propagation analysis'. AFFDL-TR-70-107, October 1970.

8. ——— — 'Fatigue crack propagation rates and threshold stress intensity factor ranges for aluminium alloy plate, extruded bar and forgings'. Engineering Sciences Data Unit Item No. 81031, November 1981.

9. Forman, R. G., Kearney, V. E. and Engle, R. M. — 'Numerical analysis of crack propagation in cyclic loaded structures'. J. Basic Eng., Trans. ASME, vol. 89, 1967, pp. 459–463.

10. Walker, K. — 'The effect of stress ratio during crack propagation and fatigue for 2024-T3 and 7075-T6 aluminium'. ASTM STP 462, 1970, pp. 1–14.

11. Wheeler, O. E. — 'Spectrum loading and crack growth'. J. Basic Engrg, vol. 4, no. 1, March 1972, pp. 181–186.

12. Willenborg, J., Engle, R. M. and Wood, H. A. — 'A crack growth retardation model using an effective stress concept'. U.S. AFFDL, TM-71-1-FBR, January 1971.

13. Gallagher, J. P. and Hughes, T. F. 'Influence of yield strength on overload affected fatigue crack growth behaviour in 4340 steel'. U.S. AFFDL-TR-74-27, July 1974.

14. Gallagher, J. P. and Stalnaker, H. D. 'Predicting flight by flight fatigue crack growth rates'. J. Aircraft, vol. 12, no. 9, September 1975.

15. Bell, P. D. and Creager, M. 'Crack growth analysis for arbitrary spectrum loading'. U.S. AFFDL-TR-74-129-vol-1, October 1974.

16. Bell, P. D. and Wolfman, A. 'Mathematical modelling of crack growth interaction effects'. Fatigue crack growth under spectrum loads, ASTM STP 595, 1976, pp. 157-171.

17. Elber, W. 'The significance of fatigue crack closure'. Damage tolerance in aircraft structures, ASTM STP 486, 1971, pp. 230 242.

18. Pinckert, R. E. 'Damage tolerance assessment of F-4 aircraft'. MCAIR 76-015, September 1976.

19. Eidinoff, H. L. and Bell, P. D. 'Application of the crack closure concept to aircraft fatigue crack propagation analysis'. Proc. 9th ICAF-Symposium, 1977: LBF-Rep. No. TR-136 (1977).

20. Bowie, O. L. 'Analysis of an infinite plate containing radial cracks originating at the boundary of an internal circular hole'. J. Math. Phys., vol. 35, 1956, pp. 60-71.

21. Liu, A. F. 'Stress intensity factor for a corner flaw'. Engrg Fracture Mech., vol. 4, 1972, pp. 175-179.

22. Wood, H. A. and Engle, R. M. 'USAF damage tolerant design handbook: Guidelines for the analysis and design of damage tolerant aircraft structures. AFFDL-TR-79-3021, March 1979.

23. Clark, W. G. and Hudak, S. J. 'Variability in fatigue crack growth rate testing'. Jl. Testing & Evaluation, JTEVA, vol. 3, no. 6, November 1975, pp. 454-476.

24. Hewitt, R. L. 'Some effects of material property data selection on crack propagation analysis'. National Aero. Estab. LTR ST-1369, May 1982.

25. Clark, G. 'Significance of fatigue stress intensity in fracture toughness testing'. Int. Jl. of Fracture, vol. 15, no. 5, October 1979, pp. R179 181.

26. Roman, I. and Ono, K. 'Model for fracture toughness alteration due to cyclic loading'. Int. Jl. of Fracture, vol. 19, 1982, pp. 67 80.

27. 'Damage tolerance of aeronautical alloys'. Centre D'Essais Aeronautique De Toulouse, vol. 1.

28. 'Damage Tolerant Design Handbook'. Metals and Ceramics Information Centre, HB-01, January 1975.

29. Schijve, J. and de Rijk, P. 'The fatigue crack propagation in 2024-T3 alclad sheet materials from seven different manufacturers'. NLR-TR M.2162, May 1966.

30. ——— 'Airplane damage tolerance requirements'. Military Specification MIL-A-8344 (USAF), July 1974.

31. Pike, V. J. and Kirkby, W. T. 'Influence of assumed crack growth pattern on damage—tolerance life prediction for corner—cracks at holes'. Royal Aircraft Estab. Tech. Rep. 80017, 1980.

TABLE 1

Frequency of load occurrence in F · W 200 flight sequence

g-level*	Occurrences per program
7·5	2
6·75 to 7·25	6
6·25 to 6·75	18
5·75 to 6·25	14
5·25 to 5·75	88
4·75 to 5·25	205
4·25 to 4·75	275
3·75 to 4·25	634
3·25 to 3·75	913
2·75 to 3·25	1,364
2·25 to 2·75	1,430
1·75 to 2·25	2,319
1·25 to 1·75	4,233
0·75 to 1·25	10,060
0·25 to 0·75	15,678
−0·25 to 0·25	1,706
−0·75 to −0·25	104
−1·25 to −0·75	28
−1·75 to −1·25	14
−2·25 to −1·75	2
−2·75 to −2·25	4
−3·25 to −2·75	2
Total	39,099

* The *g*-levels indicated are proportional to the loads applied in the specimen tests; they are not necessarily an accurate representation of forces seen in the F+W test article because of the different flying load cases

TABLE 2

Frequency of load occurrence in RAAF 'all-time-average' 500 flight sequence

g-level*	Occurrences per program
7·8	1
7·25 to 7·75	0
6·75 to 7·25	2
6·25 to 6·75	106
5·75 to 6·25	139
5·25 to 5·75	361
4·75 to 5·25	871
4·25 to 4·75	1,347
3·75 to 4·25	2,448
3·25 to 3·75	3,524
2·75 to 3·25	4,874
2·25 to 2·75	5,261
1·75 to 2·25	14,679
1·25 to 1·75	28,299
0·75 to 1·25	9,151
0·25 to 0·75	33,126
−0·25 to 0·25	3,163
−0·75 to −0·25	177
−1·25 to −0·75	14
−1·75 to −1·25	1
−2·25 to −1·75	1
Total	107,545

* The g-levels are based on a unique linear relation between stress and g, and are proportional to the loads applied in the specimen tests. They are based on the relation between the highest load and g which is relevant to the case of no carriage of centreline tanks. As noted in the text however, a small fraction of the flying is with centreline tanks and this makes the above g estimations not completely accurate as a measure of the forces seen in the aircraft.

TABLE 3

R values in F · W 200-flight sequence (without ground loads)

Peak load (g)	$R \leqslant 0{\cdot}7$	$0{\cdot}7 < R \leqslant 0{\cdot}6$	$0{\cdot}6 < R \leqslant 0{\cdot}5$	$0{\cdot}5 < R \leqslant 0{\cdot}4$	$0{\cdot}4 < R \leqslant 0{\cdot}3$	$0{\cdot}3 < R \leqslant 0{\cdot}2$	$0{\cdot}2 < R \leqslant 0{\cdot}1$	$0{\cdot}1 < R \leqslant 0$
1	0	0	52	0	0	0	0	0
1·5	0	0	0	0	0	0	0	0
2	20	0	0	0	0	0	0	0
2·5	0	0	0	0	0	52	0	0
3	0	0	0	0	0	0	0	0
3·5	0	0	0	0	0	0	0	0
4	0	0	0	0	0	14	0	0
4·5	0	0	0	2	0	14	0	0
5	0	0	0	0	0	0	0	0
5·5	0	0	0	0	0	0	0	0
6	0	0	0	0	0	0	0	0
6·5	0	0	0	0	0	0	0	0
7	0	0	0	0	0	0	0	0
7·5	0	0	0	0	0	0	0	0

Continued

Table 3 (Continued)

Peak load (g)	$0 \leqslant R < 0{\cdot}1$	$0{\cdot}1 \leqslant R < 0{\cdot}2$	$0{\cdot}2 \leqslant R < 0{\cdot}3$	$0{\cdot}3 \leqslant R < 0{\cdot}4$	$0{\cdot}4 \leqslant R < 0{\cdot}5$	$0{\cdot}5 \leqslant R < 0{\cdot}6$	$0{\cdot}6 \leqslant R < 0{\cdot}7$	$0{\cdot}7 \leqslant R$
1	52	0	0	0	0	110	0	0
1·5	52	24	34	398	0	0	1099	0
2	52	0	116	0	0	948	0	241
2·5	0	0	271	0	863	102	0	0
3	0	14	0	682	0	270	0	0
3·5	156	50	400	0	62	152	0	20
4	52	10	202	231	0	95	0	0
4·5	52	4	112	20	66	117	0	0
5	0	11	110	15	104	0	0	0
5·5	58	0	52	12	5	0	0	0
6	0	18	18	0	0	14	0	0
6·5	0	12	0	0	6	0	0	0
7	0	6	0	0	0	0	0	0
7·5	0	2	0	0	0	0	0	0

TABLE 4

Tensile and fracture properties of A7-U4SG-T651 55 mm thick rolled plate (batch serial GZ)

(*a*) *Static tensile*

	Specification	*GZ*
0·1 % proof stress (MPa)	—	451
0·2 % proof stress (MPa)	390	457
Ultimate tensile strength (MPa)	450	502
Elongation (%) ($5{\cdot}65\sqrt{A}$)	5	10·7

(*b*) *Fracture toughness*

25 mm thick LT specimens

	GZ
Fracture toughness, K_{1c} (MPa m$^{\frac{1}{2}}$) (average of 8 tests)	32·0
Standard deviation (MPa m$^{\frac{1}{2}}$)	0·5

TABLE 5

Test conditions and specimen numbers

Loading condition	Specimen type	Test details				Specimen number
		Material thickness	*R*-value	Initial max. load kN	Final max. load kN	
Constant amplitude	*CCT*	5 mm	+0·7	17·33	24·32	GZ1AG3
			+0·2	8·00	11·22	GZ1AF3
			+0·2	10·06	12·07	GZ1AF2
			0·7	10·47	—	GZ1AG2
		20 mm	+0·7	95·52	143·28	GZ1AA1
			+0·2	41·72	62·58	GZ1AB1
			0·7	40·48	56·67	GZ1AC1
F + W sequence	*CCT*	5 mm	gross area stress: 15·97 MPa/g			GZ1AJ1
		20 mm	gross area stress: 17·98 MPa/g			GZ1AE1
		20 mm	gross area stress: 13·33 MPa/g			GZ1AB2
	Hole-18 simulation	5 mm	gross area stress: 44·04 MPa/g			GZ1E2A
	Frame-bottom simulation	20 mm	gross area stress: 43·80 MPa/g			GZ1E1B
RAAF 'all-time-average' sequence	*CCT*	20 mm	gross area stress: 14·12 MPa/g			GZ1AA2
	Frame-bottom simulation	20 mm	gross area stress: 28·63 MPa/g			GZ1D1B

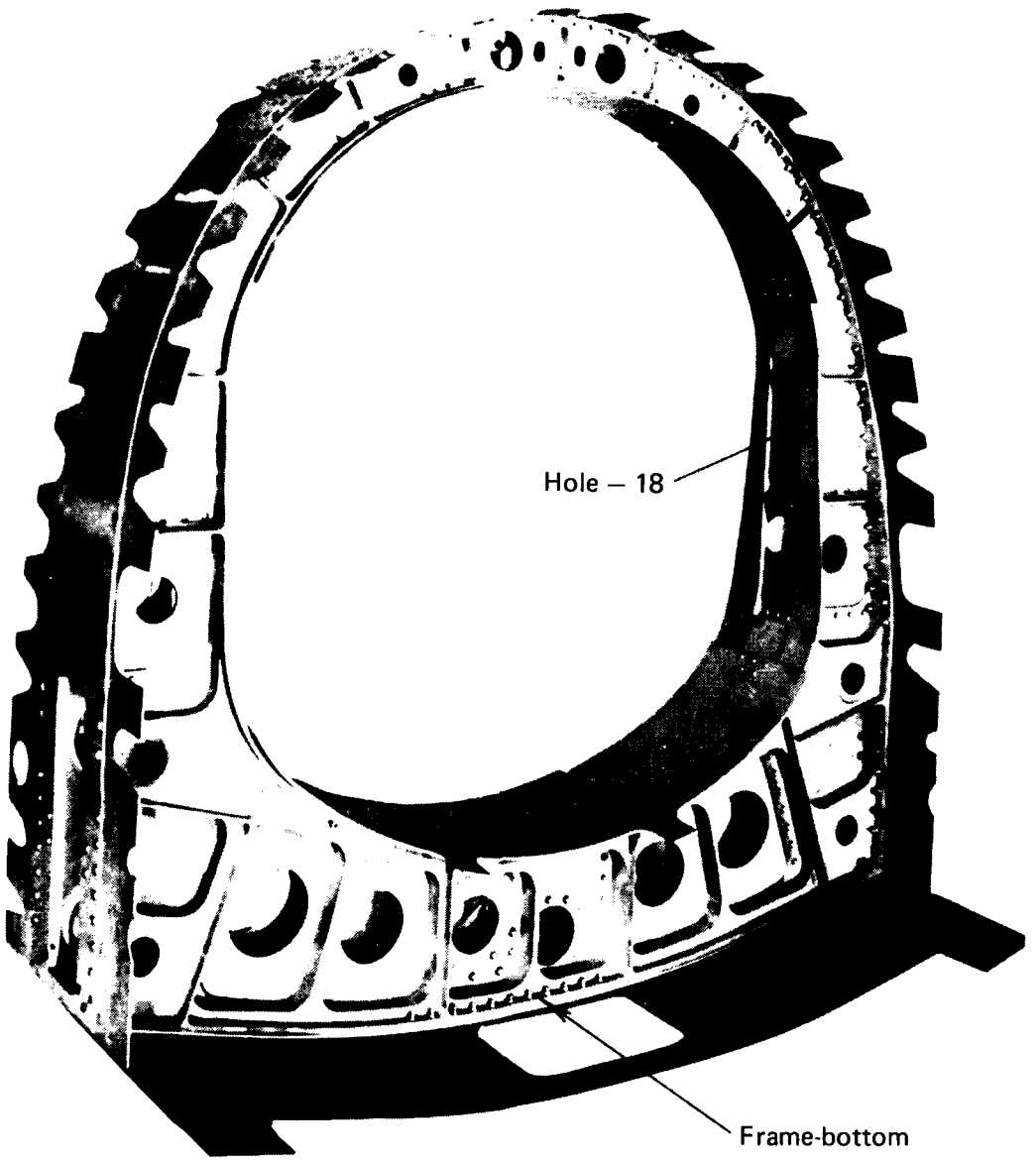

FIG. 1 FRAME 26, MIRAGE III

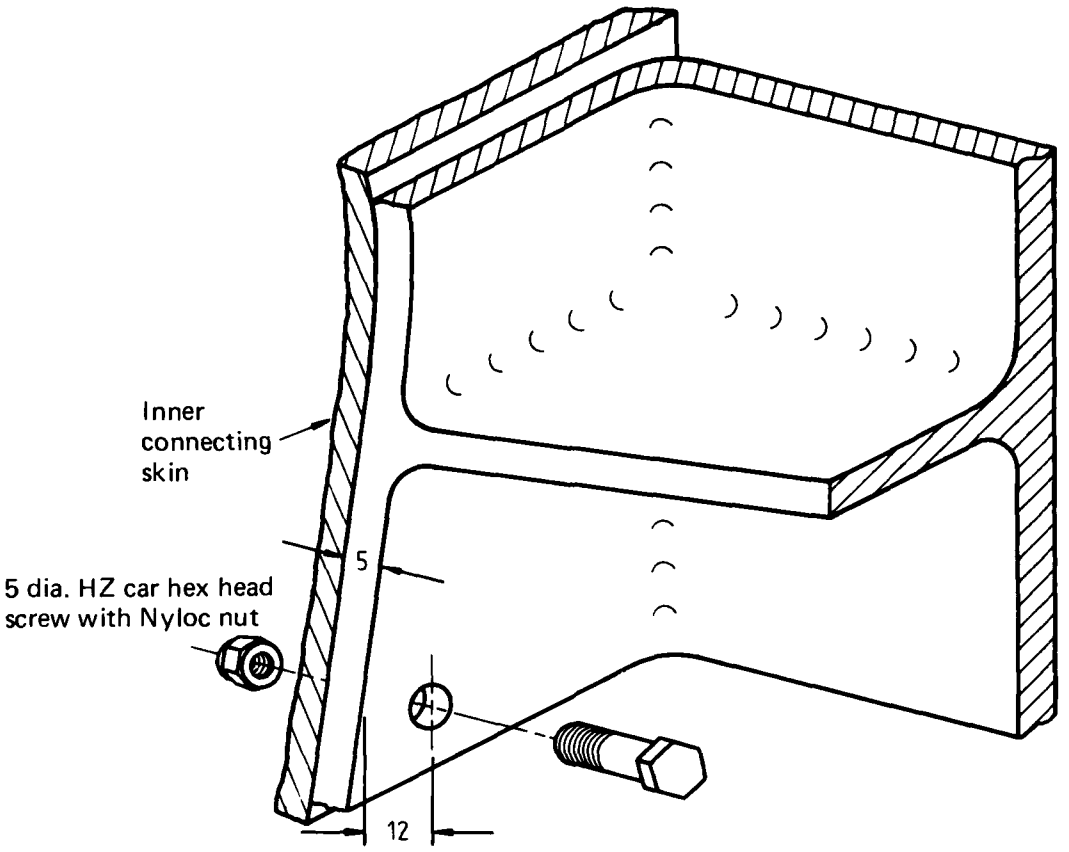

(a) Hole 18 and surrounding flange area

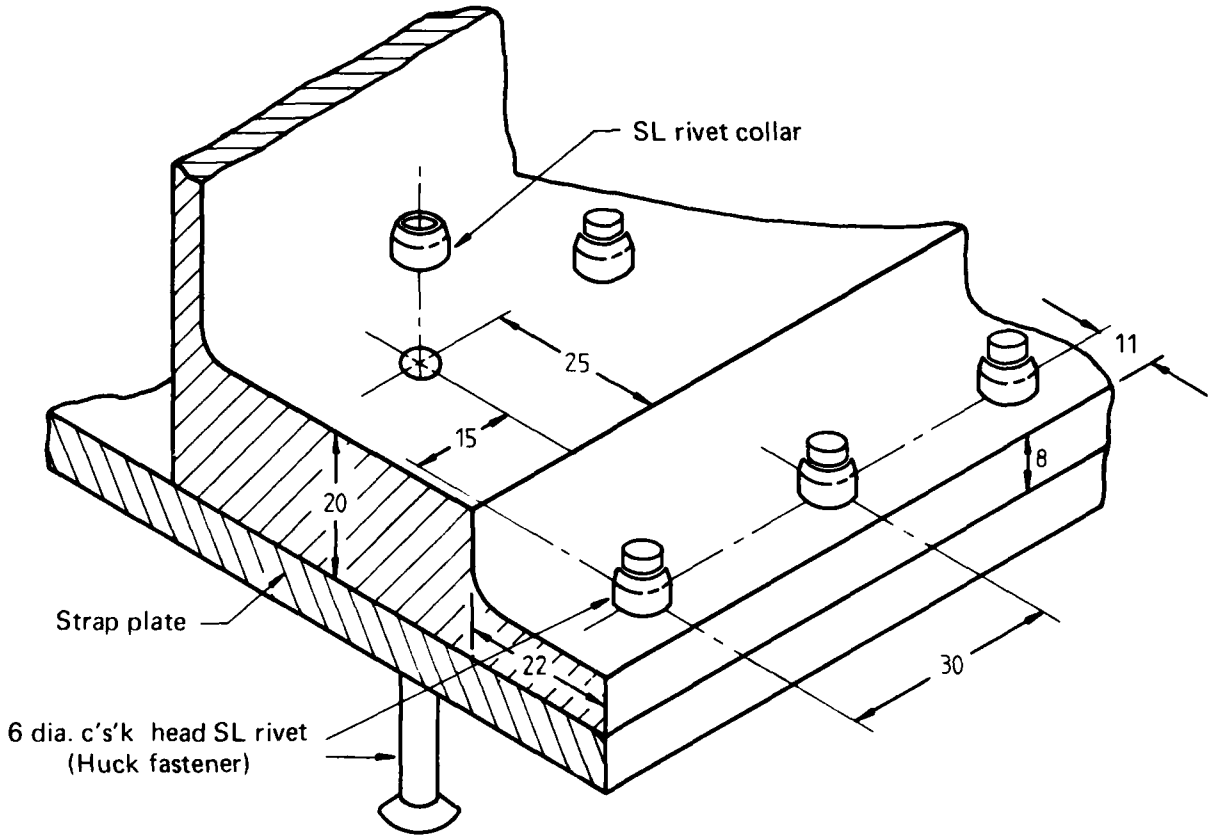

(b) Bottom part of frame near ℄

FIG. 2 REGIONS OF MIRAGE FRAME 26 MODELLED

Plate designation GZ

Hatched specimens used in tests – other spares

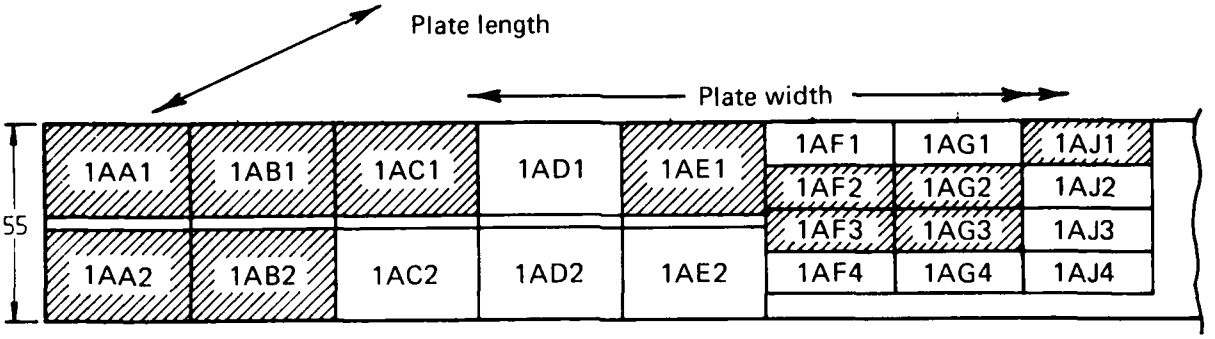

(a) Centre cracked tension specimens

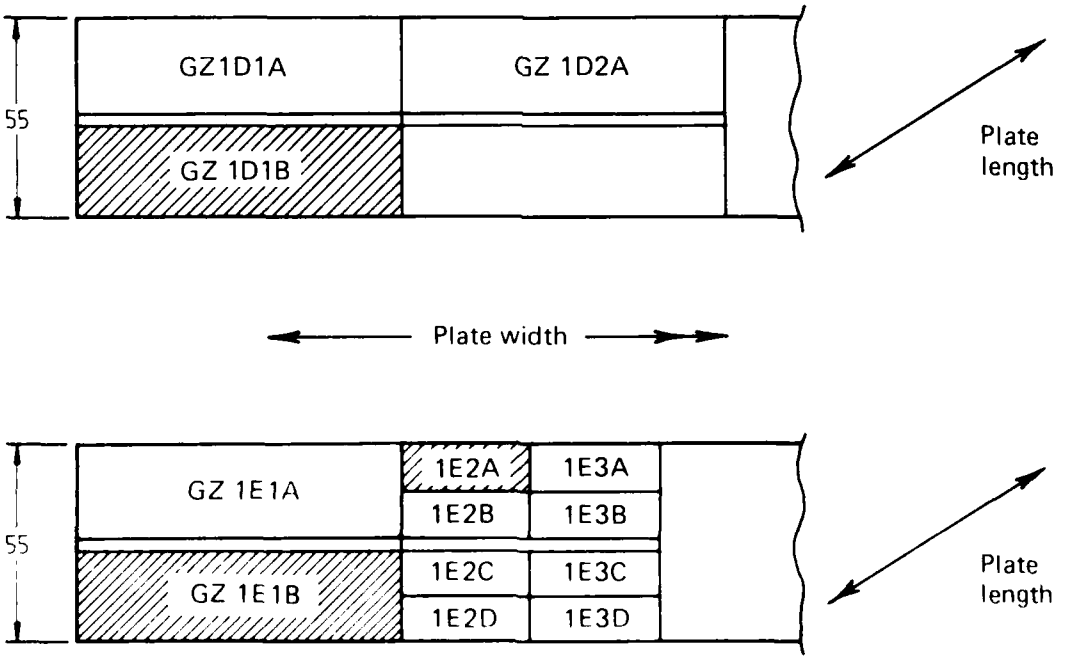

(b) Simulation specimens

FIG. 3 LOCATION OF SPECIMENS WITHIN THICKNESS OF ROLLED PLATE

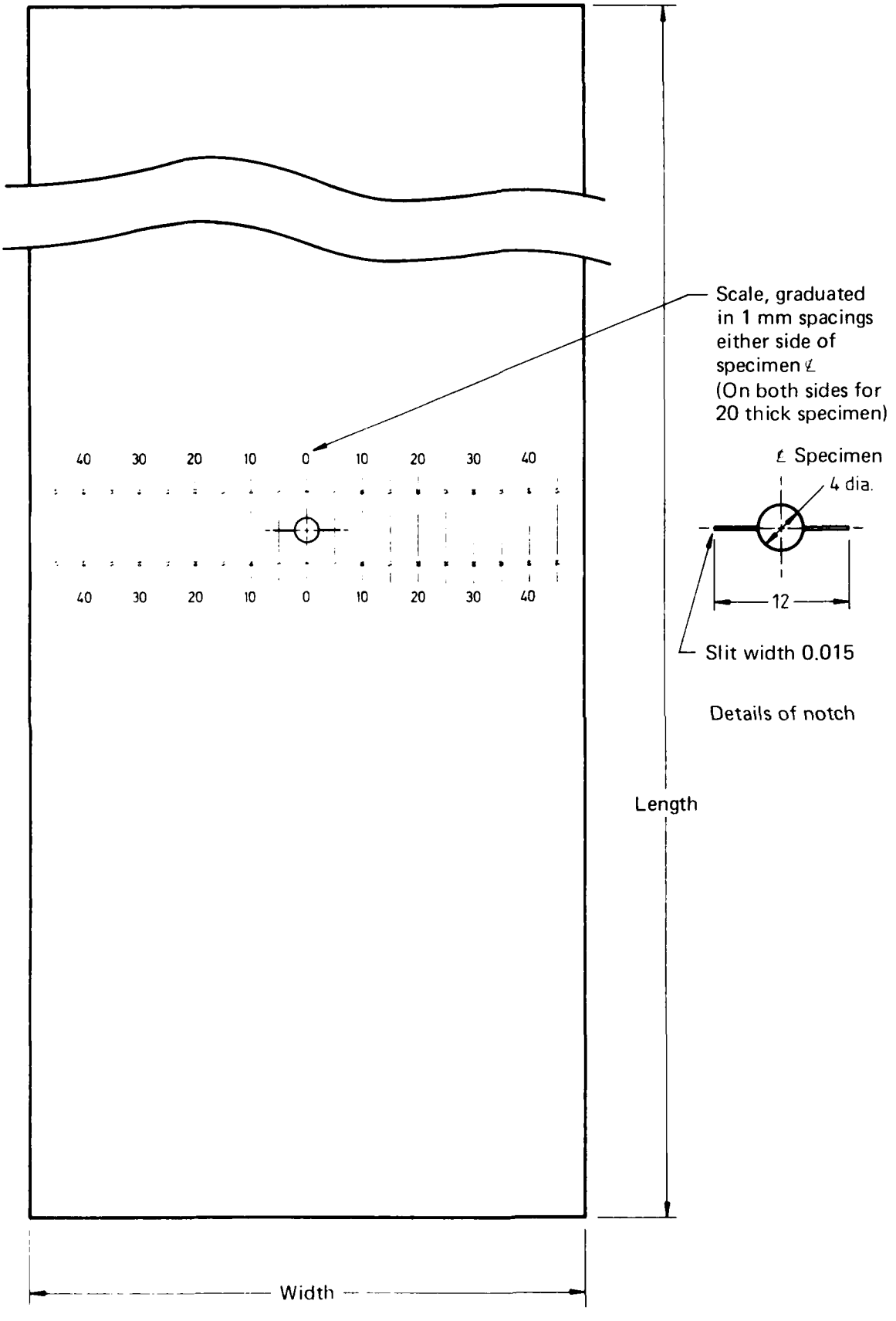

	Length	Width	Thickness
(a)	300	100	20
(b)	300	75	5

FIG. 4 CENTRE–CRACKED–TENSION SPECIMENS

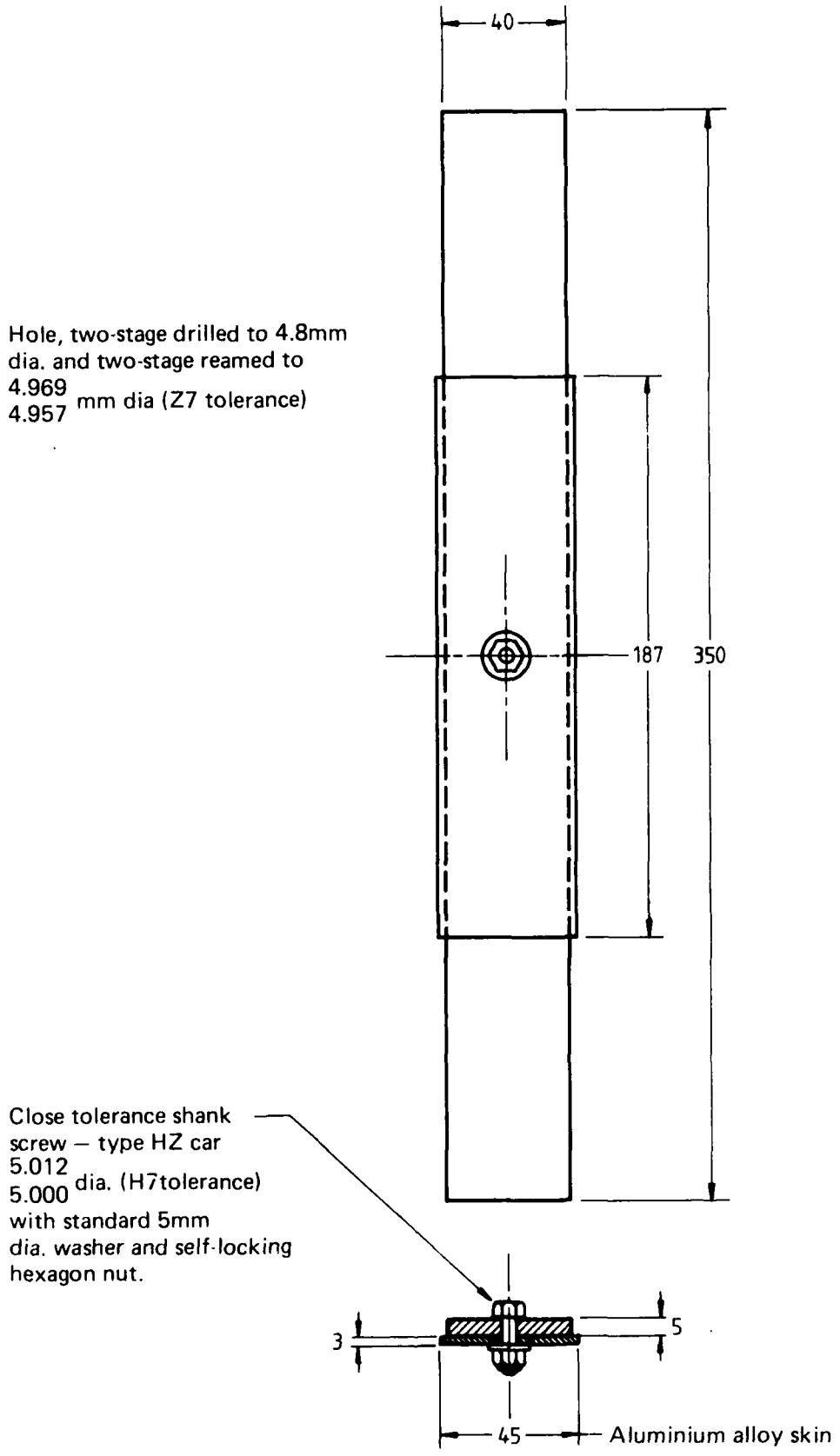

FIG. 5 SIMULATION SPECIMEN – HOLE 18

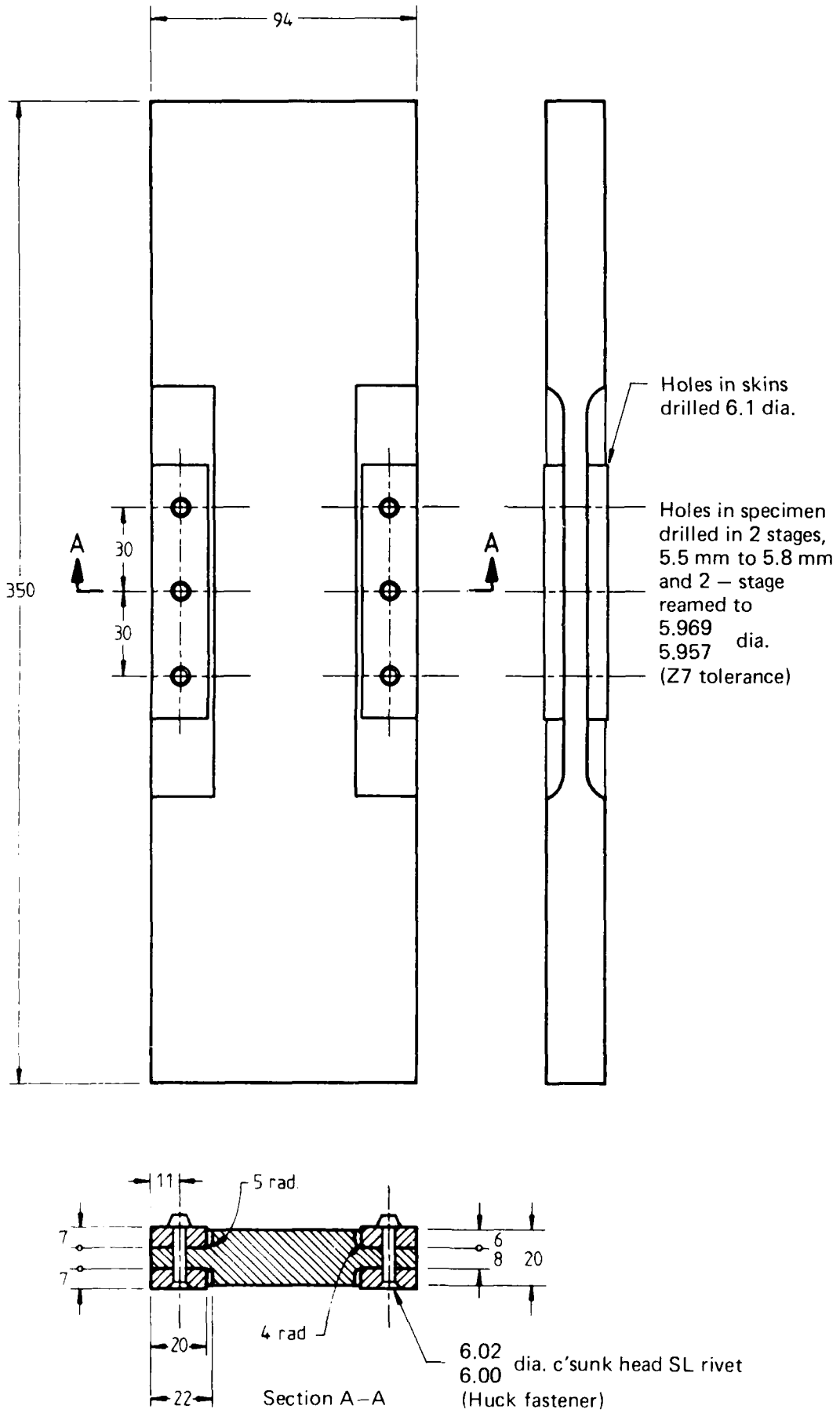

FIG. 6 SIMULATION SPECIMEN BOTTOM SECTION OF FRAME 26

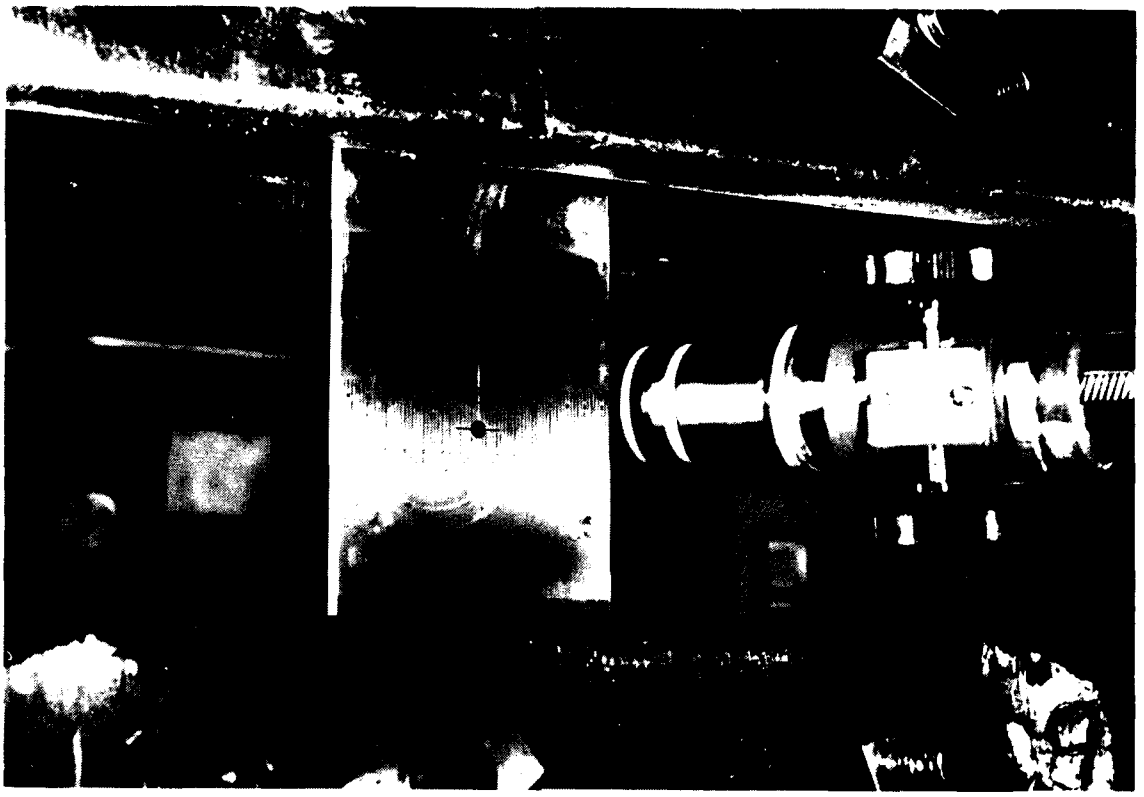

(a) CCT test

(b) Frame-bottom simulation test

FIG. 7 TEST ARRANGEMENTS

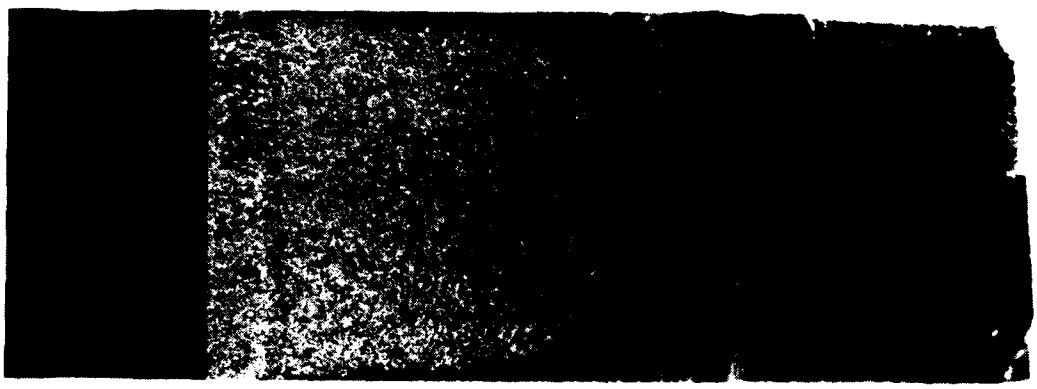

(a) Crack-front curvature

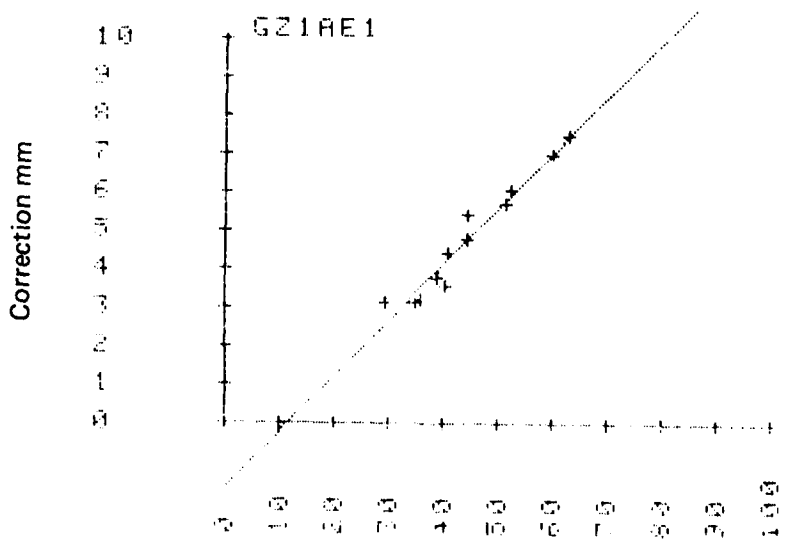

(b) Curvature correction

FIG. 8 CRACK CURVATURE CORRECTION METHOD (SPECIMEN GZ1AE1)

(i) Full cross-section x 3.

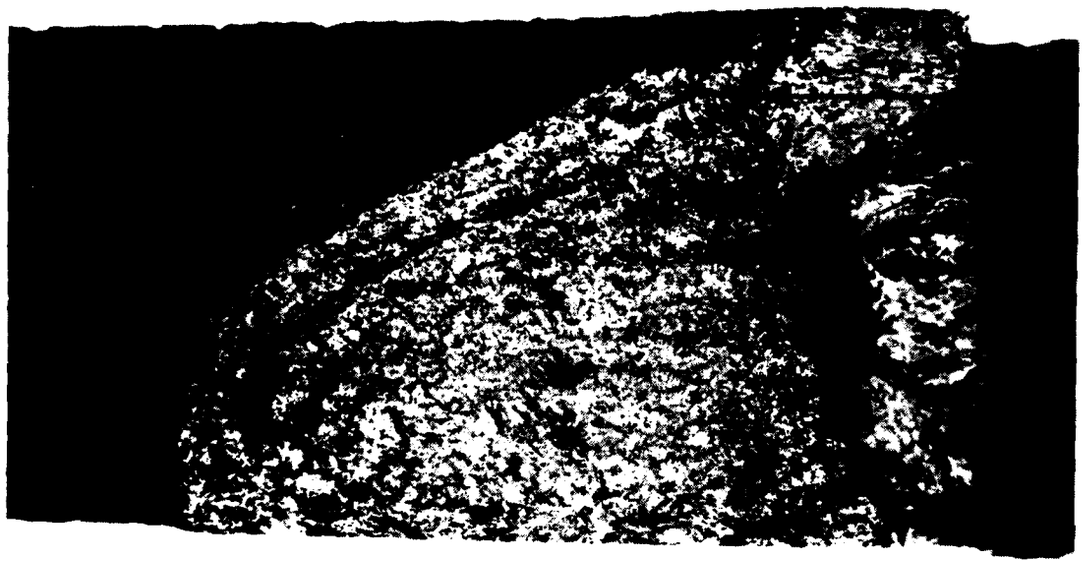

(ii) Detail of crack x 15
Crack depths measured along line indicated.

FIG. 9(a) FRACTURE OF HOLE–18 SIMULATION SPECIMEN (GZ1E2A)

(i) Full cross-section x 1.5

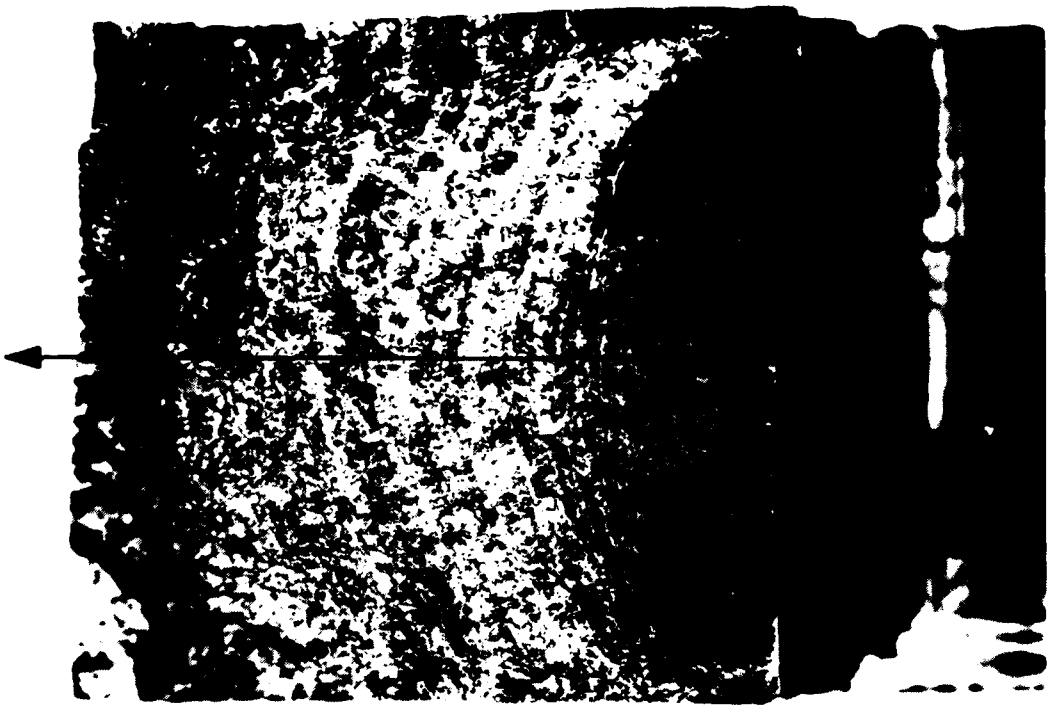

(ii) Detail of crack x 12
Crack depths measured along line indicated.

FIG. 9(b) FRACTURE OF FRAME-BOTTOM SIMULATION SPECIMEN TESTED UNDER F + W SEQUENCE (GZ1E1B)

(i) Full cross-section x 1.5

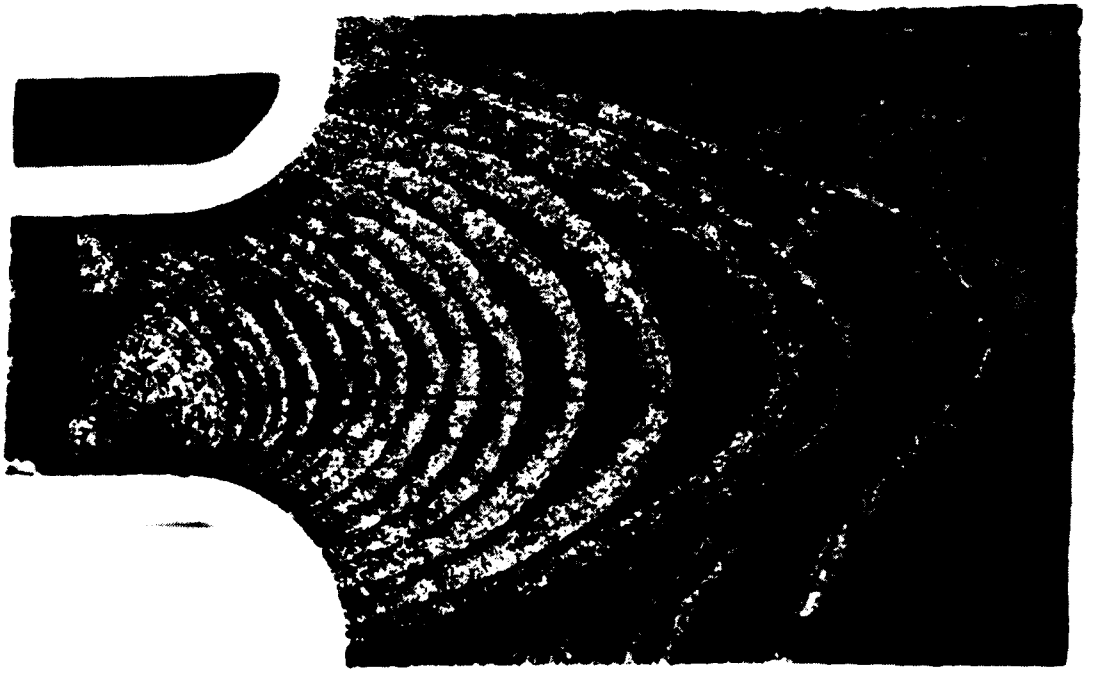

(ii) Detail of fatigue crack from Huck fastener hole. x 4.5
Crack depths measured along line indicated.

FIG. 9(c) FRACTURE OF FRAME-BOTTOM SIMULATION SPECIMEN TESTED UNDER RAAF 'ALL-TIME-AVERAGE' SEQUENCE (GZ1D1B

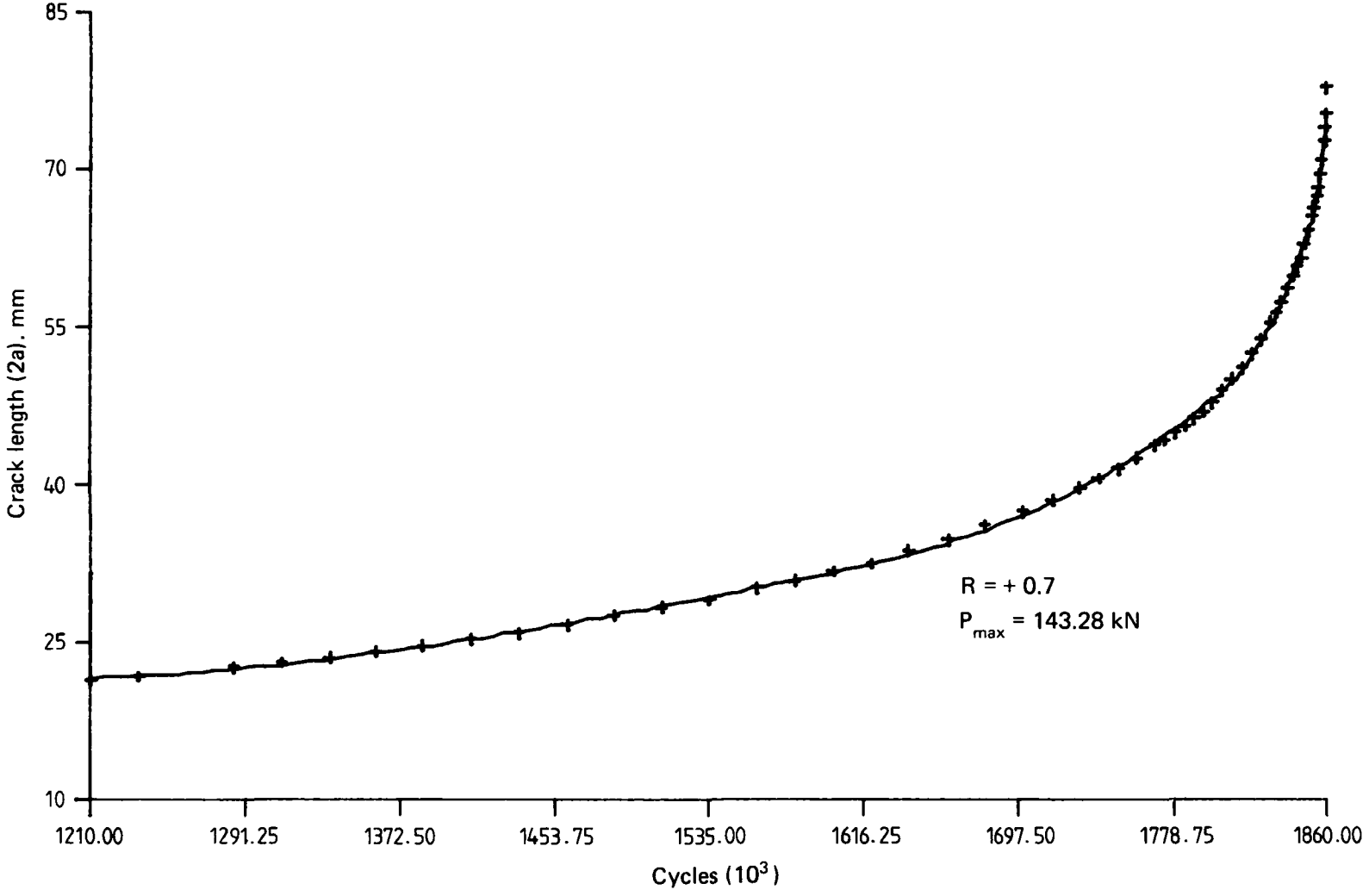

FIG. 10 CUBIC-SPLINE FIT TO CRACK GROWTH DATA. 20 mm THICK CCT SPECIMEN, CONSTANT-AMPLITUDE.

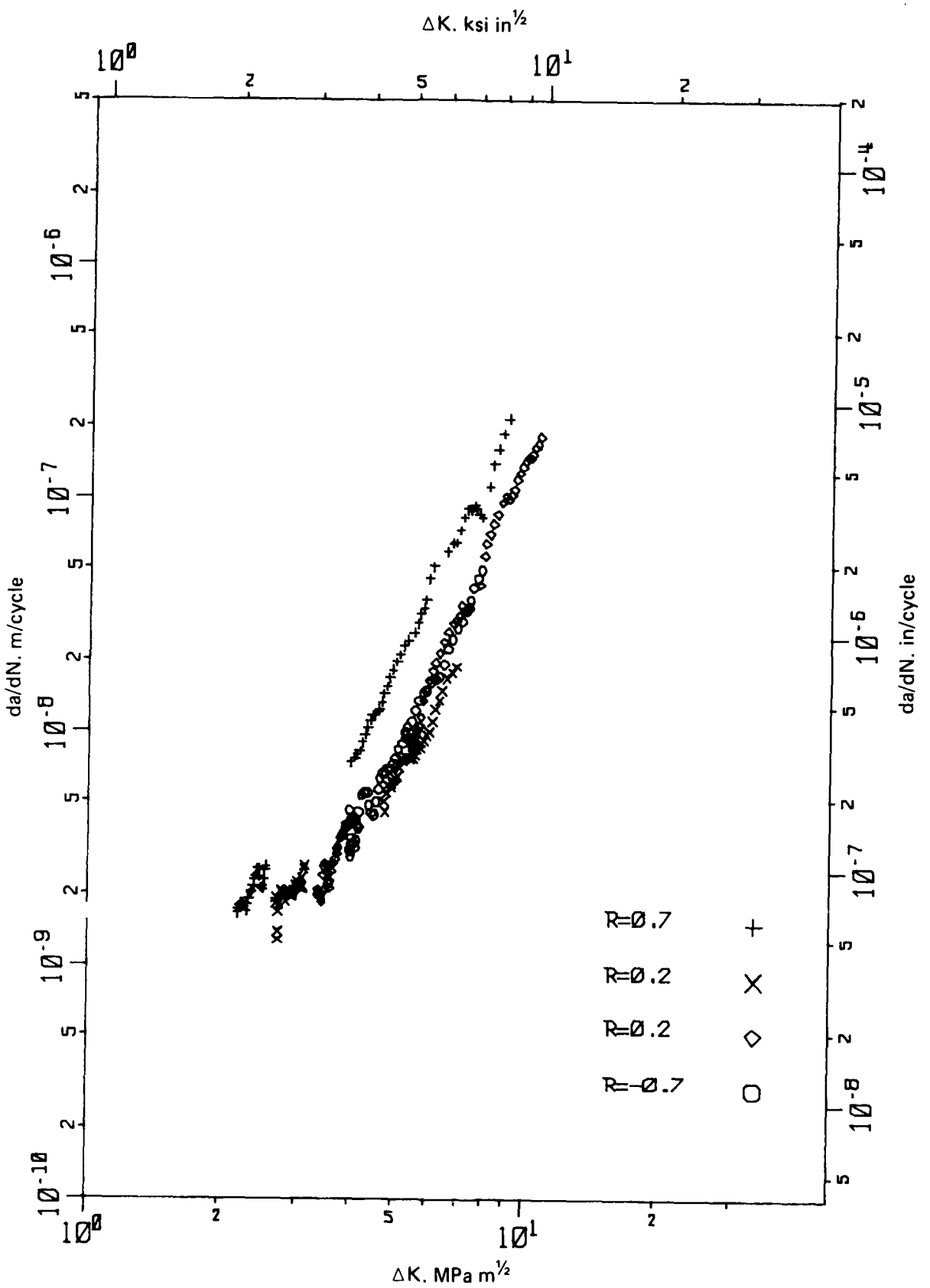

FIG. 11 da/dN – ΔK DATA FOR 5mm THICK CCT SPECIMENS.

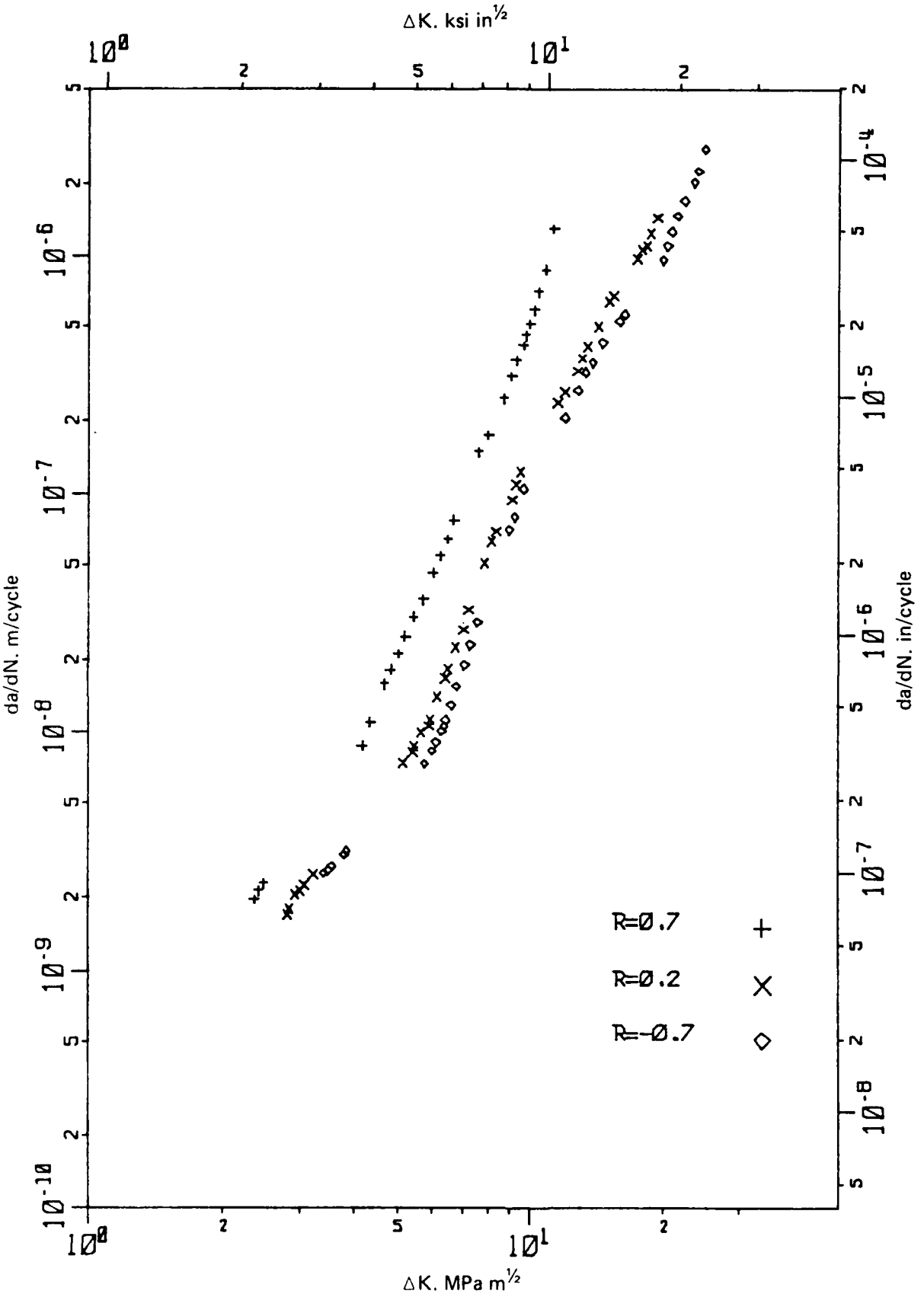

FIG. 12 da/dN – ΔK DATA FOR 20mm THICK CCT SPECIMENS.

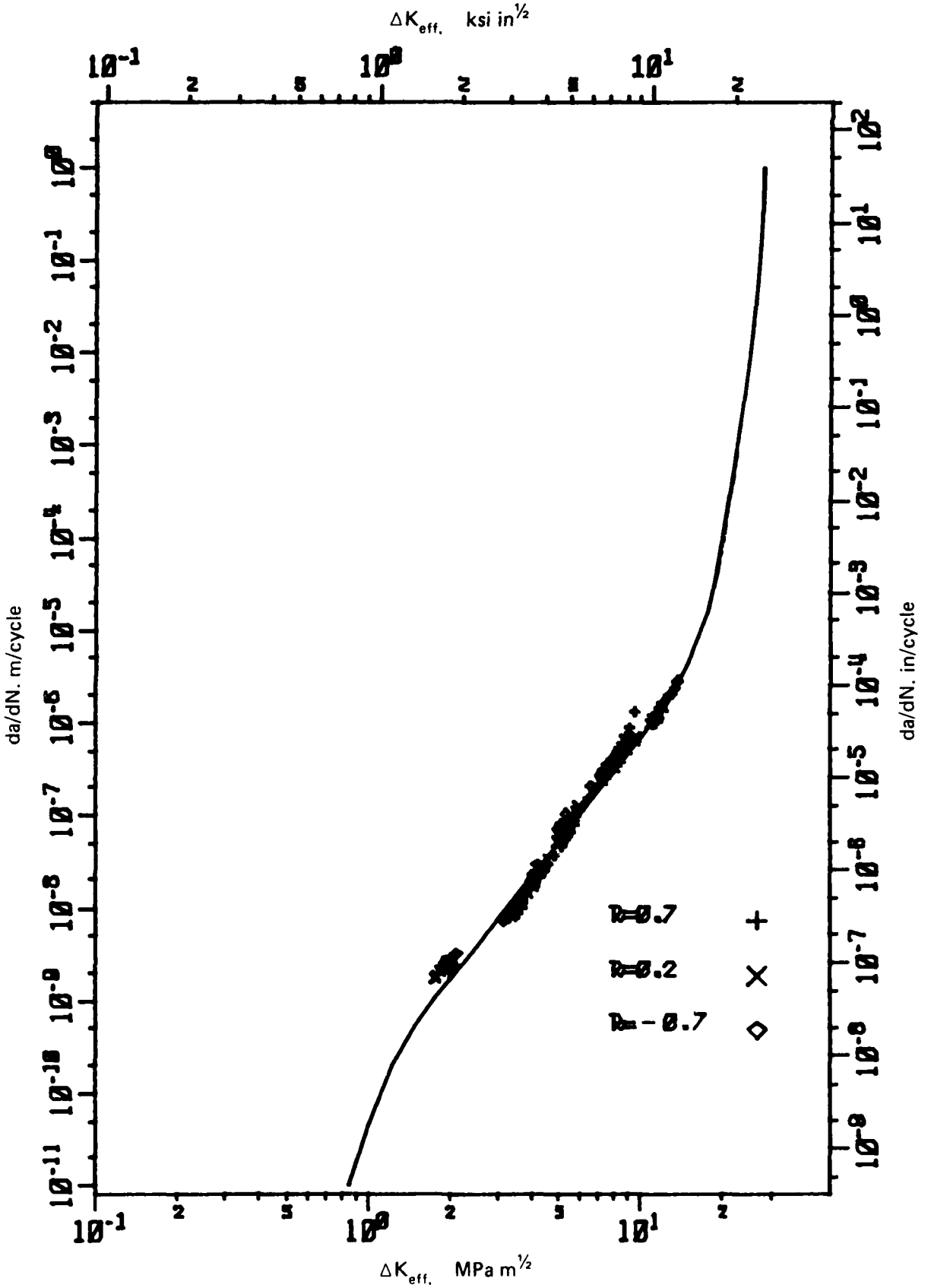

FIG. 13 CORRELATION OF MEAN STRESS EFFECT ON CRACK GROWTH RATE BY $\Delta K_{eff.}$ (SCHIJVE)

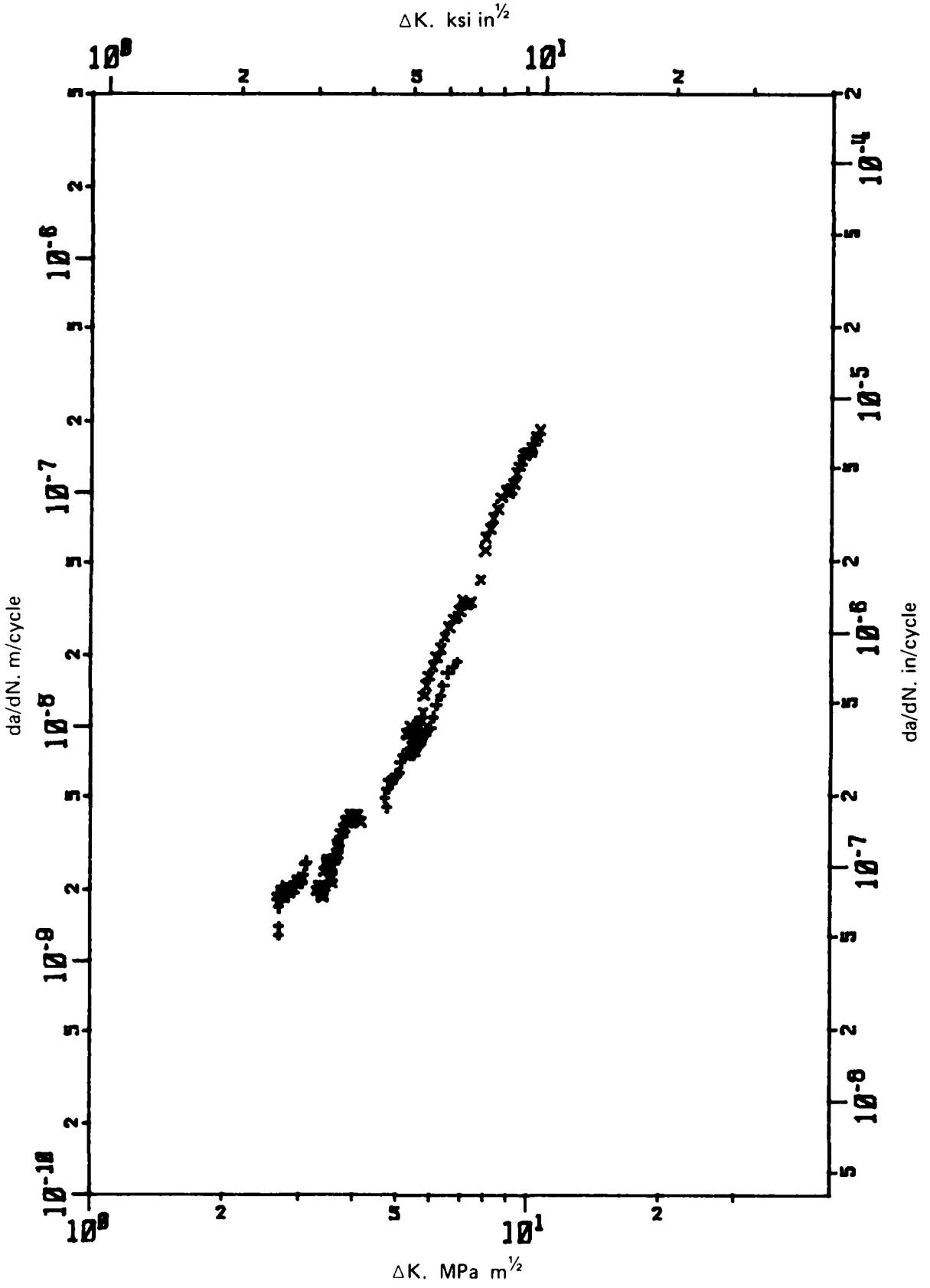

FIG. 14 SCATTER IN CRACK GROWTH RATE DATA. 5mm THICK CCT SPECIMENS TESTED AT R = 0.2.

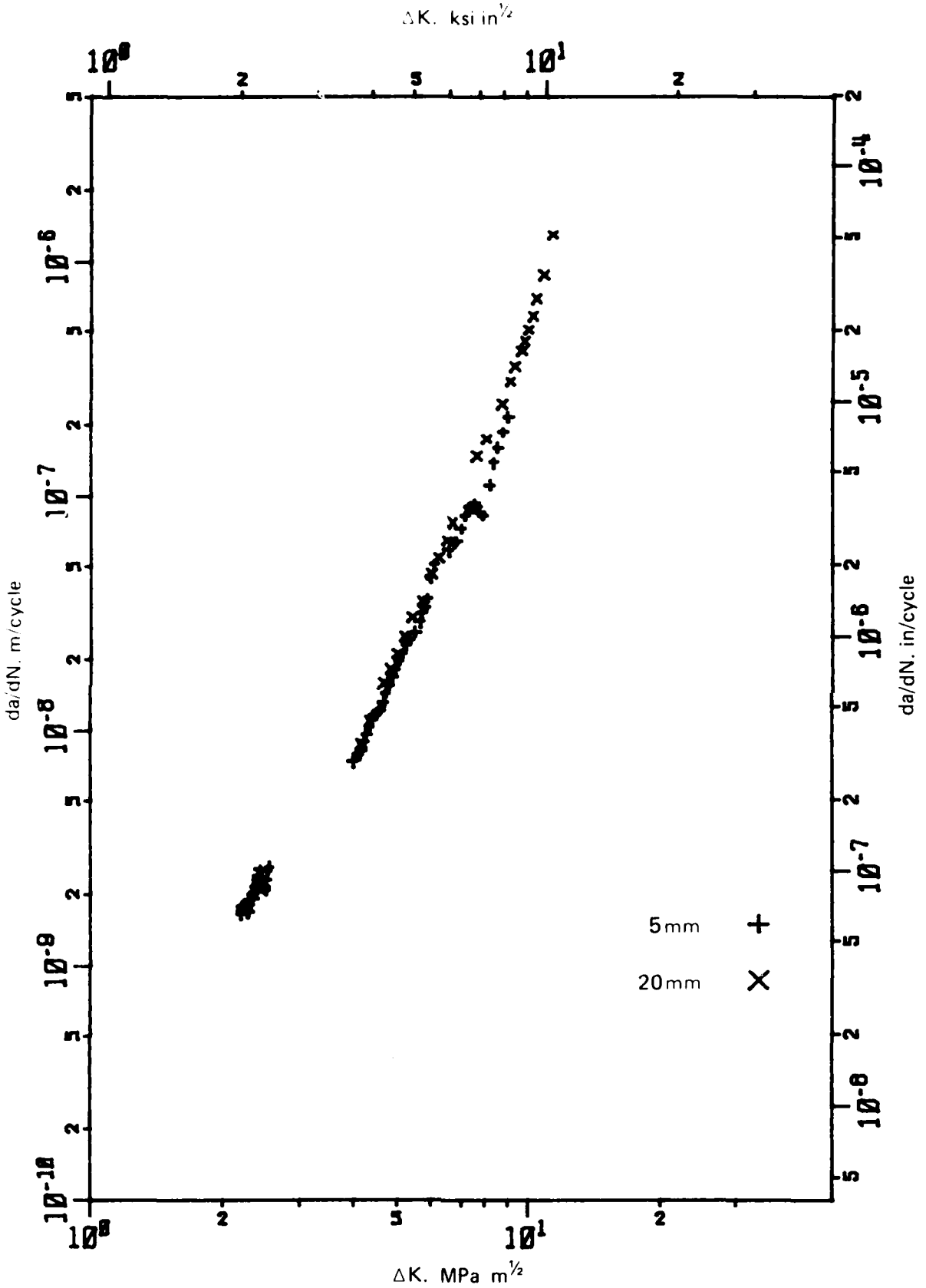

FIG. 15 da/dN – ΔK DATA FOR 5mm AND 20mm THICK CCT SPECIMENS TESTED AT R = 0.7.

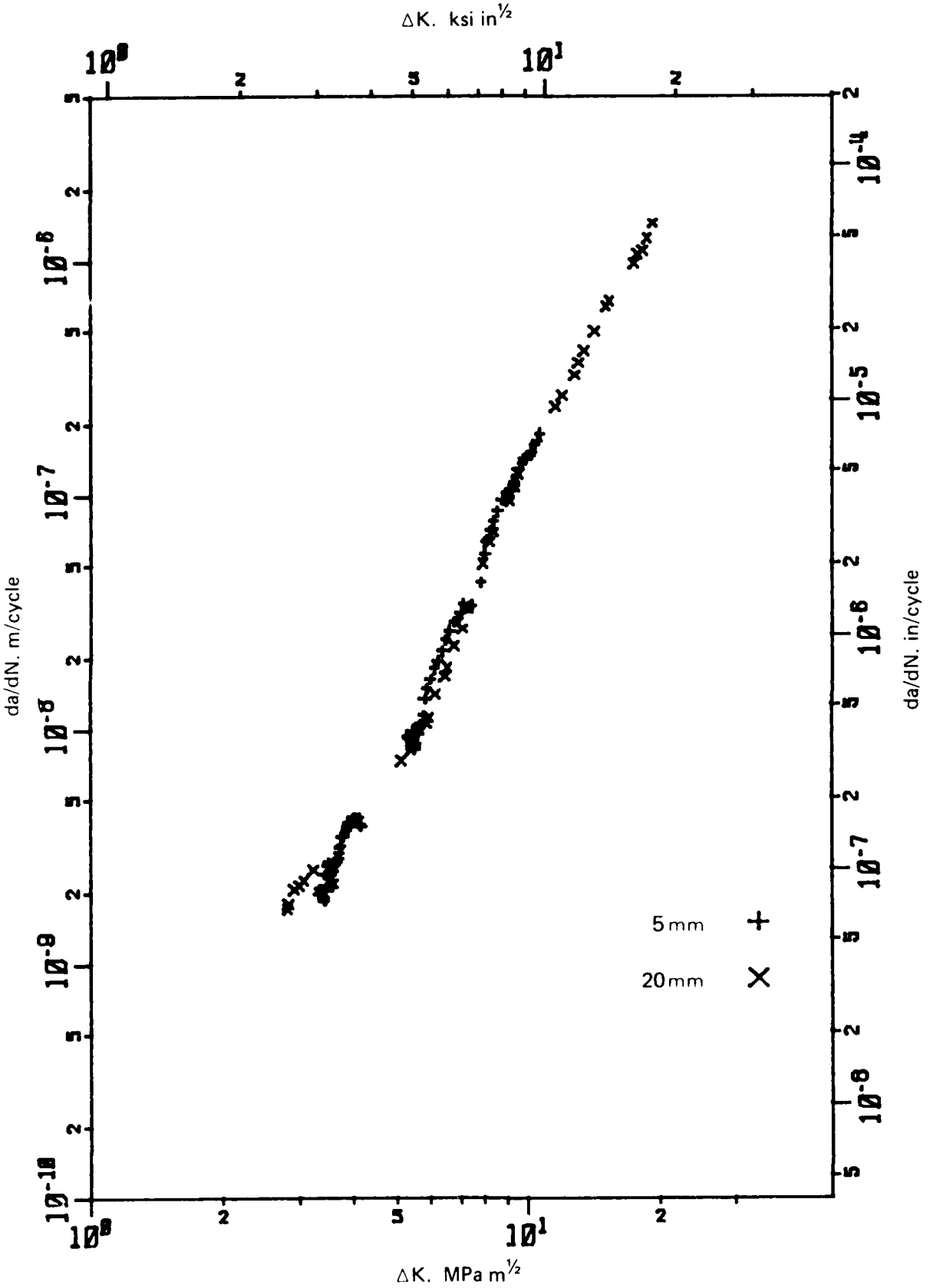

FIG. 16 da/dN – ΔK DATA FOR 5mm AND 20mm THICK CCT SPECIMENS TESTED AT R = 0.2.

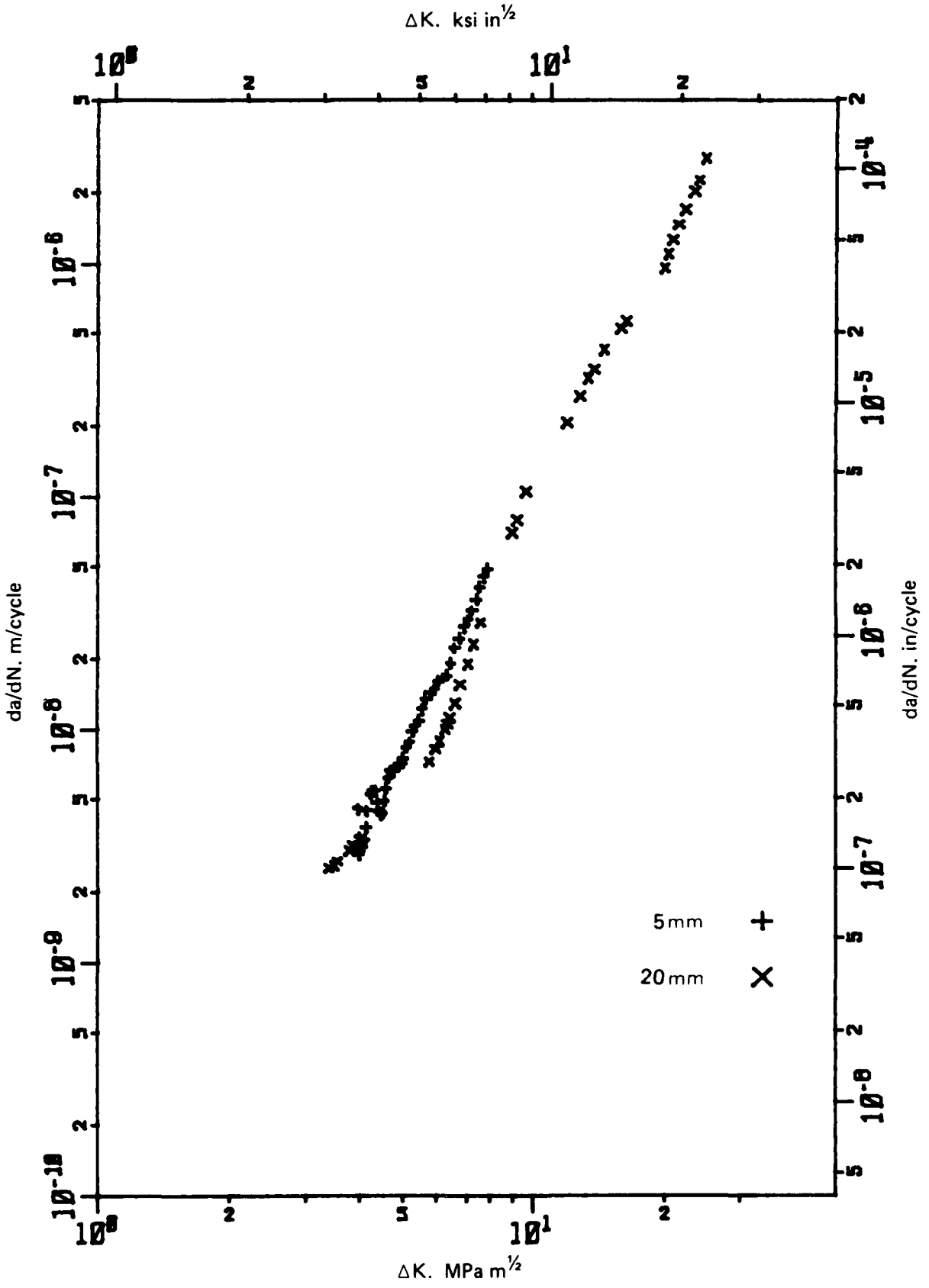

FIG. 17 da/dN – ΔK DATA FOR 5mm AND 20mm THICK CCT SPECIMENS TESTED AT R = –0.7.

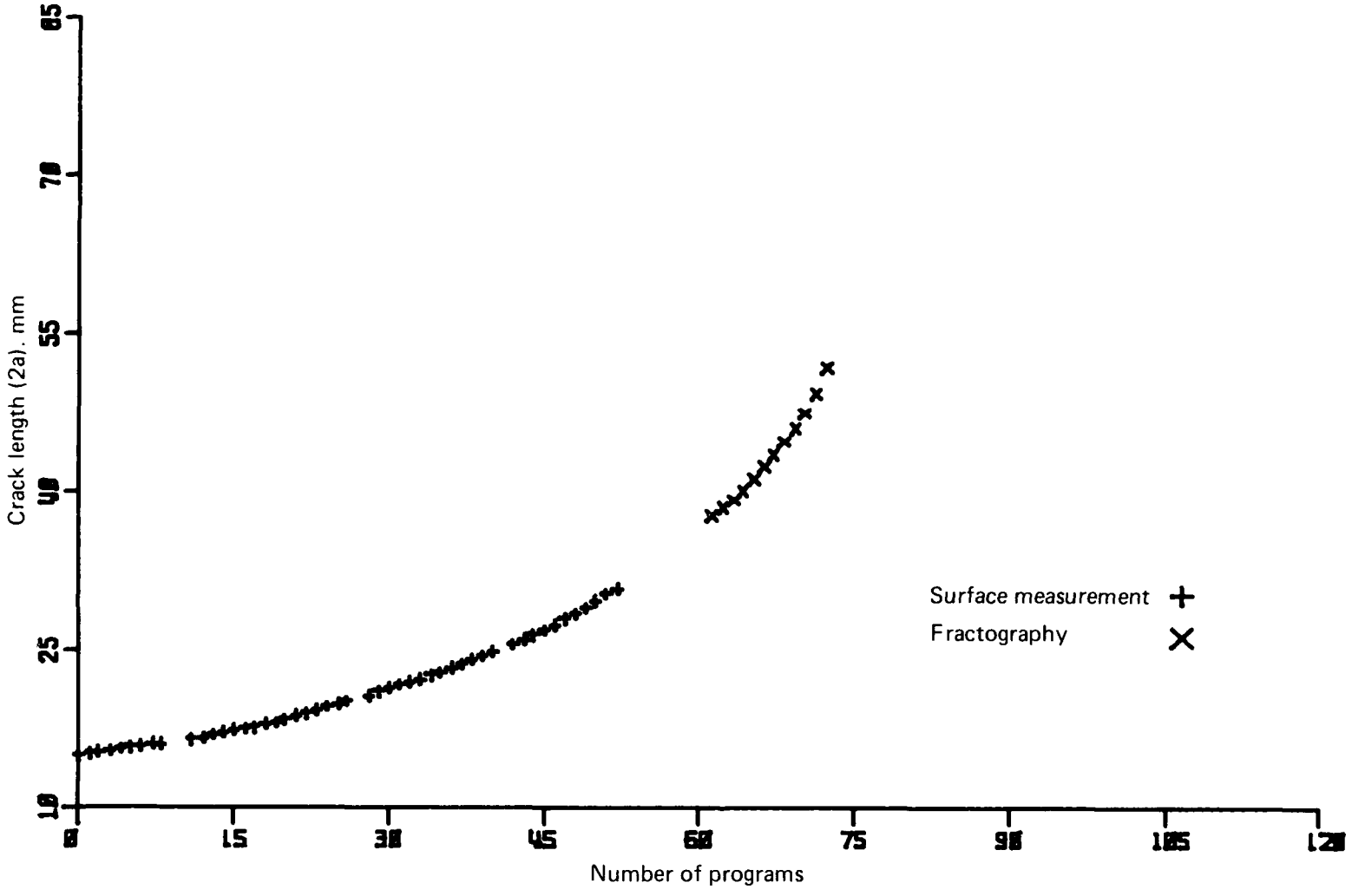

FIG. 18 CRACK GROWTH IN 5mm THICK CCT SPECIMEN TESTED UNDER THE F + W SEQUENCE (15.97 MPa/g).

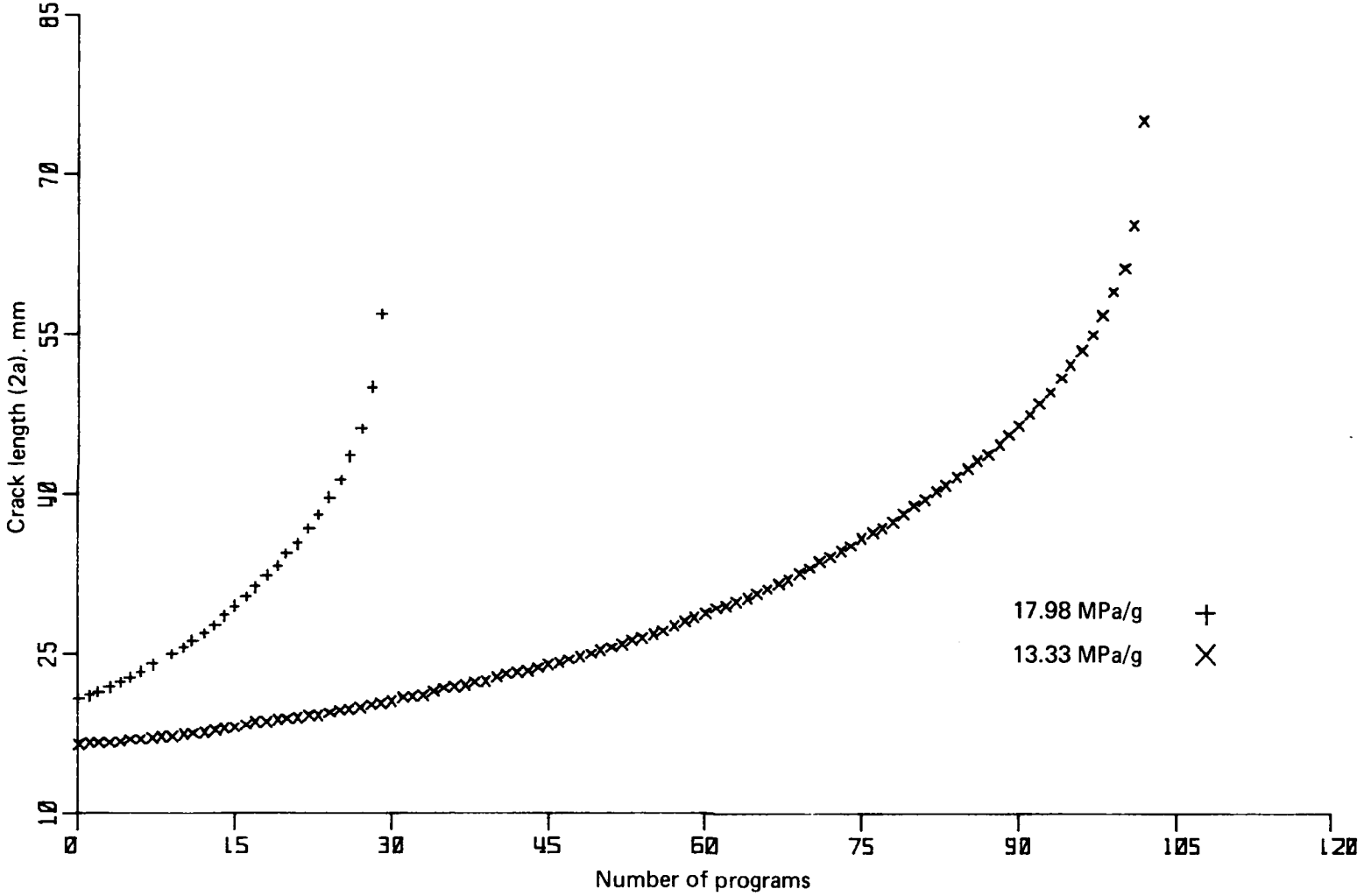

FIG. 19 CRACK GROWTH IN 20mm THICK CCT SPECIMENS TESTED UNDER THE F + W SEQUENCE.

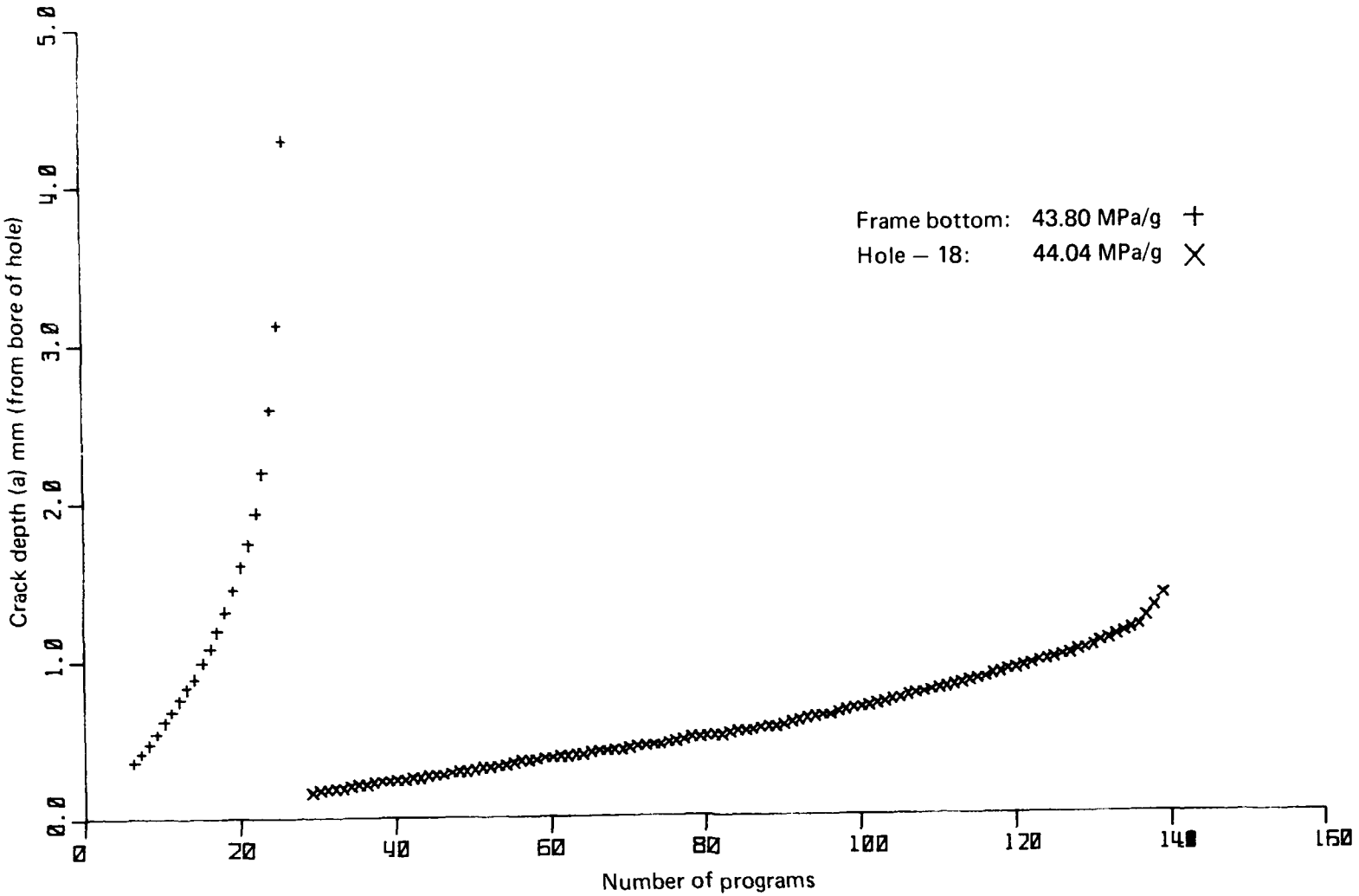

FIG. 20 CRACK GROWTH IN SIMULATION SPECIMENS; F + W SEQUENCE.

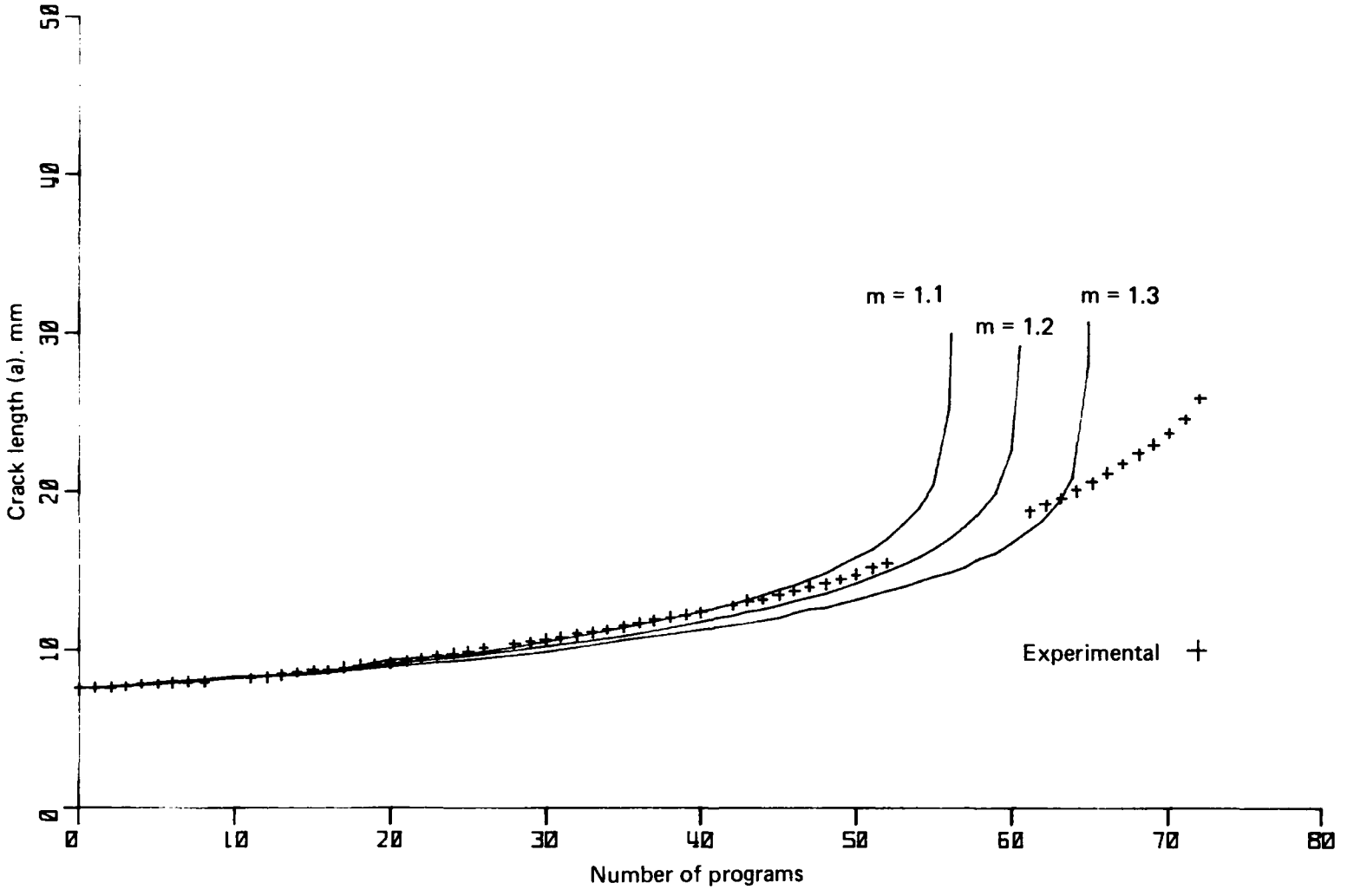

FIG. 21 CALIBRATION OF WHEELER EXPONENT, m.
5mm THICK CCT SPECIMEN TESTED UNDER THE F + W SEQUENCE
(15.97 MPa/g).

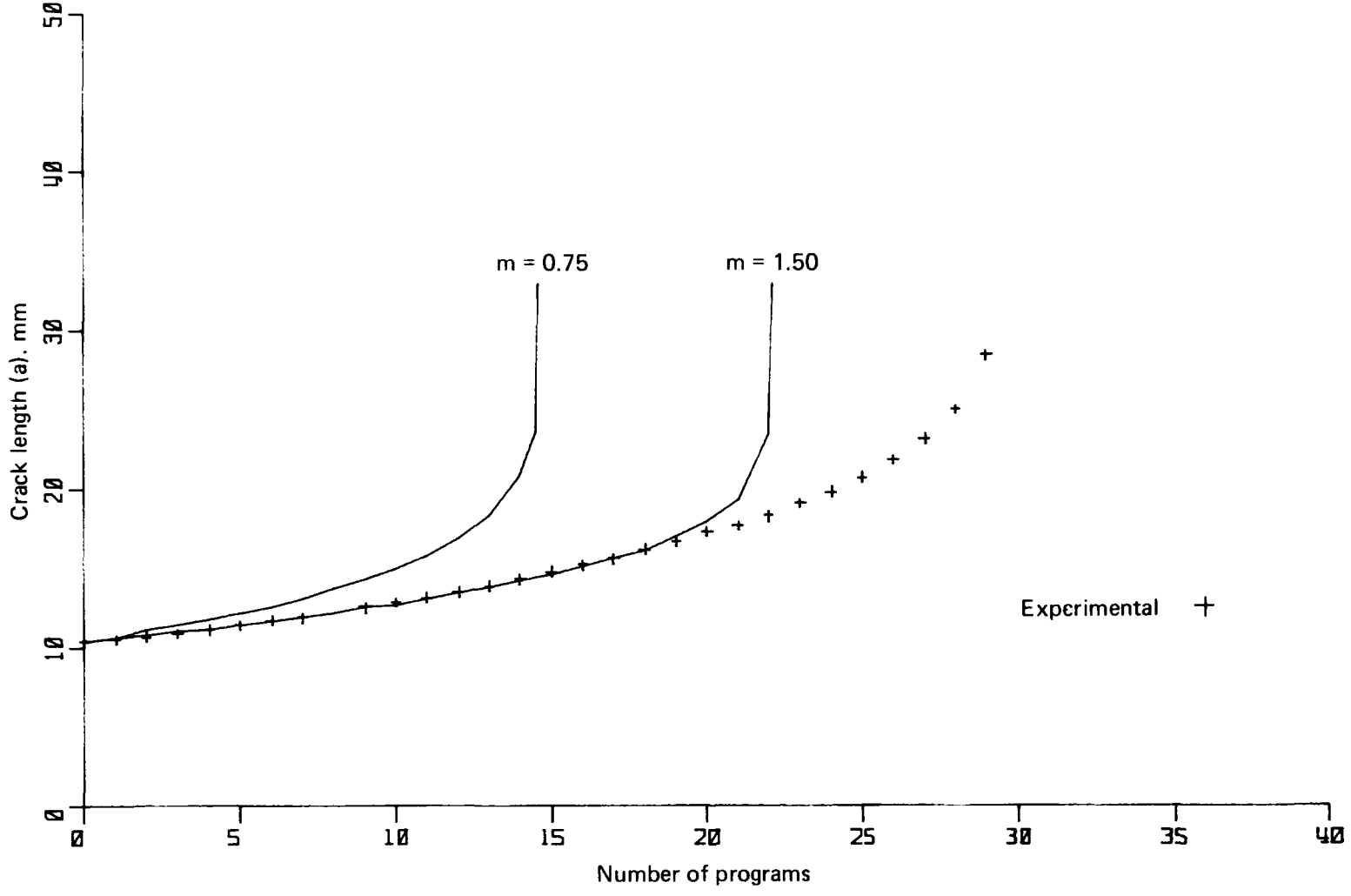

FIG. 22 CALIBRATION OF WHEELER EXPONENT, m.
20mm THICK CCT SPECIMEN TESTED UNDER THE F + W SEQUENCE
(17.98 MPa/g).

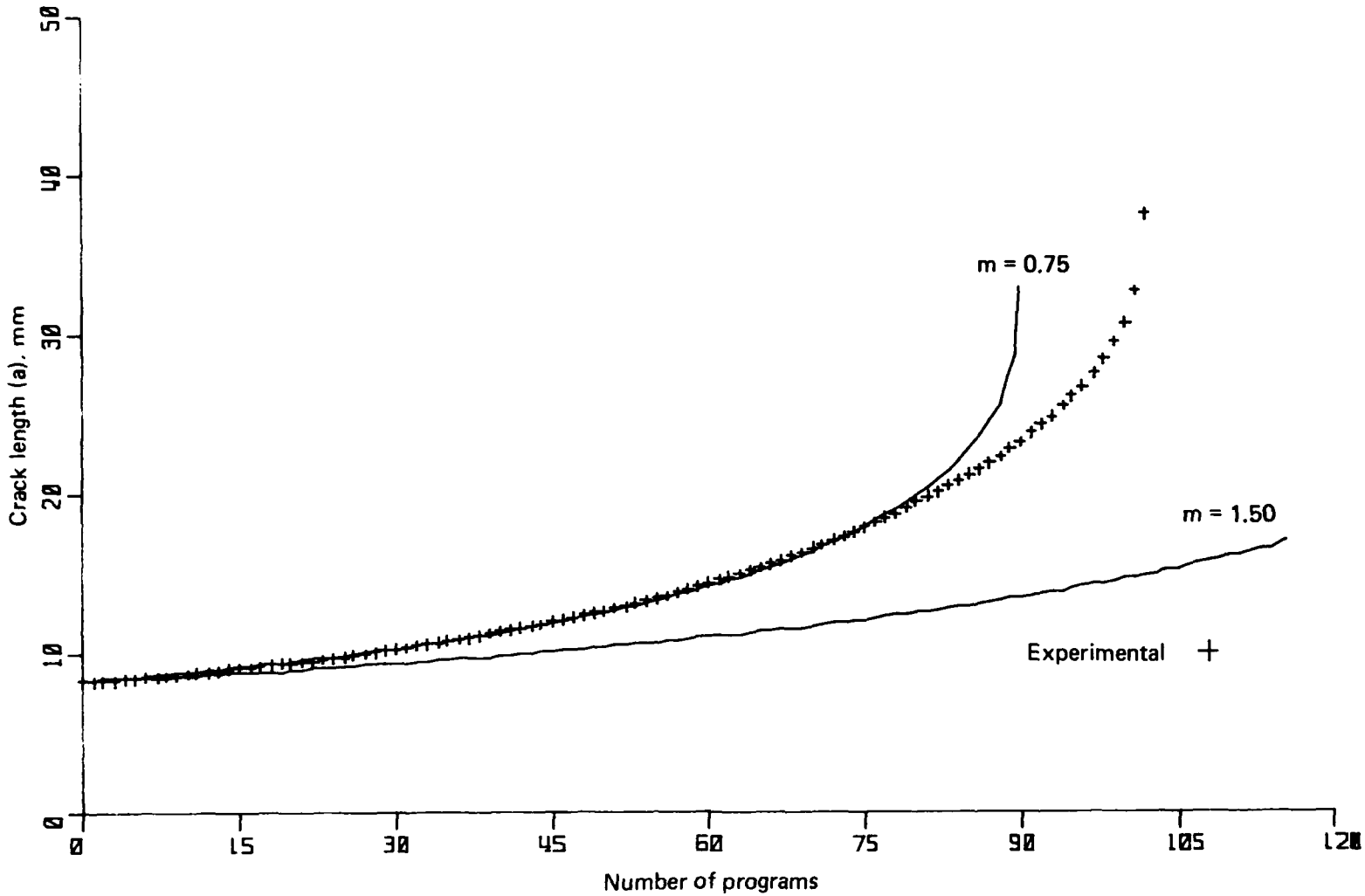

FIG. 23 CALIBRATION OF WHEELER EXPONENT, m.
20mm THICK CCT SPECIMEN TESTED UNDER THE F + W SEQUENCE
(13.33 MPa/g).

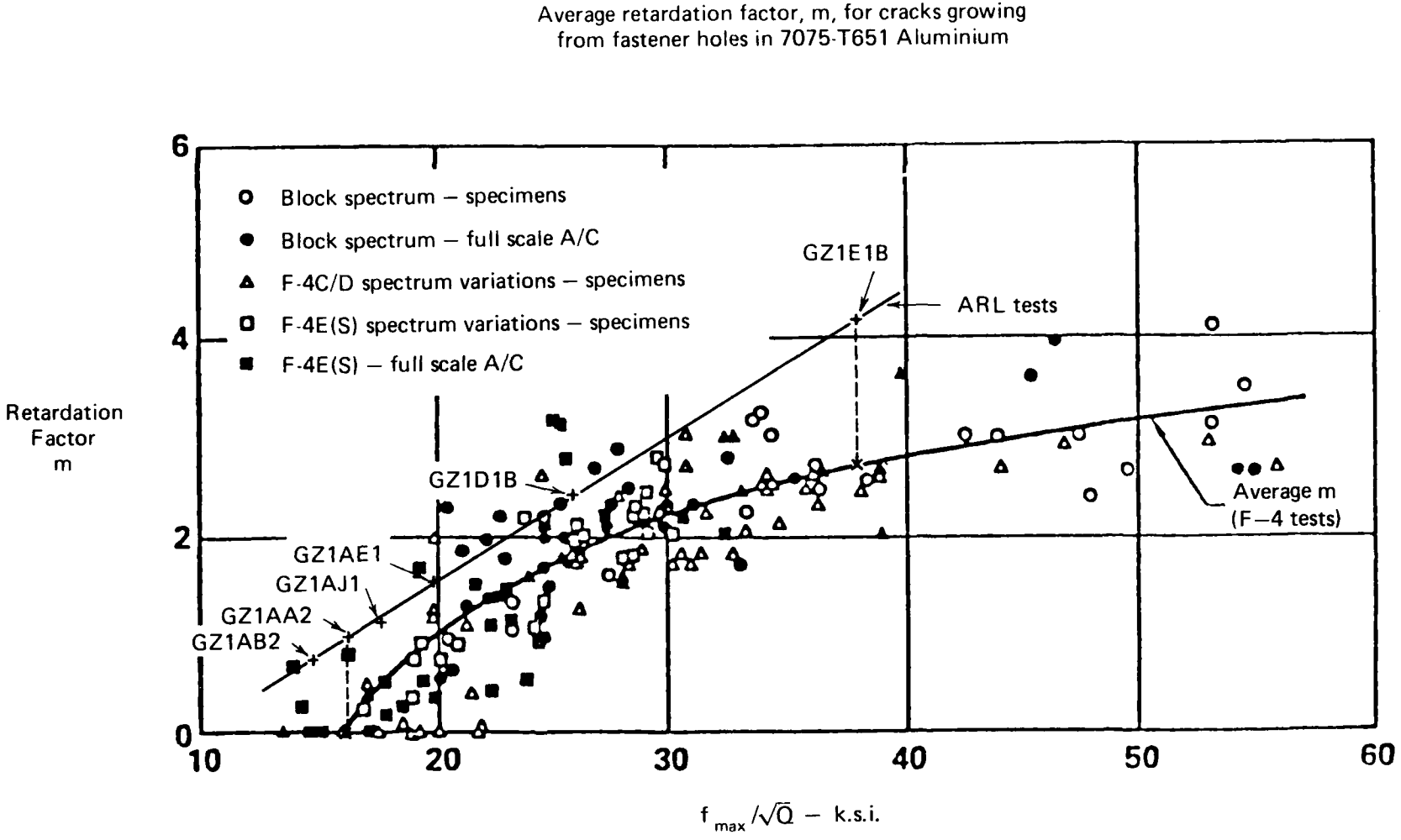

FIG. 24 DEPENDENCE OF WHEELER RETARDATION EXPONENT, m, ON MAXIMUM STRESS IN SEQUENCE AND CRACK SHAPE, REF. 18.

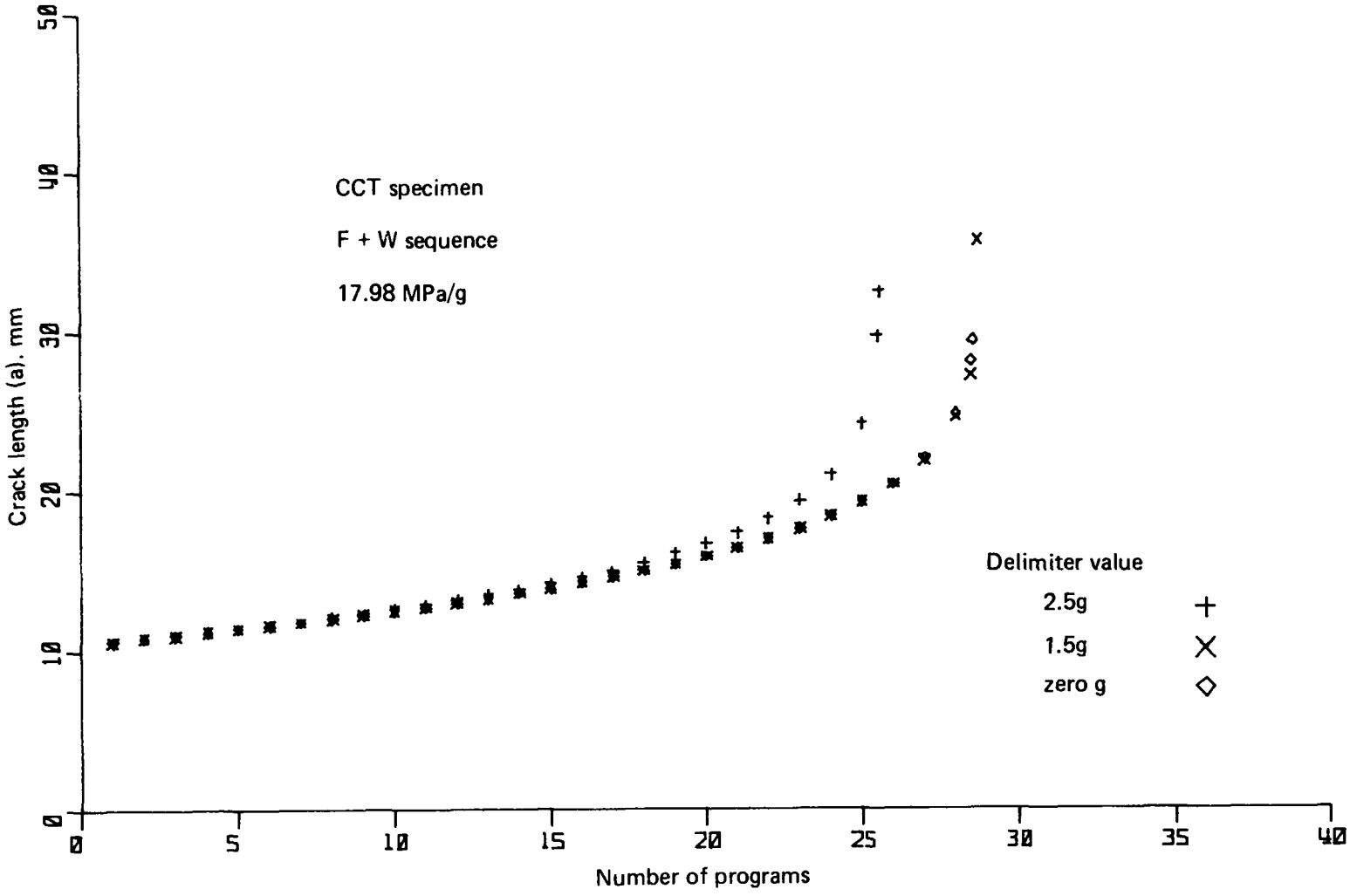

FIG. 25 INFLUENCE OF g–DELIMITER ON CRACK GROWTH PREDICTION (USING THE MODIFIED WILLENBORG RETARDATION MODEL, S = 2.30).

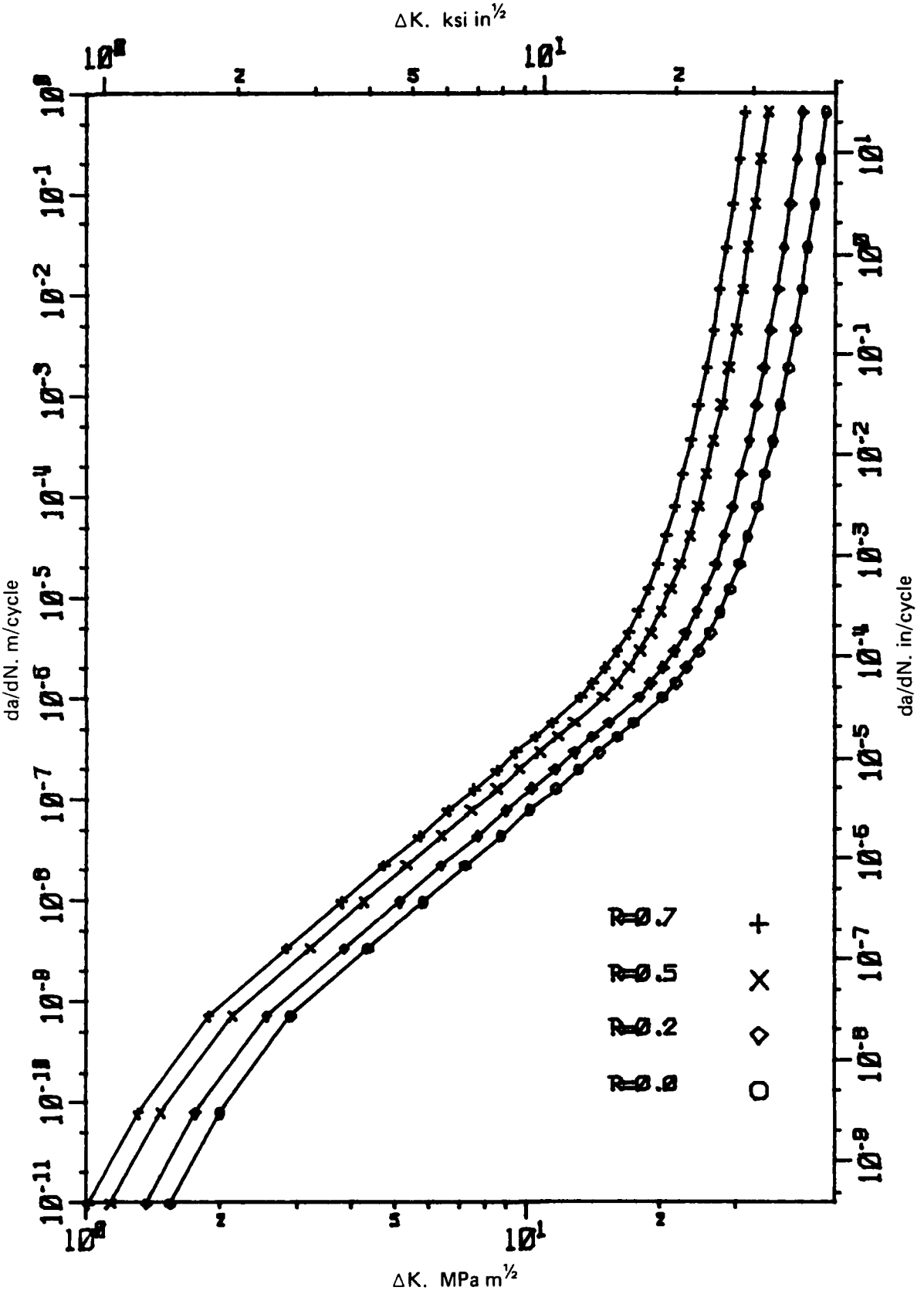

FIG. 26 da/dN – ΔK DATA FOR 20mm THICK CCT SPECIMENS – CONVERTED FROM ΔK_{eff} (SCHIJVE) TO ΔK.

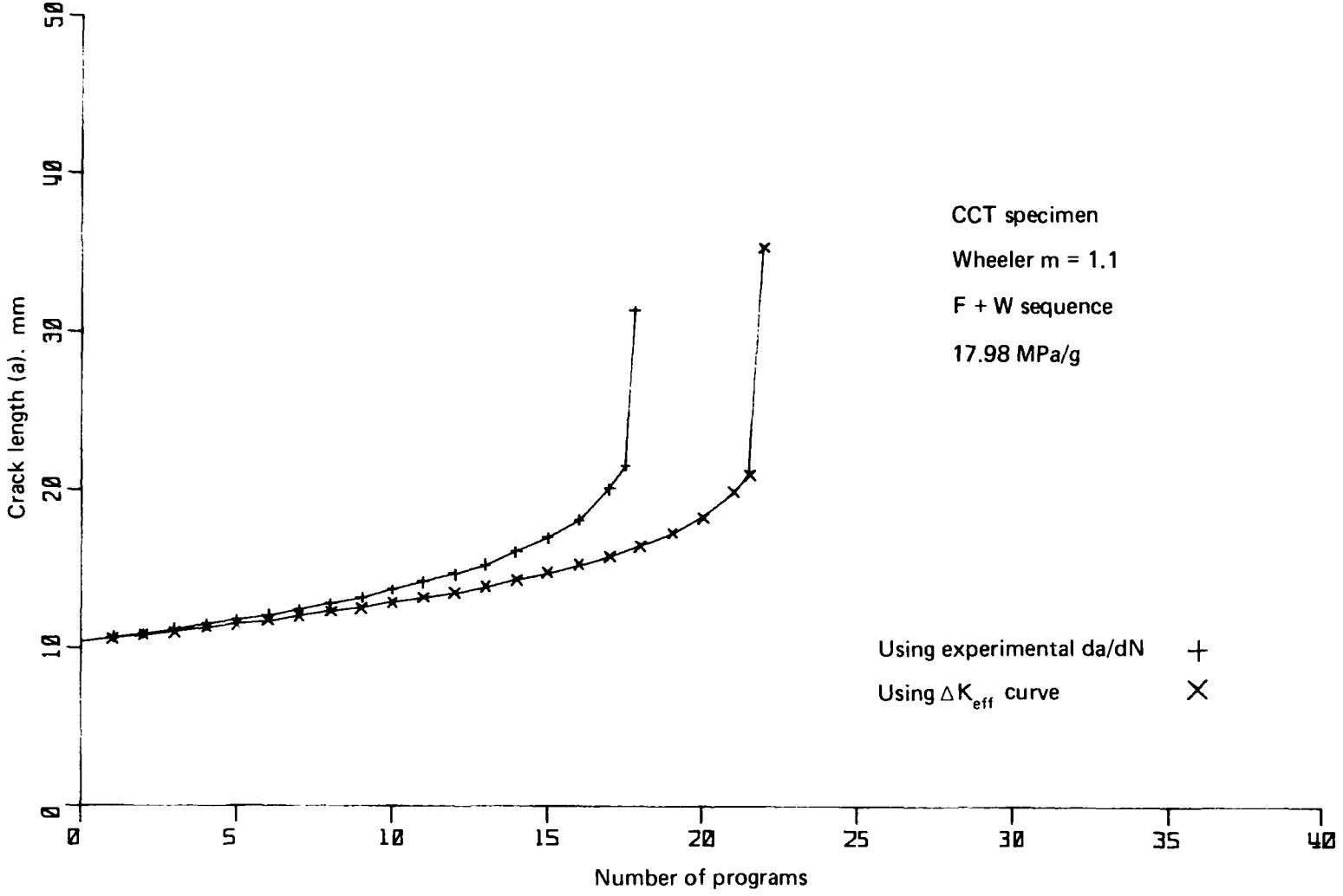

FIG. 27 INFLUENCE OF da/dN – ΔK REPRESENTATION ON CRACK GROWTH PREDICTION.

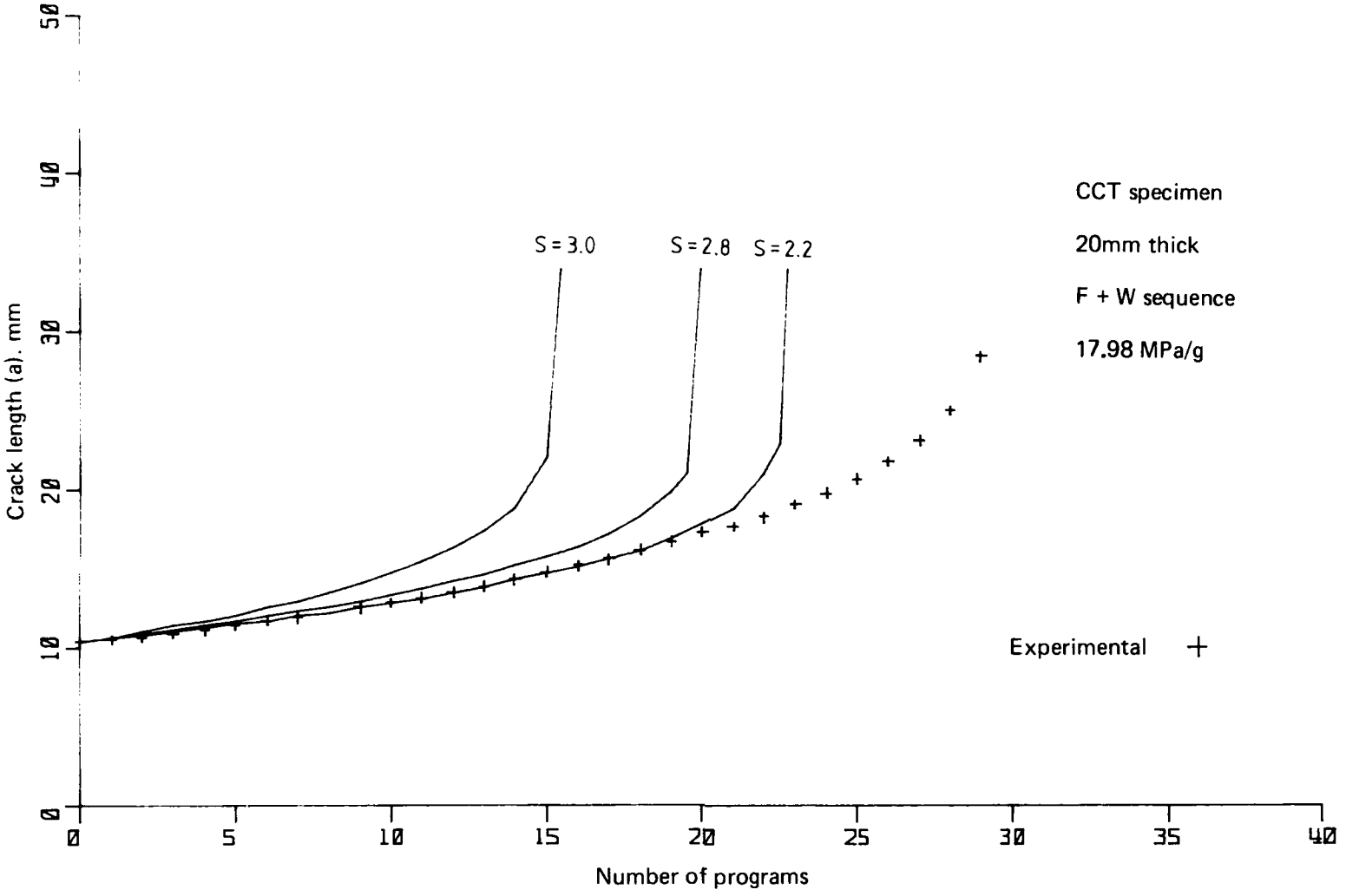

FIG. 28 CALIBRATION OF THE MODIFIED WILLENBORG SHUT-OFF RATIO, S.

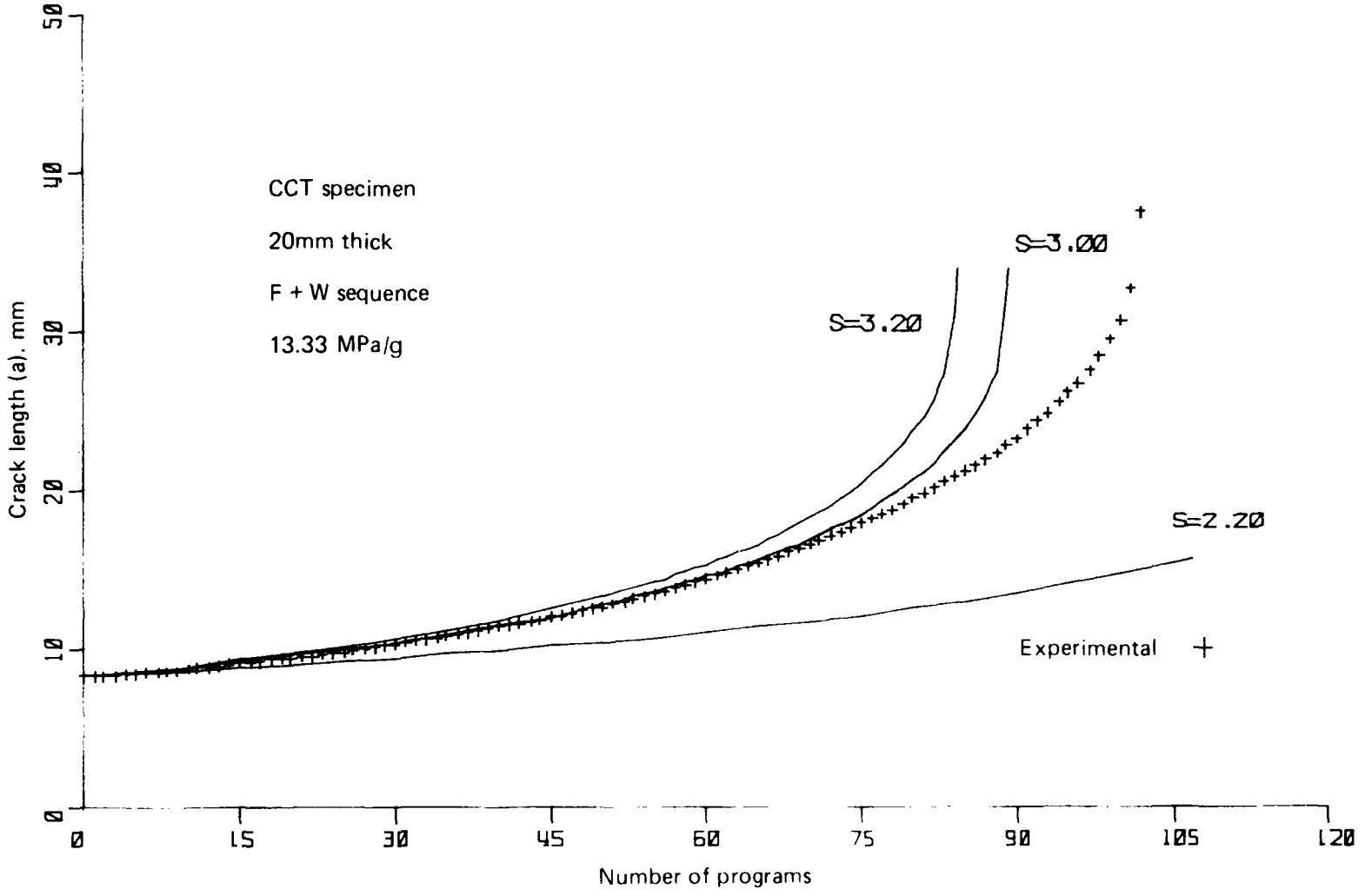

FIG. 29 CALIBRATION OF THE MODIFIED WILLENBORG SHUT-OFF RATIO, S.

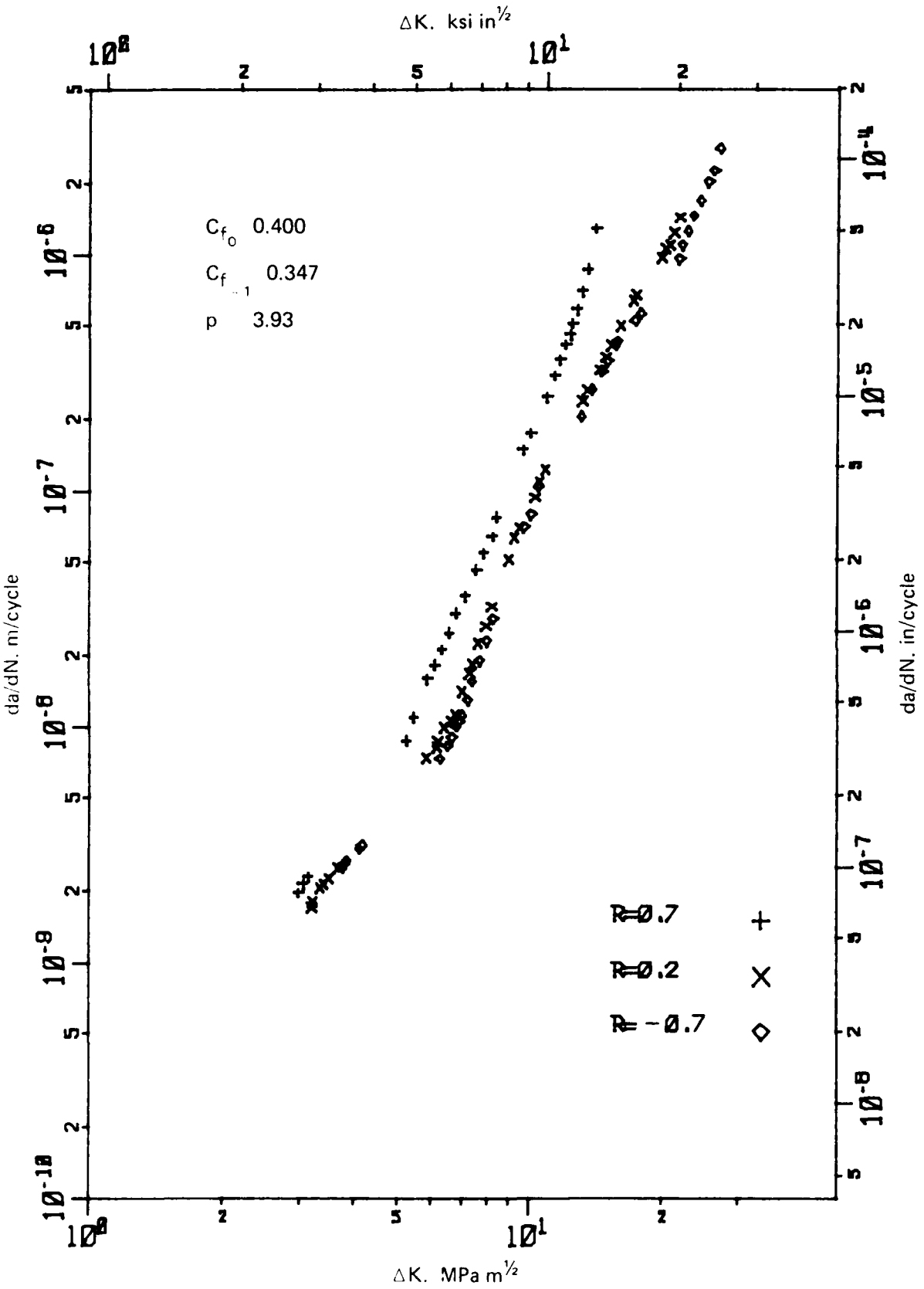

FIG. 30 da/dN – ΔK DATA FOR 20mm THICK CCT SPECIMENS TRANSLATED TO R = 0.

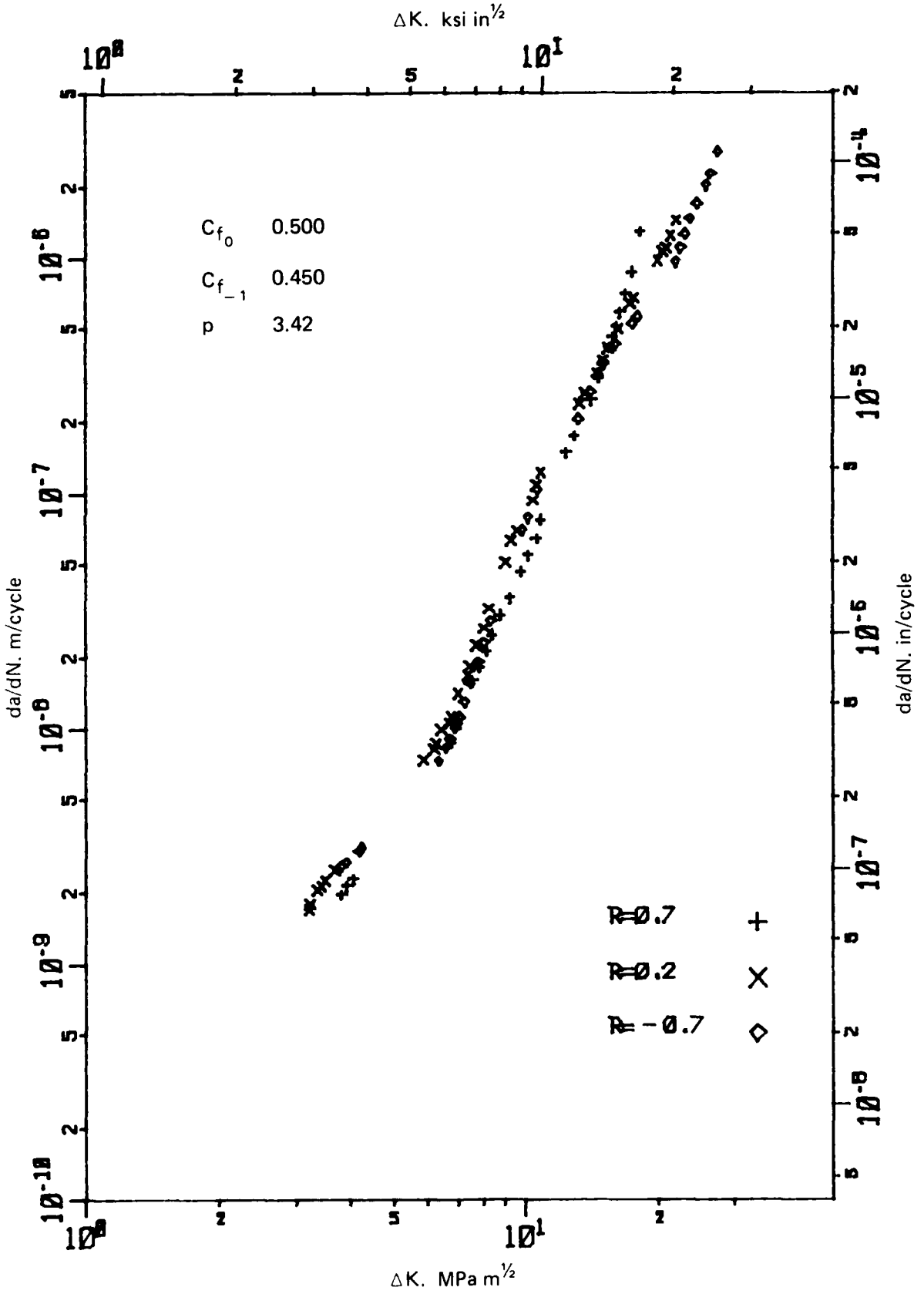

FIG. 31 da/dN - ΔK DATA FOR 20mm THICK CCT SPECIMENS TRANSLATED TO R = 0.

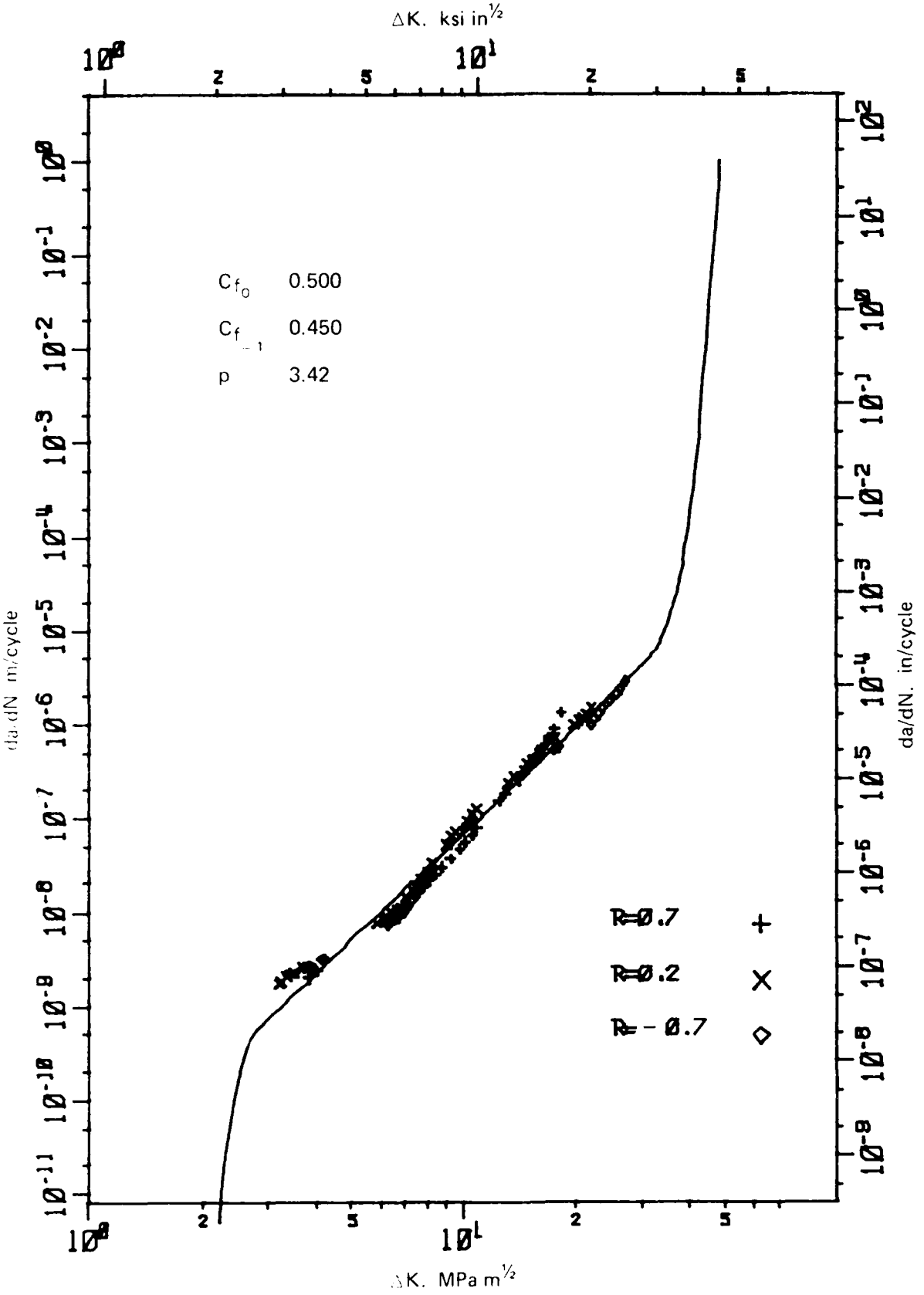

FIG. 32 da/dN – ΔK DATA FOR 20mm THICK CCT SPECIMENS TRANSLATED TO R = 0.

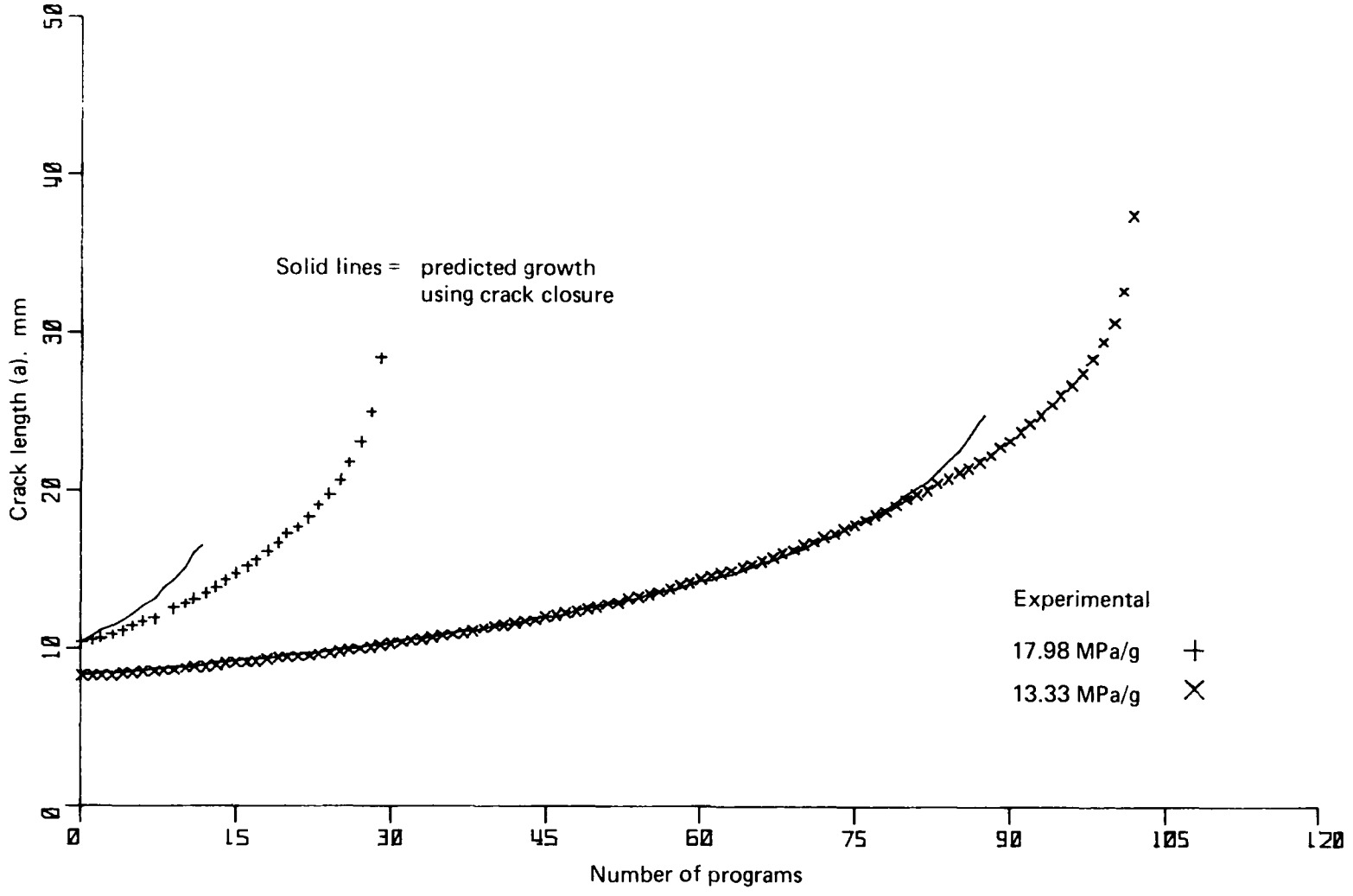

FIG. 33 EXPERIMENTAL AND PREDICTED CRACK GROWTH IN 20mm THICK CCT SPECIMENS TESTED UNDER THE F + W SEQUENCE.

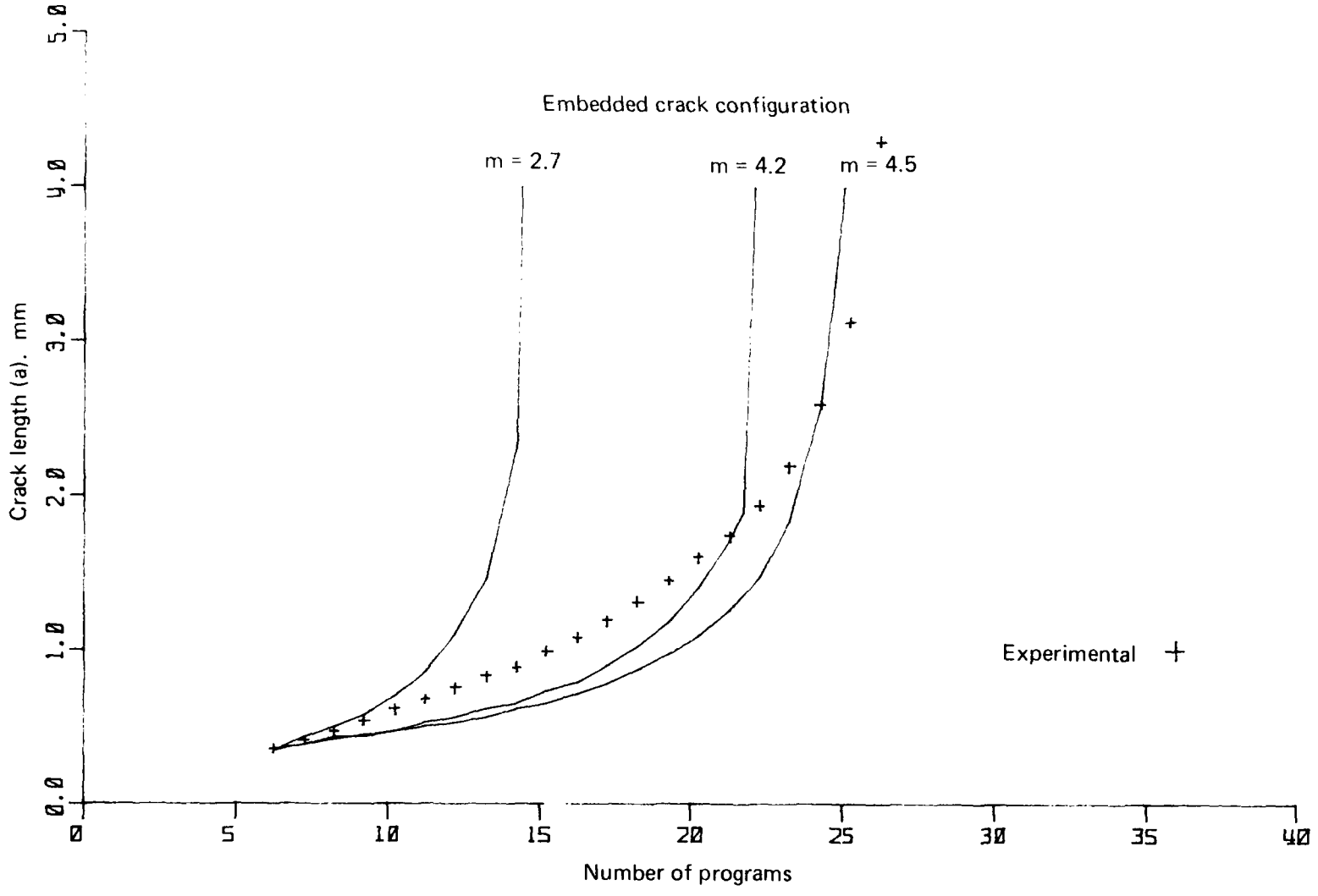

FIG. 34 CRACK GROWTH PREDICTION, USING WHEELER RETARDATION, FOR THE FRAME-BOTTOM SIMULATION SPECIMEN TESTED UNDER THE F + W SEQUENCE (43.80 MPa/g).

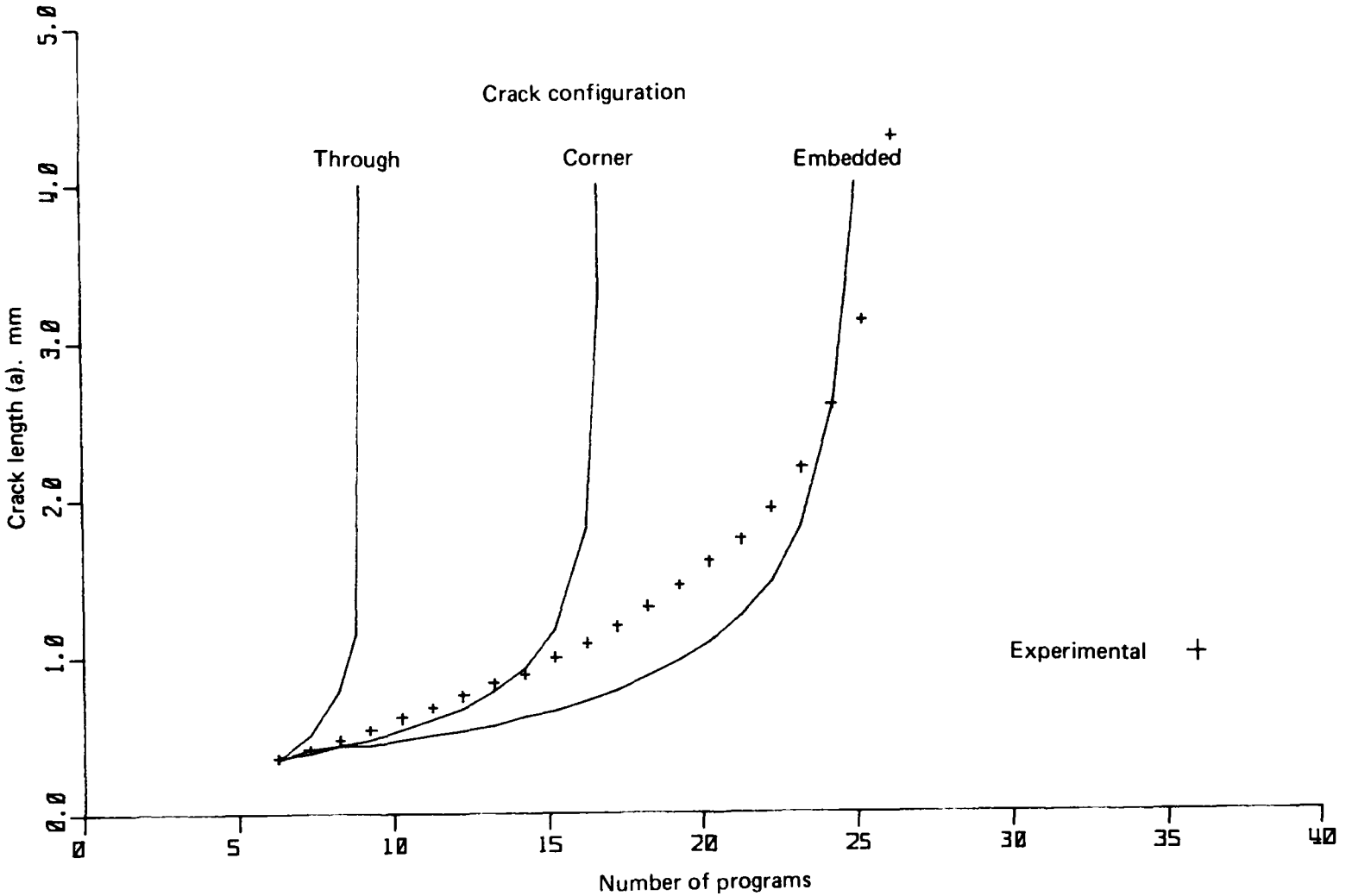

FIG. 35 INFLUENCE OF CRACK GEOMETRY ON CRACK GROWTH PREDICTION FOR THE FRAME-BOTTOM SIMULATION SPECIMEN TESTED UNDER THE F + W SEQUENCE (43.80 MPa/g) AND USING THE WHEELER EXPONENT m = 4.50.

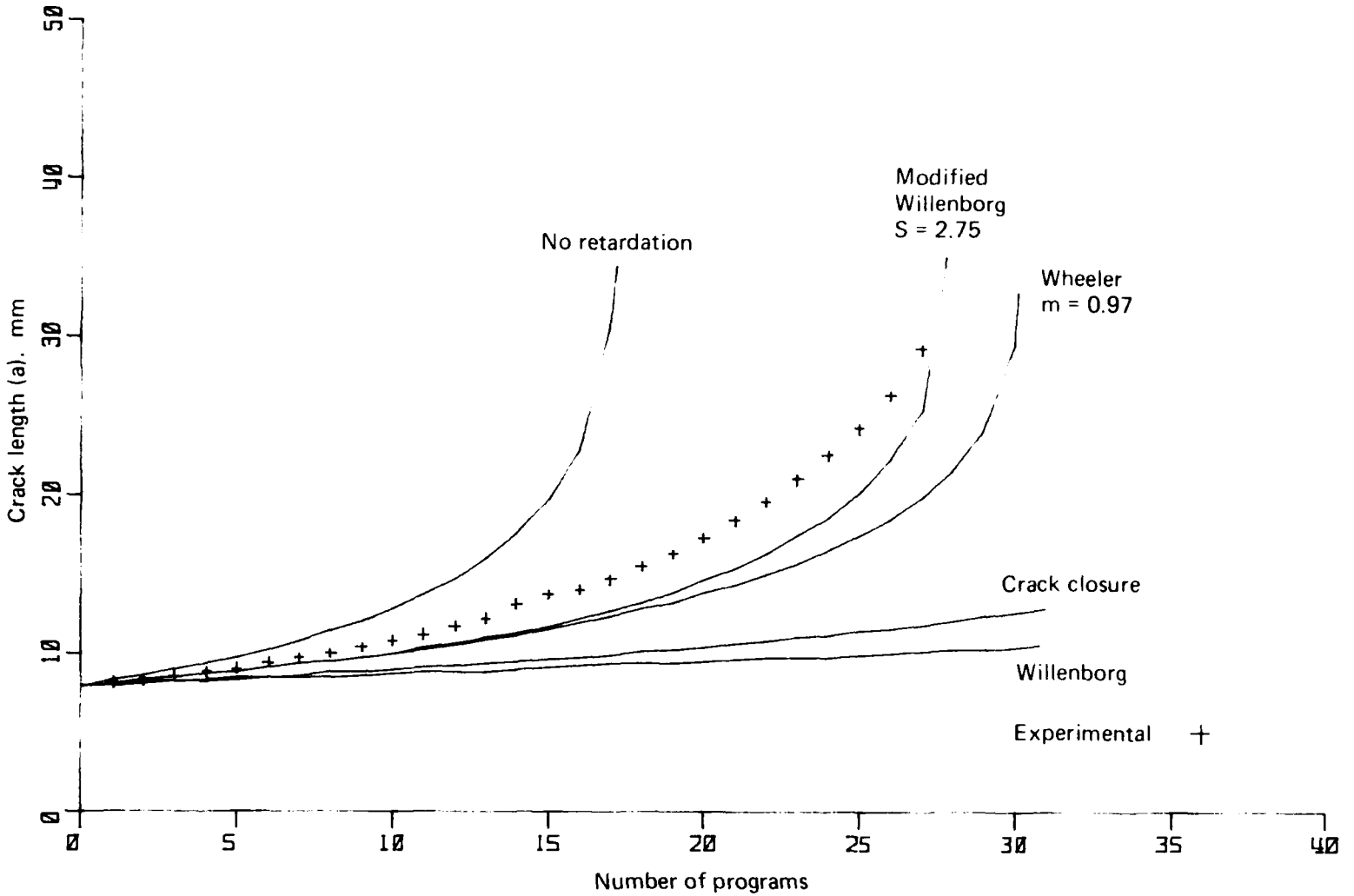

FIG. 36 CRACK GROWTH IN 20mm THICK CCT SPECIMEN UNDER THE RAAF 'ALL-TIME-AVERAGE' SEQUENCE (14.12 MPa/g).

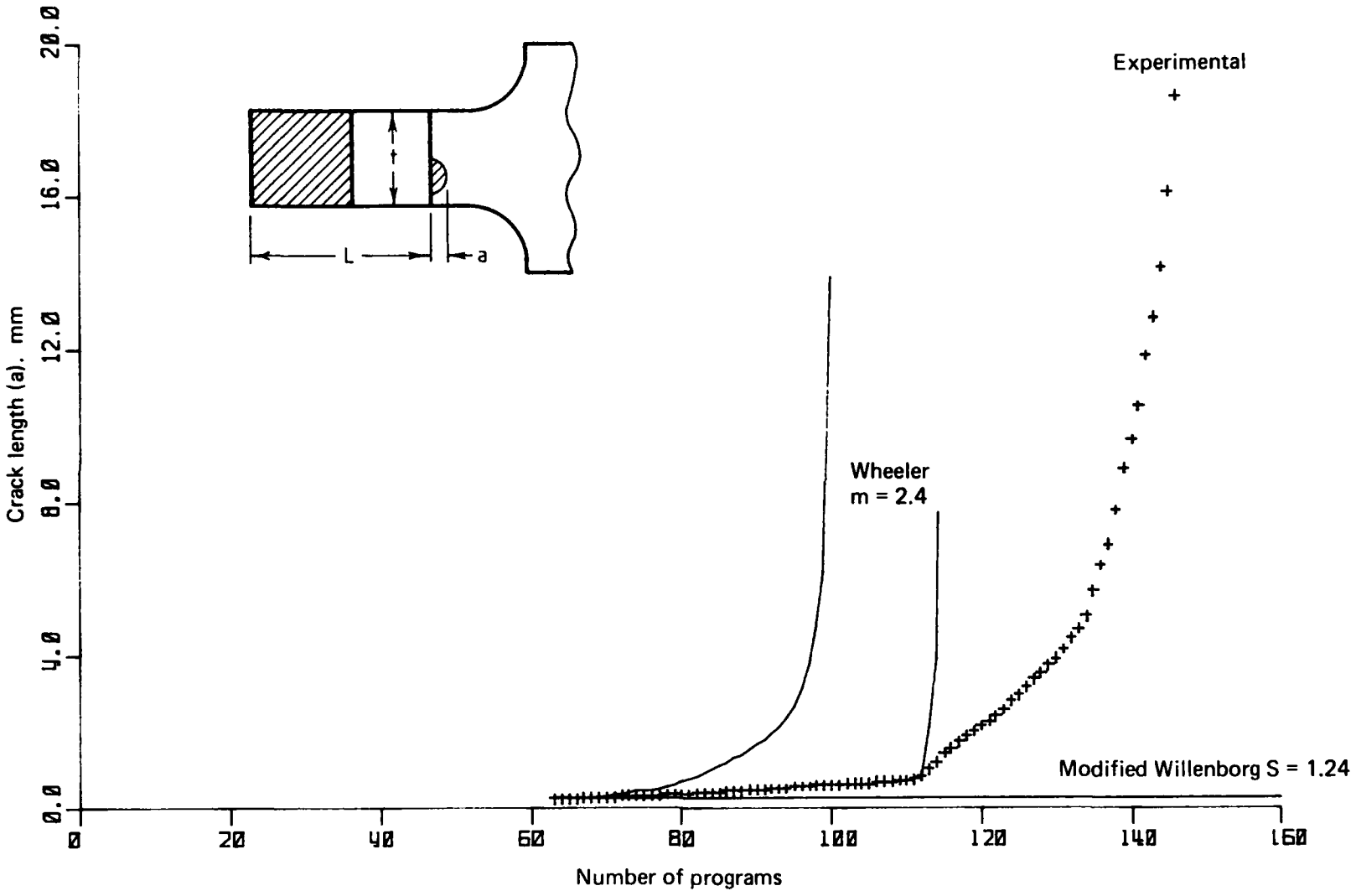

FIG. 37 CRACK GROWTH PREDICTION FOR FRAME-BOTTOM SIMULATION SPECIMEN TESTED UNDER THE RAAF 'ALL-TIME-AVERAGE' SEQUENCE (28.63 MPa/g).

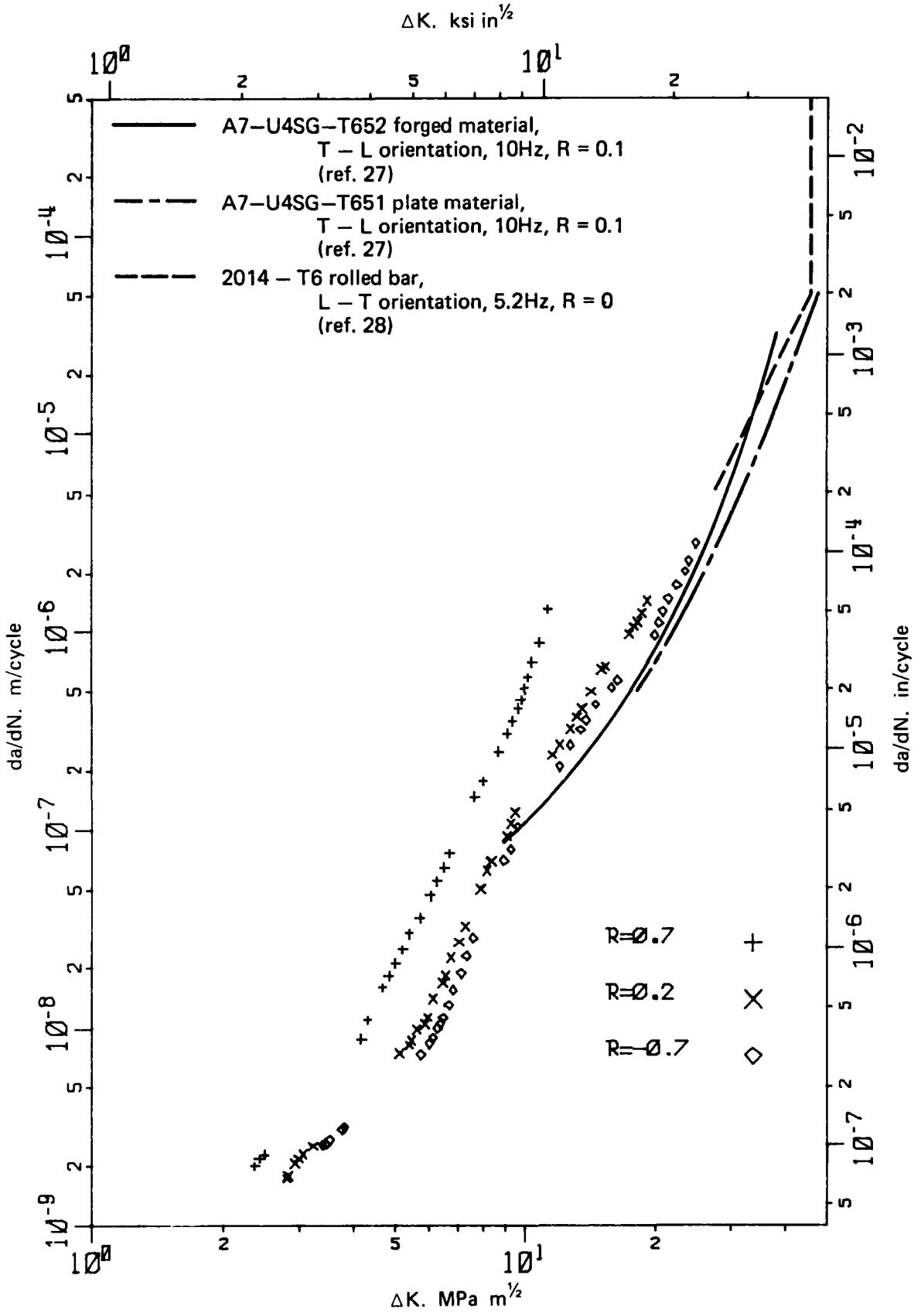

FIG. 38 COMPARISON OF PRESENT AND PUBLISHED da/dN –ΔK DATA.

DISTRIBUTION

AUSTRALIA

DEPARTMENT OF DEFENCE

Central Office

Chief Defence Scientist
Deputy Chief Defence Scientist
Superintendent, Science and Technology Programmes } (1 copy)
Controller, Projects and Analytical Studies
Defence Science Representative (U.K.) (Doc. Data sheet only)
Counsellor, Defence Science (U.S.A.) (Doc. Data sheet only)
Defence Central Library
Document Exchange Centre, D.I.S.B. (18 copies)
Joint Intelligence Organisation
Librarian H Block, Victoria Barracks, Melbourne
Director General—Army Development (NSO) (4 copies)
Defence Industry and Materiel Policy, FAS

Aeronautical Research Laboratories

Director
Library
Divisional File—Structures
Superintendent—Materials
Authors: J. M. *Finney*
F. G. Harris
R. A. Pell
C. S. Dentry
C. T. Stefoulis
J. Y. Mann
B. C. Hoskin
C. K. Rider
D. G. Ford
G. S. Jost
J. G. Sparrow
G. Clark
J. M. Grandage
L. M. Bland
B. J. Wicks
N. T. Goldsmith

Materials Research Laboratories

Director/Library

Defence Research Centre

Library

Navy Office
Navy Scientific Adviser
RAN Aircraft Maintenance and Flight Trials Unit
Directorate of Naval Aircraft Engineering
Directorate of Naval Aviation Policy
Superintendent, Aircraft Maintenance and Repair
Directorate of Naval Ship Design

Army Office
Army Scientific Adviser
Engineering Development Establishment, Library
Royal Military College Library
US Army Research, Development and Standardisation Group

Air Force Office
Air Force Scientific Adviser
Aircraft Research and Development Unit
Scientific Flight Group
Library
Technical Division Library
Director General Aircraft Engineering—Air Force (4 copies)
Director General Operational Requirements—Air Force
HQ Operational Command (SMAINTSO)
HQ Support Command (SLENGO)
RAAF Academy, Point Cook
Air Attache Paris

Central Studies Establishment
Information Centre

DEPARTMENT OF DEFENCE SUPPORT

Government Aircraft Factories
Manager
Library

DEPARTMENT OF AVIATION

Library
Flying Operations and Airworthiness Division

STATUTORY AND STATE AUTHORITIES AND INDUSTRY

CSIRO
Materials Science Division, Library
Trans-Australia Airlines, Library
Qantas Airways Limited
Gas and Fuel Corporation of Victoria, Manager Scientific Services
SEC of Vic., Herman Research Laboratory, Library
Ansett Airlines of Australia, Library
B.H.P., Melbourne Research Laboratories
Commonwealth Aircraft Corporation

Library
Mr R. C. Beckett
Mr R. Stephens
Hawker de Havilland Aust. Pty Ltd, Bankstown
Library
Mr V. Romeo
Australian Aircraft Consortium
General Manager
WGCDR G. R. Susans

UNIVERSITIES AND COLLEGES

Melbourne	Engineering Library
R.M.I.T.	Library

CANADA

CAARC Coordinator Structures
International Civil Aviation Organization, Library
NRC
Aeronautical and Mechanical Engineering Library
Division of Mechanical Engineering, Director

FRANCE

ONERA, Library
AMD-BA
Mr M. Peyrony
Mr D. Chaumette

INDIA

CAARC Coordinator Structures
Defence Ministry, Aero Development Establishment, Library
Hindustan Aeronautics Ltd, Library
National Aeronautical Laboratory, Information Centre

INTERNATIONAL COMMITTEE ON AERONAUTICAL FATIGUE

Per Australian ICAF Representative (25 copies)

ISRAEL

Technion-Israel Institute of Technology
Professor J. Singer
Professor A. Buch
Israel Aircraft Industries
Mr A. Brot

JAPAN

National Research Institute for Metals, Fatigue Testing Division
Institute of Space and Astronautical Science, Library

NETHERLANDS

National Aerospace Laboratory (NLR), Library

Universities

Technological University
of Delft — Professor J. Schijve

NEW ZEALAND

Defence Scientific Establishment
Library
Mr P. Conor
Transport Ministry, Airworthiness Branch, Library
RNZAF, Vice Consul (Defence Liaison)

SWEDEN

Aeronautical Research Institute, Library
Swedish National Defense Research Institute (FOA)

SWITZERLAND

F + W (Swiss Federal Aircraft Factory), Dr H. R. Boesch

UNITED KINGDOM

Ministry of Defence, Research, Materials and Collaboration
CAARC, Secretary
Royal Aircraft Establishment
Bedford, Library
Farnborough, Materials and Structures Department
National Engineering Laboratory, Library
British Library, Lending Division
CAARC Co-ordinator, Structures
Aircraft Research Association, Library
British Ship Research Association
Fulmer Research Institute Ltd, Research Director
Motor Industry Research Association, Director
Rolls-Royce Ltd
Aero Division Bristol, Library
Welding Institute, Library
British Aerospace
Kingston-upon-Thames, Library
Hatfield-Chester Division, Library
British Hovercraft Corporation Ltd, Library
Short Brothers Ltd, Technical Library

UNITED STATES OF AMERICA

NASA Scientific and Technical Information Facility
Applied Mechanics Reviews
Metals Information
The John Crerar Library
The Chemical Abstracts Service
Boeing Comaany
  Mr R. Watson
  Mr J. C. McMillan
United Technologies Corporation, Library
Lockheed-California Company
Lockheed Missiles and Space Company
Lockheed Georgia
McDonnell Aircraft Company, Library
Nondestructive Testing Information Analysis Center

Universities and Colleges

Iowa	Professor R. I. Stephens

SPARES (20 copies)

TOTAL (195 copies)

Department of Defence

DOCUMENT CONTROL DATA

1. a. AR No.	1. b. Establishment No.	2. Document Date	3. Task No.
AR 003-015	ARL-STRUC-R-401	April, 1984	AIR 82/125

4. Title	5. Security	6. No. Pages
MODELLING FOR FATIGUE CRACK GROWTH PREDICTION IN MIRAGE IIIO FRAME 26	a. document: Unclassified b. title: U. c. abstract: U.	32 7. No. Refs: 31

8. Author(s)	9. Downgrading Instructions
J. M. Finney, F. G. Harris, R. A. Pell, C. S. Dentry and C. T. Stefoulis	

10. Corporate Author and Address	11. Authority (*as appropriate*)
Aeronautical Research Laboratories, P.O. Box 4331, Melbourne, Victoria, 3001	a. Sponsor c. Downgrading b. Security d. Approval a) AIR FORCE OFFICE DGAIRENG

12. Secondary Distribution (*of this document*

Approved for public release

Overseas enquirers outside stated limitations should be referred through ASDIS, Defence Information Services Branch, Department of Defence, Campbell Park, CANBERRA, ACT, 2601.

13. a. This document may be ANNOUNCED in catalogues and awareness services available to . . .

No limitations

13. b. Citation for other purposes (*i.e. casual announcement*) may be (*select*) unrestricted (*or*) as for 13 a.

14. Descriptors	15. COSATI Group
Crack propagation	11130
Fatigue (materials)	01030
Damage tolerance	
Mathematical models	
Mirage IIIO aircraft	

16. Abstract

Constant- and variable-amplitude fatigue crack growth data have been obtained for A7-U4SG-T651 (2214) aluminium alloy applicable to frame 26 of Mirage IIIO aircraft, enabling calibration of computer models of crack growth. Of the four crack growth retardation models examined Wheeler, Willenborg, modified Willenborg and Crack Closure- the Wheeler and modified Willenborg models are the most satisfactory but both require calibration by test. Even so, crack growth is not accurately predicted when the specimen geometry and the test sequence are varied from those used in calibrating the models.

Apart from the crack growth models, the main sources of inaccuracy in predicting crack growth are the inadequacy of the growth rate basic data, incorrect assumptions of crack shape, and uncertainty in stress history. Thus, crack growth life may not be confidently predicted to better than a factor of two on actual life and, in some cases, the factor may be as high as ten.

This page is to be used to record information which is required by the Establishment for its own use but which will not be added to the DISTIS data base unless specifically requested.

16. Abstract (*Contd*)

17. Imprint

Aeronautical Research Laboratories, Melbourne

18. Document Series and Number	19. Cost Code	20. Type of Report and Period Covered
Structures Report 401	24 1230	—

21. Computer Programs Used

—

22. Establishment File Ref(s)

—

END

FILMED

2-85

DTIC